

Wing-Huen Ip (Editor)

New Results in the Observations and Space Exploration of Asteroids

Proceedings of An International CJMT-1 Workshop
on Asteroidal Science

October 16-17, 2012, Macao

Macau University of Science and Technology

Editors

Wing-Huen Ip
National Central University, Taiwan
Macau University of Science and Technology, Macao
Email: wingip@astro.ncu.edu.tw

Issued Date: March 2014

Publisher and Distribution: Macau University of Science and Technology

Preface

An international workshop on asteroidal science was held between October 16 and 17, 2012, at the Macau University of Science and Technology gathering together experts on asteroidal study in China, Japan, Macao and Taiwan. For this reason, we have called it CJMT-1 Workshop. Though small in sizes, the asteroids orbiting mainly between the orbit of Mars and of Jupiter have important influence on the evolution of the planetary bodies. Topics ranging from killer asteroids to space resources are frequently mentioned in news reports with prominence similar to the search for water on Mars. This also means that the study of asteroids is very useful in exciting the imagination and interest in science of the general public. Several Asian countries have therefore developed long-term programs integrating ground-based observations and space exploration with Japan being the most advanced and ambitious as demonstrated by the very successful Hayabusa mission to asteroid 25143 Itokawa. In this volume we will find descriptions of the mission planning of Hayabusa II to the C-type near-Earth asteroid, 1999 JU₃. Not to be outdone, China's Chang'E 2 spacecraft was re-routed to a flyby encounter with asteroid 4179 Toutatis in December 2012. It is planned that in the next CJMT workshop, we will have the opportunity to learn more about the in-depth data analysis of the Toutatis observations and the progress reports on the Hayabusa II mission which launch date is set to be July 2014. Last but not least, the presentations on the ground-based facilities as described in this volume will pave the way for coordinated observations of asteroidal families and Trojan asteroids - across Asia from Taiwan to Uzbekistan. Such international projects will serve as an important symbol of good will and peaceful cooperation among the key members of this group. Finally, I want to thank the Space Science Institute, Macao University of Science and Technology, for generous support, and its staff members, especially, Eason Gu and Tom Lin, for their kind assistance in the organization of the workshop and the editing of the Proceedings volume.

Wing-Huen Ip

Table of Contents

| | |
|---|----|
| Group Photo | 1 |
| Development of an Asian-wide observation network for the solar system small bodies: a JSPS Asia-Africa Science Platform during 2009-2011 | 2 |
| Searching Physical Parameters of Asteroids From Light curves Based on Ellipsoid Shape Model | 20 |
| The shape inversion of asteroids and error estimates of spin parameters in Yunnan Observatory..... | 31 |
| Current Knowledge of Jupiter Trojans – toward the Solar Power Sail mission | 43 |
| Overviews of Hayabusa2: The C-Class Asteroid Sample Return Mission of Japan... 60 | |
| Scientific Use Of LIDAR data Of Hayabusa-2 Mission | 74 |
| Near Infrared Spectroscopy and Thermal Infrared Imagery on Hayabusa2: Hydrated and Physical State of C-Class Asteroid 1999JU3 | 97 |

Group Photo



SECOND ROW (FROM LEFT): Wudong Dong, Sinsuke Abe, Bin Li, Noriyuki Namiki, Xiaoping Lu, Haibin Zhao, Yan Xia, Chien-Hsien Lin
FIRST ROW (FROM LEFT): Yuan Li, Fumi Yoshida, Tatsuaki Okada, Wing-Huen Ip, Bao Mei, Hsing-Wen Lin, Xiaobin Wang

Development of an Asian-wide observation network for the solar system small bodies: a JSPS Asia-Africa Science Platform during 2009-2011

Takashi Ito and Fumi Yoshida

*National Astronomical Observatory
Osawa 2-21-1, Mitaka
Tokyo 181-8588, Japan
Ito.t@nao.ac.jp*

Abstract — During 2009-2011, a group of astronomical scientists worked on a long-term observational program funded by Japan Society for the Promotion of Science. This program was largely focused on observations of the solar system small bodies, particularly those of the young asteroid families and of the potentially hazardous asteroids that have possibility to collide with the Earth. This program involved many scientists in four Asian countries: Japan, South Korea, Taiwan, and Uzbekistan. Major part of the observational activity took place at Maidanak Observatory, Ulugh Beg Astronomical Institute, Uzbekistan. In this article we make a brief summary as to what the program aimed at, what we did during the three year program, and what we have accomplished not only in academic standpoint but in the viewpoint of establishing a community of scientists. The designated budget program was already finished, but our science activity goes on, and we are preparing for an application for the next program along the same scientific objectives, this time including more people from more countries that could make a great scientific partnership between the existing members.

1. Introduction

Japan Society for the Promotion of Science (JSPS) is one of the governmental agencies in Japan that supports activities of scientists in and around Japan mainly in terms of funding. Nowadays a large number of scientific programs are going on with the help of JSPS, together with numerous employment of young scientists. According to the webpage of JSPS¹, their purposes and objectives are as follows:

The Japan Society for the Promotion of Science (JSPS), or Gakushin for short, is an independent administrative institution, established by way of a national law for the purpose of contributing to the advancement of science in all fields of the natural and social sciences and the humanities. JSPS plays a pivotal role in the administration of a wide spectrum of Japan's scientific and academic programs. While working within the broad framework of government policies established to promote scientific advancement, JSPS carries out its programs in a manner flexible to the needs of the participating scientists.

For scientists working on scientific projects over many countries like us, JSPS is regarded as a major funding agency for international collaboration programs,

¹ <http://www.jsps.go.jp/english/aboutus/index2.html>

particularly those with countries in Asia. A large number of international collaboration programs with a variety of frameworks are going on under the conduct of JSPS, from a short-term small bilateral collaboration between two countries to a very large multinational collaboration involving a huge amount of grant for several years. For achieving our scientific objectives that we will describe later, we had been looking for a relatively large funding source for multinational collaborations in the Asian region. For that purpose we submitted a grant application to one of the JSPS international programs in 2008 autumn. The category that we chose was called “Asia-Africa Science Platform”, specialized in collaborations with countries in the Asian or African regions. The following four items (1-4) are for explaining what Asia-Africa Science Platform is, being largely cited from JSPS’s webpage and from their attached materials²:

1. Objective: The Asia-Africa Science Platform is designed to create high potential research hubs in selected fields within the Asian and African region, while fostering the next generation of leading researchers. It does this by establishing sustainable collaborative relations among universities and research institutes in Japan and other Asian and African countries. Under the program, these “core institutions” will collaborate in research fields of special importance or significance to Asia and/or Africa and that is deemed to be of high priority within Japan. Core institutions in Japan and other Asian and African countries conduct exchanges under the leadership of Japanese core institutions. These exchanges will take the form of joint research, seminars and other scientific meetings, and researcher exchanges, which are to be organized and carried out effectively under the program. It is anticipated that the hubs formed by the core institutions will continue to carry out research activities after the funded project has ended.
2. Targeted Research Topics: Research topics of special importance or significance to Asia and/or Africa and deemed to be of high priority within Japan. (All fields of the humanities, social sciences and natural sciences.)
3. Eligible Countries: Asian and African countries (core institutions may only be established in Asian and African countries; however, individual researchers from other countries or regions, including non-Asian and non-African, are eligible to participate in projects.)
4. Implementation method: (1) A full-time researcher employed at a Japanese university or research institute acts as the project coordinator. His/her institution or department sets up the implementation framework and carries out the project. (2) JSPS provides financial support for carrying out project-related joint research, scientific meetings and researcher exchanges by Japanese core institutions. (3) JSPS makes a call for proposals to universities/research institutions, and conducts reviews and selections. The actual operation of the selected projects is left to the core institutions themselves. Counterpart core institutions in Asian and African countries are encouraged to obtain financial support from science-promotion agencies or other funding organizations in their respective countries.

For this program we organized a group of scientists that work on observational and theoretical studies of the solar system small bodies. Our application was focused on long-term observation of the solar system small bodies, particularly that of young asteroid families and of potentially hazardous asteroids. Our application involved many scientists from four countries: Japan, South Korea (Republic of Korea), Taiwan, and Uzbekistan. Fortunately our application was approved by JSPS in early 2009, and actual funding began from 2009 April for three years until 2012 March, five million Japanese yen being supplied each year for our research plan (note that 1 US dollar was equivalent to ~80 Japanese yen as of 2012 July).

Not only achieving scientific objectives on the solar system small body study, but our program aimed at building an Asian-wide astronomical observation and human network that can be used in the long-term future not only for the solar system small

² <http://www.jsps.go.jp/english/e-aaplat/>

body studies but for other astronomical observations, such as observation of gamma ray bursts, variable stars, or transit-timing variation of extrasolar planets.

The most important station of our observation network is located in Uzbekistan, called Maidanak Observatory, operated by Ulugh Beg Astronomical Institute, Uzbek Academy of Science. We showed a schematic diagram of how our network worked in Figure 1.

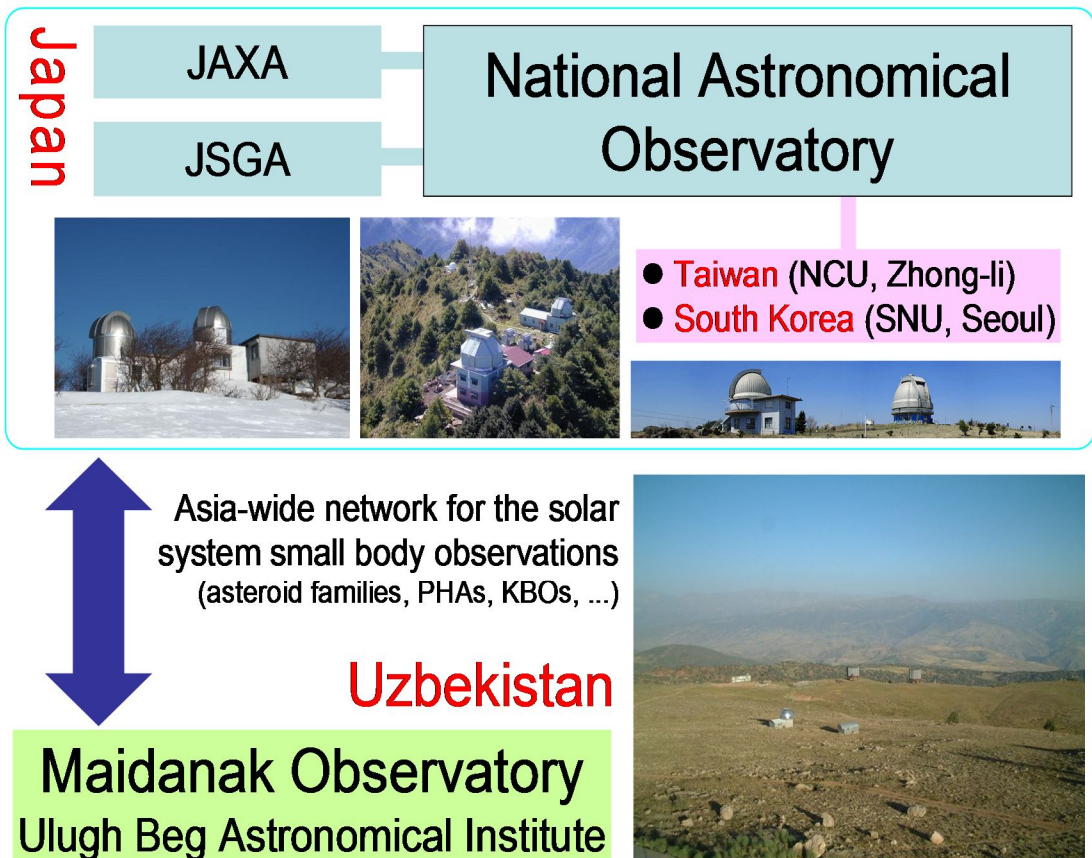


Figure 1. Schematic diagram of how our science platform works between the four relevant countries and institutes. The photos are, from the top left: Mount Nyukasa Station (JAXA, Japan), Lulin Observatory (NCU, Taiwan), Okayama Astrophysics Observatory (OAO) of NAOJ, and Maidanak Observatory (Uzbekistan).

We assigned core institutes in each of the four countries: In Uzbekistan, Ulugh Beg Astronomical Institute (UBAI; corresponding scientist for this program was Shuhrat A. Ehgamberdiev). In Taiwan, National Central University (NCU; Chen Wen-Ping), In Republic of Korea, Seoul National University (SNU; Im Myungshin). And in Japan, National Astronomical Observatory of Japan (NAOJ; Takashi Ito). In Japan, two other major institutes collaborate with and help NAOJ to accomplish the missions of the program: Japan Aerospace Exploration Agency(JAXA), and Japan Spaceguard Association (JSAG). Each country group owns different scientific objective and activity direction at Maidanak Observatory, but in this article we will focus on our (Japanese) activity in and around Maidanak. Detailed plans and activity reports of our program during the three-year grant period are summarized and now accessible on the JSPS homepage³ for public, although all the contents are written in Japanese.

2. Maidanak Observatory

³ http://www.jsps.go.jp/j-aaplat/10ichiran_aaplat2.html

Maidanak Observatory belongs to UBAI which is a member institute of Uzbek Academy of Science, and is located at the center of the Eurasian continent (GMT+5). Mt. Maidanak where this observatory resides is close to the border between Afghanistan: longitude +66°.89641E and latitude +38°.67332N, at a distance of about 120 km south of Samarkand, lying on the spurs of the Pamir and Alai mountain system with the altitude of 2593 m. The vegetation of Mt. Maidanak is typical that of high-mountain dry sub-tropics, bushes being prevailing (see the photos in Figure 2).



Figure 2. Maidanak Observatory. (Top left) The main 1.5 m telescope on August 5, 2003. (Top right) An observatory sunset with sheep and a local shepherd, on October 11, 2011. (Middle left and right) The telescope dome for our asteroid observation program and the 0.6 m telescope, on November 11, 2007. (Bottom left and right) Typical views that you will find when you walk around Maidanak Observatory, on November 14, 2007.

The history and the sky condition of Maidanak Observatory are very well described in Ehgamberdiev et al. (2000a), and we would like to make its brief citation summary in what follows: The Maidanak summit was selected for astronomical observations in the late 1960s as a result of a ten-year long site assessment campaign organized by UBAI. In the early 1970s when the high-quality atmospheric condition of Mt. Maidanak has been recognized, the summit was occupied by a Satellite Laser Ranging (SLR) station. Meanwhile the Moscow State University (MSU) and a few other Soviet Union institutions constructed their astronomical facilities at a neighboring

summit situated 5 km to the west of Mt. Maidanak. So, there are actually two Maidanak summits. By the early 1990s, about ten telescopes as well as the corresponding observatory infrastructure (roads, buildings, mechanical shops, and so on) were completed at the western summit. At present, all the astronomical facilities belong to UBAI and are operated in the framework of scientific agreements between UBAI and MSU, Ukrainian and Lithuanian astronomical institutions. One of the largest significances of Maidanak Observatory is its longitudinal location. There is practically no other scientific observation facility in the vicinity of the longitude of 70°E except Maidanak Observatory, and it has been used as a key station of time-variable astronomical observations, such as gamma ray bursts or variable stars. You can get more detailed information about this observatory from UBAI's homepage⁴. Incidentally, we should mention that Maidanak Observatory is operated together with its base station at its mountain foot, the Kitab station, which once used to be famous for a part of the International Latitude Service activity in the early twentieth century (note that International Latitude Observatory of Mizusawa, currently the Mizusawa VLBI observatory of NAOJ, was also one of the stations of this activity together with the Kitab station). See Ehgamberdiev et al. (2000b) for more detail about the Kitab station and its history.

At the site of Maidanak Observatory (Figure 2), there are more than 200 clear nights per year with a median seeing of 0".69 (Ehgamberdiev et al., 2000a). This observatory was once Soviet Union's center for astronomy and astrophysics. But ever since the collapse of Soviet Union, the observatory had been virtually abandoned mainly due to budget deficit. Our observing project at Maidanak Observatory started in 2004 as a collaboration between Japan and Uzbekistan, but it is not only about asteroid observation but about facility rejuvenation, funding for employing observers, and education of young scientists for future academic activity in Uzbekistan. Using one of the 0.6 m telescopes of this observatory, the Japanese group has been observing the solar system small bodies, particularly some members of the young asteroid families. The 0.6 m telescope that we use for our observing program of young asteroid family members was made by Carlzeiss Jena, initially with a CCD camera FLI IMG1001E (1024 x 1024 pixels, FOV = 10'.7 x 10'.7, and pixel scale = 0".67 at this telescope) that UBAI provided us (note that this CCD camera was later replaced during this program, as we will mention in the following sections). Since the old telescope can do only sidereal tracking, maximum exposure time is around three minutes for typical main belt asteroid observation: Longer exposure time would cause trailing loss. Due to the exposure time limitation, we are only able to observe asteroids with the apparent magnitude of ~17 (in *R* band) by this instrument. We will describe one of our scientific results about the young asteroid families in Section 6.

3. Rejuvenation of observational facilities

As wrote above, Maidanak Observatory had not been virtually invested for a long time since early 1990s. Naturally, many of their facilities are obsolete and not maintained well. For example as to the 0.6 m telescope we use, although the telescope body itself is fine, we had two serious problems: The mirrors attached to this telescope had not been cleaned or re-aluminized for many years, and the CCD camera was quite incompetent mainly due to the low quality CCD chip. Therefore we started our activity first from cleaning the mirrors and replacing the CCD camera for our asteroid observations.

⁴ <http://www.astrin.uzsci.net/>

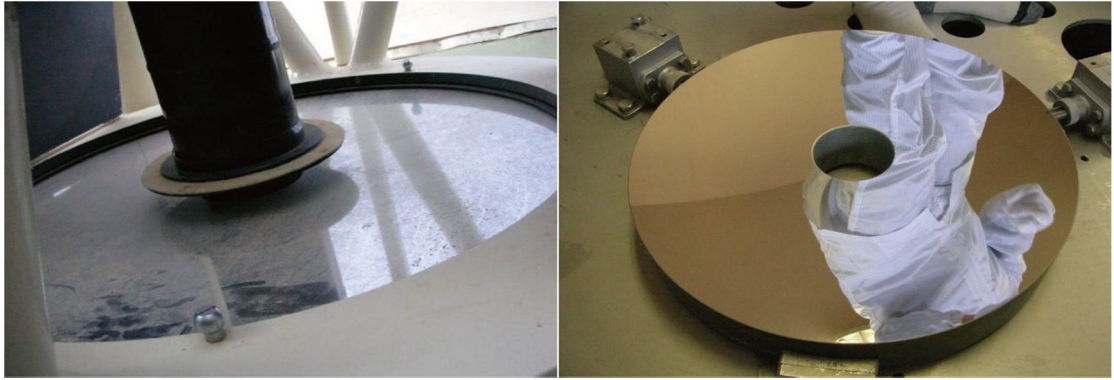


Figure 3. The main mirror of the 0.6 m telescope at Maidanak Observatory that we use for our asteroid observation. (Left) Before cleaning, on November 11, 2007. (Right) Just after cleaning and re-aluminization at OAO, on April 13, 2010.

As for the cleaning and re-aluminizing the telescope mirrors, our plan was as follows: First, detach the mirrors from the telescope (main one and sub one) at Maidanak, send the mirrors to Okayama Astrophysics Observatory (OAO) of NAOJ, Okayama, Japan, that is equipped with a large factory for mirror cleaning and re-aluminizing. After finishing cleaning and re-aluminizing the mirrors, send them back to Maidanak and attach them to the original telescope. The initial state of the main mirror of the 0.6 m telescope was substantially bad – as bad as you even could not see your face at all on the mirror, with the average light reflection rate of $\sim 45\%$ (see the left photo of Figure 3). After a series of complicated paperwork for exporting the mirrors, the mirrors arrived at OAO in early 2010. After that, thanks to the full cooperation of the OAO staff members, the mirrors are cleaned and re-aluminized beautifully to an unbelievable extent (see the right photo of Figure 3). Note that at this time NAOJ took care of the main mirror of another telescope of UBAI: the 0.48 m telescope at Parkent, not so far from Tashkent, along with a request from UBAI's director, Dr. Shuhrat A. Ehgamberdiev.

As for replacement or upgrade of the CCD camera for our observation, at first it looked fairly hopeless, mainly due to very high price of a cutting-edge CCD equipment including its maintenance cost. However, this time we encountered with a luck to get an offer from Department of Astronomy, Kyoto University, Japan. They offered us to release one of their CCD cameras (for free!) that they had stopped using, while it is still usable, for our observation activity at Maidanak. The camera is made by PixelVision with a CCD chip named SITe SI004AB (1600 x 1600 pixels, FOV =



Figure 4. (Left) The Japanese group working on an extensive check of the CCD camera that Kyoto University provided for our program. From the right, Kiichi Okita (NAOJ), Hiroshi Ohtani (Kyoto University), and Fumi Yoshida (NAOJ). (Right) A snapshot when the Japanese group members are giving a detailed instruction to the UBAI staff team as to how to construct, install, and operate the CCD camera and its controlling software. Both photos were taken on November 13, 2011 at the Kitab station of UBAI.

$13'.2 \times 13'.2$ and pixel scale = $0''.495$ at this telescope, and pixel size = $18 \mu\text{m}$), which had been used at Ouda Observatory, Nara, Japan, for several years. Although the camera needed some restoration and repair as it had not been used for a couple of years, we completed them at OAO, and exported the camera to Uzbekistan in 2011 summer. Then in 2011 November, four Japanese members of this program visited Uzbekistan to construct and check the functions of the entire CCD system. Unfortunately, bad weather and heavy snowfall prohibited us to reach Maidanak Observatory in this trip, but we did many kinds of extensive tests about the CCD camera at the Kitab station of UBAI located at the mountain foot of Maidanak Observatory, also giving a comprehensive set of instructions to the UBAI staff members that now take care of the CCD camera at Maidanak for our observation (Figure 4). Currently the Kyoto CCD camera is equipped with a new filter set ($U-B-V-R-I$), and is successfully installed at the 0.6 m telescope for the asteroid observation. UBAI organized a local observation team for our program, and it carries out observations scheduled by the Japanese group on a regular basis.

4. Tutorial session for young astronomers

As was stated in "1. Objective" in the Asia-Africa Science Platform of JSPS, our program also had to aim at fostering the next generation of leading researchers in each of the countries involved in this field through the program. For this purpose, every year we invited young astronomers or engineers to Japan, mainly from Uzbekistan and sometimes from other countries, dispatching them to the observatories that the Japanese member institutes are operating. Hereafter we call the series of invitations "tutorials" for young astronomers. The major purpose of the tutorials is for the young



Figure 5. (Top left) A tutorial session at OAO with a pair of young astronomers coming from Uzbekistan and Taiwan, on February 18, 2010. (Top right) A photo taken right after a tutorial session at Mount Nyukasa Station was finished for three young astronomers from Uzbekistan, on February 4, 2011. (Bottom left) In the middle of a tutorial session at BSGC/JSGA for a young Uzbek astronomer, on February 9, 2012. (Bottom right) A group photo when we invited UBAI's general director, Dr. Shuhrat A. Ehgamberdiev to the Chofu headquarters of JAXA, on September 7, 2010.

generation people to know how cutting-edge observation systems work with highly advanced digital technology, and how astronomical observations are done automatically, as little human interference involved as possible. Also, we hope that they understand scientific significance of our own observation program – what kind of importance the solar system small bodies have in the context of planetary astronomy, and which type of observational data is particularly important for our specific objectives focused on young asteroid families and potentially hazardous asteroids. In collaboration with several domestic observatories in Japan, we dispatched the invited young scientists there and had them stay at each of them for several days, having them learn and practice how to observe the solar system small bodies using particular observation system and hardware/software (Figure 5). The major observatories that cooperated this tutorials are: OAO (of NAOJ), Mount Nyukasa Station (of JAXA), Bisei Spaceguard Center in Okayama (BSGC of JSGA), and the NAOJ headquarters in Mitaka, Tokyo.

Nowadays most of the astronomical observations carried out in the world are computerized and half-automatic, involving as little human interference as possible. However, unfortunately the facilities at Maidanak Observatory have a long way to reach this standard. What we need in future is a larger investment on this observatory in order to introduce modern telescope operating systems including hardware and software. But more importantly, we need to have young generation scientists and engineers that are very well aware of the world standard of the modern astronomical observations. Most of the participants to the tutorials were quite impressed to see the computerized, semi-automatic observation system for the first time, and we hope that this experience will be the fundamentals when they build a similar modern system in their home institutes in the near future, particularly at Maidanak Observatory.

5. Maidanak Observatory Users' Meeting

Most of the major astronomical observatories hold annual or semi-annual meetings for the observers (users) using there, asking them to present their latest academic achievement and to exchange information about observational details. This is the so-called observatory's users' meeting (UM) which is supposed to be a precious opportunity for the observatory to pick up opinions and comments from their observers for the purpose of future improvement and development of their facility and service. However, Maidanak Observatory (and any other observatories that UBAI operates) had somehow never held its users' meeting before our program began. Now that UBAI wants to have as many international collaborators as possible, the situation at that time where they were away from opportunities to get observers' opinions was obviously not ideal. Hence, Fumi Yoshida (NAOJ), the practical science leader of the Japanese group, took initiative and called upon the first Maidanak Observatory Users' Meeting in 2009 spring. What was very lucky for us was that, right after the call for meeting by Yoshida, the Korean group led by Im Myungshin agreed to this idea, and proposed not only hosting the meeting in SNU, Seoul, but offering substantial amount of funding aid for the meeting.



Figure 6. Group photos taken at each of the Maidanak Users' Meetings during our program period. (Top) At the first meeting in SNU, Seoul, on June 30, 2009. (Mid) At the second meeting in UBAI, Tashkent, on June 21, 2010. (Bottom) At the third meeting in NAOJ, Tokyo, on January 31, 2012.

The monumental first Maidanak Users' Meeting was held on June 30, 2009, at Seoul National University in Seoul, Republic of Korea. More than 50 participants gathered at the meeting not only from the four countries registered in this program, but from Russia and Egypt (Figure 6, top). Most of the participants did not know each other then, but as presentations went on, they began understanding what others are trying to do at Maidanak Observatory, which is exactly what we believe was the commencement of the Maidanak community. At the business session of the meeting there were substantial amount of opinion exchanges including very harsh, hostile, and adversarial comments as to how sloppy and disorganized the operation of Maidanak Observatory is compared with the modern world standard observatories. The Maidanak staff members rebutted against some of the opinions, but accepted most others, and they promised to improve the operation and facilities as soon as possible. At the same time, we agreed to the point that we have to find more ways for investment on Maidanak Observatory for the sake of the community future. Obviously, the meeting in Seoul was a remarkable highlight of the entire three- year program.

Following the great success of the first Maidanak Users' Meeting in Seoul, the second Maidanak Users' Meeting was hosted by UBAI in Tashkent, Uzbekisntan, on June 21-22, 2011. Evidently this was the most authentic form of having a Maidanak Users' Meeting, and the whole institute of UBAI worked very hard on its preparation to have a fruitful meeting with many participants from foreign countries. More than 40 participants gathered at the meeting not only from the four countries registered in this program, but from Russia, Ukraine and Spain (Figure 6, middle). Particularly the participation of Russian scientists and engineers to the meeting was quite meaningful and significant, as a large part of the Maidanak facilities still depend on the experience and expertise of Russian scientists that have been involved with Maidanak



Figure 7. (Top left) The main banquet of the first Maidanak Users' Meeting in Seoul, on June 30, 2009, with Korean traditional palace dishes. (Top right) Takashi Ito, an author of this article, is giving an invited lecture at the second Maidanak Users' Meeting at the UBAI headquarters, Tashkent, on June 22, 2010. (Bottom left) A part-time working woman is preparing a lunch for visitors at Maidanak Observatory by burning wood pieces due to frequent power outages, during the after-meeting tour of the second Maidanak Users' Meeting, on June 24, 2010. (Bottom right) Fumi Yoshida, the other author of this article as well as the main organizer of the third Maidanak Users' Meeting in Tokyo, Japan, is preparing a formal Japanese tea ceremony for the participants, on February 1, 2012.

Observatory for a long time, ever since its site assessment in 1960s. Having their presence at the users' meeting in Tashkent, the participants felt free to ask as many questions as they wanted about technical details and future facility plans at the meeting. And the observatory side, including the helpers coming from Russia and Ukraine, returned satisfactory answers to the questions to a great deal.

The meeting was followed by a three day trip to Maidanak Observatory with nearly 30 visitors. According to a local staff member, a visit of this large group of people to Maidanak "has never happened since the collapse of Soviet Union in 1991," and we continued discussions at the observatory too, not only on scientific activity at Maidanak but at future operational plans of the observatory itself. We cannot say that the accommodation facility of Maidanak Observatory is very good at present, but we hope to return to Maidanak Observatory again within some years and have another, even more intensive discussions about our activity at this place.

The third Maidanak Users' Meeting, which was supposed to be the final one during the grant period of three years, was once planned to take place in Tokyo, Japan, in

2011 May. However, an unexpected disaster totally changed the original plan, as well as the entire future of that country – the Great East Japan Earthquake that happened on March 11, 2011, which caused deaths of nearly 20,000 people as well as financial damage of ~20 trillion Japanese yen (more than 200 billion US dollars) to the entire country. In addition to the direct damages of human casualties and economic mayhem, the country ended up with suffering from yet another disgusting problem: Severe radiation leak from a half-collapsed nuclear power plant in Fukushima caused by a huge tsunami that immediately followed the earthquake. It eventually turned out to be an accident of a nuclear power plant that is as serious as the Chernobyl disaster in 1986 in the former Soviet Union. Obviously it is impossible to describe in this short article how terribly the people in Japan got confused, scared, lost hopes, and angry in those days. It was just clear that we could never prepare a Maidanak Users' Meeting as planned in May of the same year as the disaster under a situation like that. Therefore we just had to cancel the initial plan, putting off everything until things have got settled and people have got their daily life back, which actually took a very long time.

We had to wait until the next year when we got ready to host the Maidanak Users' Meeting in Japan. Having a large amount of help and support from the NAOJ local members and its administration office, the third Maidanak Users' Meeting finally took place at the end of 2012 January at NAOJ's headquarters in Mitaka, Tokyo, Japan. Nearly 40 participants gathered at the meeting not only from the four countries registered in this program, but from Russia, Ukraine and India. For the first time the meeting was broadcast to foreign countries (such as to Taiwan) through an Internet video conference system. Now that it was nearly the end of the three-year budget plan of our Asia-Africa Science Platform, the academic achievement reported by the Maidanak users in each of the countries was quite rich and established, and the discussions there were quite intensive. Also, as most of the participants are quite aware that who are operating the facilities at Maidanak and who are responsible for them, we saw very little hesitation for anyone to ask quite straight and honest opinions and criticism against the observatory administrative people, including the UBAI director. As a result, there remained several questions that UBAI could not satisfactorily answered, and the discussions are still going on the Maidanak users' mailing list.

As a whole, we believe that the series of Maidanak Users' meeting sure worked for organizing a community in and around Maidanak Observatory – a community including not only astronomers but also engineers, technicians, administrative associates, and local residents that share the same space with scientists. This kind of community is inevitable for future development of scientific activity that will be carried out at Maidanak Observatory, and we cannot stop going on toward the direction that expands this kind of community. Fortunately, the series of Maidanak Users' Meeting seem to continue even after the JSPS budget program was terminated: It was already announced that the fourth meeting will happen in Tarusa, a small town near Moscow, Russia, on July 1-4 in 2013, by the courtesy of IKI (Space Research Institute), Moscow. The Maidanak Users' Meeting series will remain a fundamental of the development of the Maidanak community, and we feel quite happy to be a part of its initiation and establishment.

6. An example of scientific achievement

In this section we briefly review what we have scientifically achieved through our observing program at Maidanak Observatory, taking lightcurves of young family

asteroids as a typical example.

Asteroid families are outcome of catastrophic collisions of asteroids that lead to their breakup into fragments (Hirayama, 1918). They may provide important clues to how disruption events occurred and to what dynamics/physics have dominated over the history of the solar system. However, it has been believed that asteroid families are as old as 10^2 to 10^3 million years, undergoing significant orbital and collisional evolution that masks the properties of the original collisions. Newer, fresher information about the formation of asteroid families has long been sought.

In 2002, a sophisticated numerical technique identified a very young asteroid family, the Karin family, formed only 5.8 million years ago (Nesvorný et al., 2002). Later, more young asteroid families were reported (Nesvorný et al., 2003) such as the

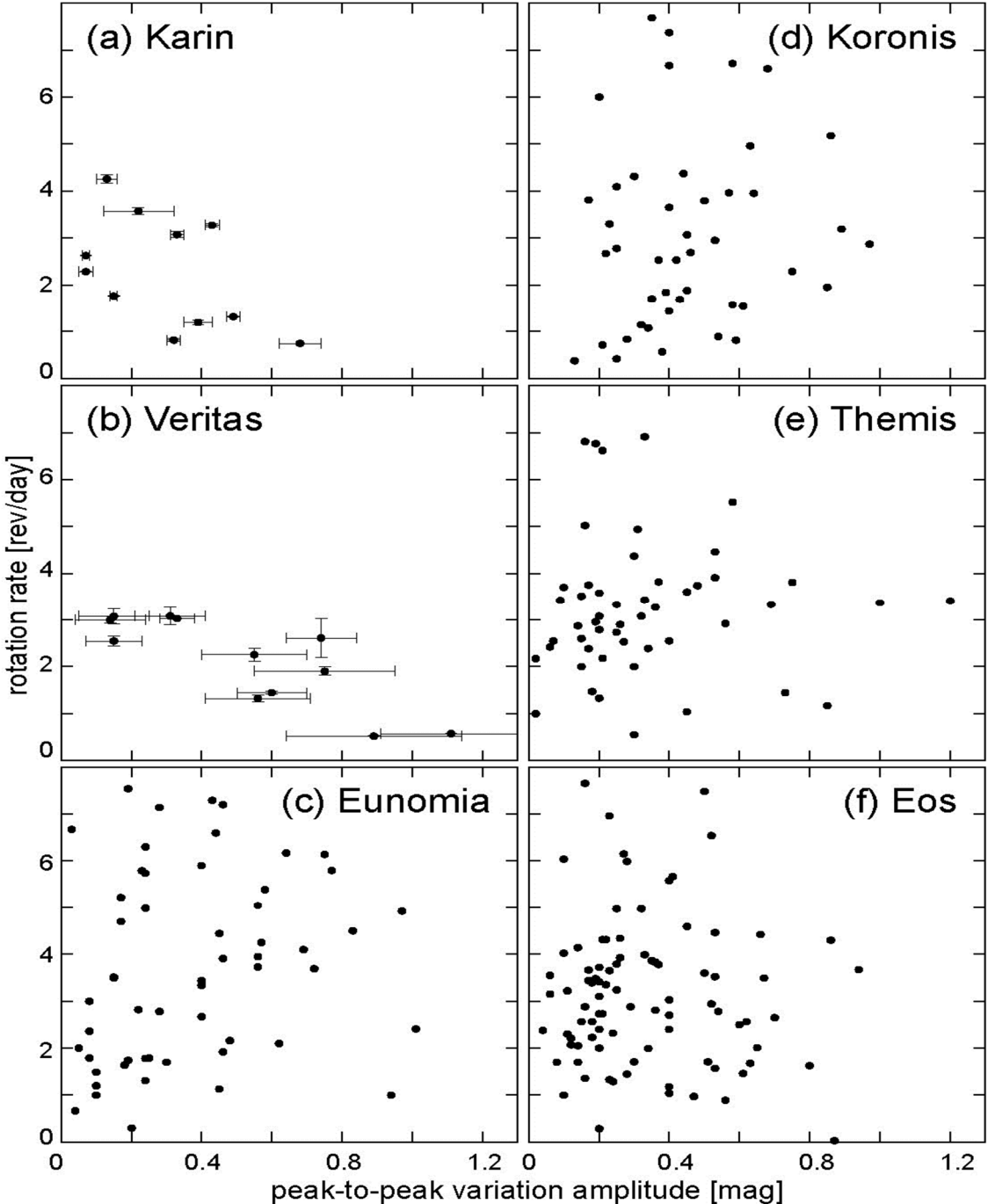


Figure 7. Peak-to-peak variation amplitude and rotation rate of the young (a, b) and old (c-f) family asteroids. (a)(b) are from our own observations.

Veritas family (8.3 Myr old) and the Iannini family (\sim 5 Myr old). Until now, even younger asteroid families have been discovered through the same numerical technique. One example is an S-type cluster, the Datura family, presumably an outcome of a disruptional collision of asteroids of only 450 ± 50 thousand years ago (Nesvorný et al. 2006a). Also, three more candidates for quite recent asteroid breakups were confirmed (Nesvorný et al. 2006b): The Emilkowalski cluster with an estimated disruption age of 220 ± 30 Kyr ago, the 1992 YC2 (16598) cluster of 50-250 Kyr ago, and the Lucascavin cluster of 300-800 Kyr ago. In addition, roughly sixty pairs of main-belt asteroids with nearly identical orbits have been reported, most of which were identified pairs formed within the past 1 Myr (Vokrouhlický et al. 2008). The origin of the paired objects are probably collisional disruption of larger parent bodies, i.e. the smallest version of young asteroid families. More and more young asteroid families will be detected in the near future. Nothing to say, accumulation of lightcurve data of the young family asteroids will eventually provide significant information about their shape, which we can compare with the result of laboratory and numerical experiments of disruptive collisions of the solar system objects.

Driven by these motivations, we have begun a long-term program to observe lightcurves (multicolor, whenever possible) of the young asteroid family members. Lightcurve observations in general yield important clues as to spin state, shape, and various surface properties of the small solar system bodies. Potential results derived from our observation of the young family asteroid members will be a strong constraint on laboratory and numerical experiments of collisional fragmentation (e.g. Michel et al. 2003; Nesvorný et al. 2006c; Kadono et al. 2009; Ito & Malhotra 2006, 2010) and of space weathering (e.g. Sasaki et al. 2001). In addition, as the age of the young family asteroids is literally young, we may be able to detect their tumbling motion (a.k.a. non-principal axis rotation, similar to Earth's Chandler wobble) in their lightcurves. Although tumbling motion can give us important insights into energy dissipation and excitation processes as well as that into internal structure of celestial bodies, it gets damped very quickly particularly for small bodies unless the excitation continues. This is the main reason why the tumbling motion of the small solar system bodies has been confirmed only for handful of cases (e.g. Mueller et al. 2002). Very young family asteroids possibly keep tumbling motion yet, and they can put epoch-making exceptions in this field.

So far we have observed lightcurves of some of the three young asteroid family members: The Karin, Veritas, and Iannini families. As for the multicolor photometry, we particularly carried out extensive observations of the largest member of the Karin family, (832) Karin, and detected potentially heterogeneous surface on this asteroid at a particular phase (Sasaki et al. 2004; Yoshida et al. 2004; Sasaki et al. 2006). In this section we give a brief summary of our preliminary results on the relationship between the peak-to-peak variation amplitude of the young asteroid family members and their rotation rate as well as their absolute magnitude. For more detail of our observation strategy and results, such as lightcurves themselves, solar phase curve, and color information, see Ito & Yoshida (2006, 2010), Yoshida et al. (2009), or Yoshida et al. (arxiv preprint).

We plotted the observation data for some members of the two young asteroid families (Karin and Veritas) in Fig. 7 and Fig. 8 together with four old and larger family asteroids, Eunomia, Koronis, Themis, and Eos for comparison. Note that the number of lightcurves that we have obtained for the Iannini family members is still too small for statistical discussion so far, and they are not plotted here.

It is well known that the peak-to-peak variation becomes larger as the solar phase

angle increases. An empirically derived correction formula is well known (Zappala et al. 1990): $A(0) = A(\alpha)/(1+m\alpha)$ where $A(0)$ and $A(\alpha)$ are the peak-to-peak variation

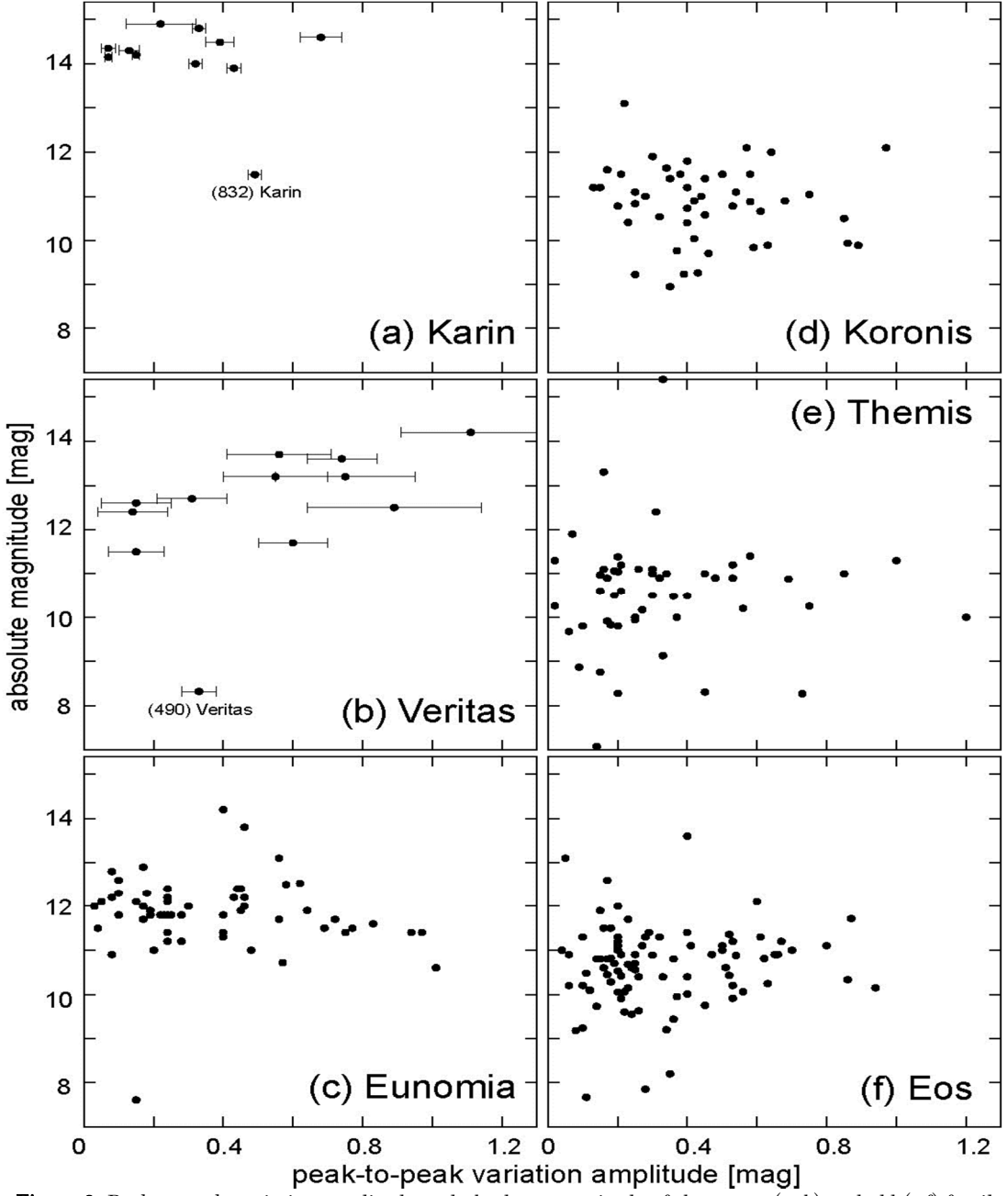


Figure 8. Peak-to-peak variation amplitude and absolute magnitude of the young (a, b) and old (c-f) family member asteroids.

amplitude of lightcurves when the solar phase angle = 0 and = α . We adopted $m = 0.030$ for the typical S-type asteroids (the Karin family asteroids) and $m = 0.015$ for the C-type asteroids (the Veritas family asteroids). We included this correction into all the data that we are going to show here. Note that the errorbars for the Veritas family members is much larger than those for the Karin family members. This is because the lightcurve data for the Veritas family asteroids is mostly from the 0.6-m telescope at Maidanak Observatory, while that for the Karin family members is to some extent from our previous observing campaign using larger telescopes, such as the Steward 2.3 m telescope ("Bok") of the University of Arizona at Kitt Peak or the 1.8 m telescope ("VATT") at the Vatican Observatory at Mt. Graham, also in Arizona. Data for the older asteroid families is from the Asteroid Data Sets at Planetary Science

Institute⁵ and the Asteroid Orbital Elements Database at Lowell Observatory⁶.

Compared with those of the older and larger asteroid family members, the relationship between peak-to-peak variation amplitude and rotation rate of the young asteroid families (Fig. 7) is very different. Although it is clear that we need more samples in future observations, both the Karin (a) and the Veritas (b) family members have the same trend in the panels: The larger the peak-to-peak variation amplitude is (i.e. the more elongated the asteroid is), the slower the asteroid rotates. This trend is not seen in any of the old asteroid family member data (the panels (c), (d), (e), (f) of Fig. 7). This trend might have an implication for the angular momentum distribution of asteroid fragments at the time of disruption. Particularly for the Karin family members that have all similar absolute magnitudes (hence similar size, see Fig. 8(a)) except the largest member ((832) Karin), this trend could mean that the angular momentum was distributed rather uniformly to each of the fragments at the disruption event. Another interesting thing, although still ambiguous until we have accumulated more data points, is that the young family asteroids do not seem to have members near the lower left corner of the panels (a) and (b) in Fig. 7. The contrast is remarkable when you compare panels (a)(b) with (c)-(f). This literally means that there are fewer members with a long rotation period and with nearly a spherical shape among the young asteroid families, while this kind of asteroid is pretty common among the old asteroid families. So far we do not have any ideas about whether this tendency is just an observation bias (i.e. it is generally difficult to observe lightcurves of asteroids with longer period and with smaller amplitude) or real dynamical characteristics particularly to the young asteroid families that were already lost from the older asteroid families due to long-term evolutions.

Note that there are very few asteroids in the upper right corner of all the panels in Fig. 7. This probably indicates the break-up limit of rubble pile asteroids: Assuming asteroids are rubble piles, they will simply break up into pieces when their rotation rate is too high, particularly when their shape is elongated. (i.e. Assuming that the volume and the density of asteroids are the same, the break-up spin rate of an elongated asteroid is lower than that of a spherical asteroid due to its higher centrifugal force when they have the same rotational angular velocity.) This is why we have few asteroids in the upper right corner of the panels (i.e. lack of fast-rotating, elongated asteroids). In other words, when we have observed young family asteroids that are not on this trend, we might want to say that they are not rubble piles but monolithic bodies.

The relationship between peak-to-peak variation amplitude and asteroids' absolute magnitude (H) is shown in Fig. 8. For some of the Karin (the panel a) and the Veritas family (the panel b) asteroids, we calculated their absolute magnitude through our observation data with different solar phase angles. For the old family members (the panels c to f), we consulted "astorb.dat" provided by Lowell Observatory⁷ in order to know their absolute magnitudes. Although it does not seem that there are any strong correlations between peak-to-peak variation amplitude and asteroid absolute magnitude, we may find an interesting feature in panel (b) for the Veritas family asteroids: the darker the asteroid is (i.e. with larger H , hence the smaller in size, assuming the same albedo for all the family members), the more elongated its shape is (i.e. the larger its peak-to-peak variation amplitude is). On one hand it might sound

⁵ <http://www.psi.edu/pds/archive/asteroids.html>

⁶ <ftp://ftp.lowell.edu/pub/elgb/astorb.html>

⁷ <ftp://ftp.lowell.edu/pub/elgb/astorb.html>

fine because at a disruption event when a large number of small fragments are created, it is natural that many of them become irregular-shaped or elongated. However, this trend is not clear for the Karin family (a) and for the older families (c-f), for which we do not yet have a good explanation.

In the very near future, an impending deluge of large-scale sky surveys such as HSC, Pan-STARRS and LSST will yield a far larger amount of information with much higher accuracy about younger asteroid families including more smaller members. They will sure be critical keys to understand the collisional and dynamical evolution of the solar system small bodies. We too will keep our series of photometric observations on the young asteroid families at Maidanak Observatory, hoping to contribute to this line of research activity.

7. Final remark

Our budget program that lasted for three years in and around Maidanak Observatory might be regarded as a middle-scale academic experiment involving several countries in an effort to answer to quite a few interesting questions that may arise in other international collaborations as well: Is it really possible to establish an Asia-wide observational network without continuous supply of million dollar money? How can we sustain a human network for this kind of observations, having a variety of people that have different scientific interest and background? What kind of way is the most efficient and effective to make the next generation scientists grow up, particularly in an international environment like this? Would it be fine to make use of economic disparity between particular countries (such as between Uzbekistan and Japan), even when the purpose is purely academic and not for profit? And, to ourselves: Was our scientific goal accomplished even to a small extent as we had expected before? Honestly, we do not have clear or appropriate answers to any of these questions now. But one thing is sure – our experiment just goes on and on, with or without budget, until our scientific objectives have been achieved and the human network that can be exploited by the future generation has been established. Also, the next generation program of this line will involve two Asian powers as well: China and India that already have extremely large resource in planetary astronomy that we rely on. It will enforce our program and hopefully accelerate the accomplishment of our scientific goals that otherwise might be rather far away.

Acknowledgements

We greatly appreciate the effort and courtesy by all the people at all the institutes in all the countries that were kindly involved with our series of observing program, particularly those working at UBAI and Maidanak Observatory, including their director, Shuhrat A. Ehgamberdiev. We also thank two expert admin associates working at NAOJ, Michiru Goto and Hiroko Kikkawa, for helping us take care of cumbersome and complicated paperwork accompanied with the use of funding. Some part of the data analysis was performed at ADC and CfCA of National Astronomical Observatory of Japan. This study is supported by the Grant-in-Aid of the Ministry of Education, Culture, Sports, Science & Technology in Japan (16740259/2004-2005, 18540426/2006-2008, 18540427/2006-2008, 21540442/2009-2011), the Sumitomo Foundation research funding (030755/2003-2004), the NAOJ special research funding by Director's discretion (2004, 2005, 2006, 2007, 2008), the Heiwa Nakajima Foundation research funding for the Asian studies (2009), and the JSPS Asia-Africa Academic Platform (2009-2011) entitled "*Development of the Asian-wide observation network for detecting and investigating potentially hazardous near-Earth objects.*"

References

- Ehgamberdiev, Sh. A., Baijumanov, A. K., Ilyasov, S. P., Sarazin, M., Tillayev, Y. A., Tokovinin, A. A., and Ziad, A. (2000a) The astroclimate of Maidanak Observatory in Uzbekistan, *Astron. Astrophys. Suppl.*, **145**, 293-304.
- Ehgamberdiev, Sh. A., Eshonkulov, S., and Litvinenko, E. (2000b) Kitab as one of the five stations of the ILS: History and present In *Polar Motion: Historical and Scientific Problems*, ASP Conference Series, (Eds. Steven Dick, Dennis McCarthy, and Brian Luzum), **208**, 163-168, ASP, San Francisco.
- Hirayama, S. (1918) Groups of asteroids probably of common origin. *Astron. J.*, **31**, 185-188.
- Ito, T. and Malhotra, R. (2006) Dynamical transport of asteroid fragments from the ν_6 resonance, *Advances in Space Research*, **38**, 817-825.
- Ito, T. and Yoshida, F. (2006) Lightcurves of the Karin family asteroids, in *Advances in Geosciences* (Eds. Anil Bhardwaj and Wing-Huen Ip), **3**, 317-329, World Scientific, Singapore.
- Ito, T. and Malhotra, R. (2010) Asymmetric impacts of near-Earth asteroids on the Moon, *Astron. Astrophys.*, **519**, A63.
- Ito, T. and Yoshida, F. (2010) Young asteroid families and their lightcurve observation at Maidanak Observatory, Uzbekistan, in *Advances in Geosciences* (Eds. Anil Bhardwaj et al.), **25**, 161-172, World Scientific, Singapore.
- Kadono, T., Arakawa, M., Ito, T., Ohtsuki, K. (2009) Spin rates of fast-rotating asteroids and fragments in impact disruption, *Icarus*, **200**, 694-697.
- Michel, P., Benz, W. and Richardson, D. C. (2003) Disruption of fragmented parent bodies as the origin of asteroid families, *Nature*, **421**, 608-611.
- Mueller, B. E. A., Samarasinha, N. H., and Michael, M. J. S. (2002) The diagnosis of complex rotation in the lightcurve of 4179 Toutatis and potential applications to other asteroids and bare cometary nuclei, *Icarus*, **158**, 205-311.
- Nesvorný, D., Bottke, W. F., Dones, L., Levison, H. F. (2002) The recent breakup of an asteroid in the main-belt region, *Nature*, **417**, 720-722.
- Nesvorný, D., Bottke, W. F., Levison, H., and Dones, L. (2003) Recent origin of the solar system dust bands, *Astrophys. J.*, **591**, 486-497.
- Nesvorný, D., Vokrouhlický, D., and Bottke, W. F. (2006) The breakup of a main-belt asteroid 450 thousand years ago, *Science*, **312**, 1490.
- Nesvorný, D. and Vokrouhlický, D. (2006) New candidates for recent asteroid breakups. *Astron. J.*, **132**, 1950-1958.
- Nesvorný, D., Enke, B. L., Bottke, W. F., Durda, D. D., Asphaug, E., and Richardson, D. C. (2006) Karin cluster formation by asteroid impact, *Icarus*, **183**, 296-311.
- Sasaki, S., Nakamura, K., Hamabe, Y., Kurahashi, E., and Hiroi, T. (2001) Production of iron nanoparticles by laser irradiation in a simulation of lunar-like space weathering, *Nature*, **410**, 555-557.
- Sasaki, S., Sasaki, T., Watanabe, J., Yoshida, F., Kawakita, H., Takato, N., Dermawan, B., Fuse, T., Ito, T., and Sekiguchi, T. (2006) A new-born asteroid 832 Karin with old and new surfaces - SUBARU Spectroscopy, *Adv. Space Sci.*, **38**, 1995-1999.
- Sasaki, T., Sasaki, S., Watanabe, J., Sekiguchi, T., Yoshida, F., Kawakita, H., Fuse, T., Takato, N., Dermawan, B., Ito, T. (2004) Mature and fresh surfaces on the newborn asteroid Karin, *Astrophys. J.*, **615**, L161-L164.
- Vokrouhlický, D. and Nesvorný, D. (2008) Pairs of asteroids probably of a common

origin, *Astron. J.*, **136**, 280-290.

Yoshida, F., Dermawan, B., Ito, T., Sawabe, Y., Haji, M., Saito, R., Hirai, M., Nakamura, T., Sato, Y., Yanagisawa, T., and Malhotra, R. (2004) Photometric observations of a very young family-member asteroid (832) Karin, *Publ. Astron. Soc. Japan*, **56**, 1105-1113.

Yoshida, F., Ito, T., Takahashi, S., Ibrahimov, M. A., and Marchalkina, A. L. (2009) Photometric observations of young asteroid families at Maidanak Observatory, in *Advances in Geosciences* (Eds. Anil Bhardwaj et al.), **15**, 119-132, World Scientific, Singapore.

Yoshida, F., Ito, T., Dermawan, B., Nakamura, T., Takahashi, T., Ibrahimov, M. A., Malhotra, R., Ip, W.-H., Chen, W.-P., Sawabe, Y., Haji, M., Saito, R., Hirai, M., Miyasaka, S., Fukushima, H., Sato, H., and Sato, Y., Lightcurves of the Karin family asteroids, arXiv:1205.2837.

Zappala, V., Cellino, A., Barucci, A. M., Fulchignoni, M. and Lupishko, D. F. (1990) An analysis of the amplitude-phase relationship among asteroids, *Astron. Astrophys.* **231**, 548-560.

Searching Physical Parameters of Asteroids From Light curves Based on Ellipsoid Shape Model

Xiaoping Lu

*Faculty of Information Technology
Macau University of Science and Technology
Avenida Wai Long, Taipa, Macau, China
xplu@must.edu.mo*

Abstract — The research about asteroids attracts more and more attention recently, especially focusing on their physical structures, such as the spin axis, the spin period and the shape. The long distance between Earth observers and asteroids makes it impossible to get the shape and other parameters of asteroids directly with the exception of the NEAs (Near Earth Asteroids). Generally photometric measurement is still the main way to obtain the research data for asteroids now, i.e. the lightcurves recording the brightness and positions of asteroids. Assuming that the shape of the asteroid is a triaxial ellipsoid with a stable spinning status, a new method is present in this article to reconstruct the shape models of asteroids from the lightcurves, with the other physical parameters together. The method searches the optimal solution by Levenberg-Marquardt algorithm to minimize the residual of the brightness. By adopting this method not only related physical parameters of asteroids can be obtained at a reasonable accuracy, but also a simple shape model of Ellipsoid can be generated for reconstructing more sophisticated shape model further. At last the numerical applications confirm the new method is efficient and stable to compute the inverse problem of asteroids shape.

1. Introduction

With the development of the technology humans have much more ability to discover the universe now. The beginning of our universe is still an interesting problem, which results in the research about asteroids because the asteroids reserve much information about the original formation of the solar system. Most of asteroids found now lie between Mars and Jupiter, commonly called as main belt asteroids (MBAs). Some astronomers guess that there would be a large planet between Mars and Jupiter, but some special reasons prevent its formation and the fragments are left to be MBAs. Generally MBAs are orbiting the sun with a stable status with the exception that some larger bodies, such as planets, passing them over and the perturbations will change their orbits. Especially some asteroids will change their orbit to approach the earth, called as near earth asteroids (NEAs). NEAs are the large potential hazards to damage the earth which is another important reason to research the asteroids.

Due to the long distance of 2.1~3.3AU between the earth and most of asteroids, until now the main research data about asteroids is the photometric brightness with the position coordinates of asteroids, the earth and the sun, generally i.e. lightcurves, which are recorded by many observatories located on the surface of the earth. Recently there are some large sky-watch missions such as UVEX, VPHAS, SSS, LSST, PanSTARRS et al, including the future mission GAIA launched in 2013 (Jordi et al., 2010) and the Chinese Chang'e 2 to flyby the asteroid 4179 sending tremendous amounts of photometric data of asteroids from the outer space. The expensive space missions are planned for only several specific asteroids and the common way for most of asteroids is nevertheless to reconstruct the physical models from lightcurves observed on the earth.

Shape models with other physical parameters such as the spinning period and spin axis, especially the albedo of asteroids are the most concerned about asteroids. The total distribution of the spin axis of MBAs can help us research the origin of the solar system because most of MBAs keep the same spin direction as they are formed. Commonly the spinning periods of MBAs are stable with some hours less than one day. But recently it is found that the thermal radiation from the sun can increase the asteroid's rate of rotation, called as YORP effect firstly by Rubincam (2000). Durech et al. (2008) observed the spinning period of asteroid 54509 will double in about 600,000 years which confirms that the spin periods of asteroids may change in a very small amplitude within a long term.

There are many methods to reconstruct the shape models of asteroids with the other physical parameters. Russell (1906) firstly started the research about the shape of asteroids and concluded a pessimistic result that the shape could not be obtained merely depending on the lightcurves of the opposition. Opposition is a special position where the sun, the earth and the asteroid are lying on the same line, i.e. the angle of Sun-Asteroid-Earth is zero. Apparently the observed brightness of asteroids is biggest on the opposition so asteroids can be easily observed on the earth. With the development of both mathematical theories and technologies in telescope more and more lightcurves viewed in various solar phase angles are recorded by many observatories located everywhere on the earth and the shape inversion algorithms can figure out the shape model in a reasonable accuracy by the high-speed computers. Lumme & Bowell (1981a,b) presented an estimation about the scattering law in the surface of atmosphereless bodies and introduced a spherical harmonics method for asteroid pole determination (Lumme et al., 1990). Hapke (1984) moved further about

the scattering law with the consideration of bidirectional reflectance and the roughness of the surface. Basing on the scattering law of Lumme and Bowell, Karttunen (1989) and Karttunen & Bowell (1989) presented a method to generate lightcurves of triaxial ellipsoid models and discussed the variations of convex model and nonconvex model. But they just noted that it was possible to determine the axial ratios of a triaxial ellipsoid model, while did not give a method to find the shape models from lightcurves. Cellino et al. (1989) adopted a model formed by merging together eight octants of ellipsoids having different semi-axes and generated the corresponding lightcurves without an inverse method, too. Adopting the tremendous sparse photometric data from the large sky surveys of GAIA and Pan-STARRS, Cellino et al. (2009) presented a genetic inversion to find the physical properties of asteroids with the assumption that the shape model of the asteroid is a triaxial ellipsoid. Furthermore Kaasalainen & Lamberg (1992a,b) built up a very efficient method to reconstruct the arbitrary surface of asteroids and the inverse shape models are confirmed by the flyby observation in space (Kaasalainen et al., 2002).

Nevertheless until now the ellipsoid model plays an important role. Firstly the photometric data observed by the observatories based on the earth is not enough accurate because of the atmosphere mist, the CCD heat, wrong operations and so on. Generally the error of photometric data is about 2% and we can not expect to obtain a very accurate shape model only from the lightcurves. Secondly the ellipsoid model is simple but it can make the inversion easy and efficient with an acceptable physical parameters while the statistical research about the spin axis and period of asteroids can obtain the needed data in a fast way. Thirdly the rough model inferred from the ellipsoid model may be the initial value for reconstructing more accurate shape model by Kaasalainen's method.

Under the similar definition employed in Kaasalainen's method and tiling the triangular facets in Lebedev way we present a fast method of the ellipsoid model in this article as the following organization. In section 2 we describe the technical details of the fast ellipsoid model including the scattering law and the photometric integration, especially the formulas for reference. After the full introduction about the method we show the performance by simulating the ellipsoid model and the real asteroid model in section 3. The result confirms that this method is efficient in computing the physical parameters and obtaining a rough ellipsoid model. At last the summing up and future plan will be discussed in section 4.

2. Ellipsoid Model For Asteroids

The disk-integrated photometric data i.e. brightness in lightcurves, contains much information about the asteroid which can be applied to obtain the related parameters. The periodic variation of brightness is mainly due to the variation of the shape as the asteroid spins around its axis. We assume that the shape of asteroid is a triaxial ellipsoid with three semi-axis $a \geq b \geq c > 0$, which spins in the period P expressed in hours around its shortest axis whose spherical coordinate is denoted as (λ, β) in the J2000 ecliptic frame system. As the convention the brightness data recorded in lightcurves is reduced to unit distances of between the asteroid and the sun, the earth respectively and corrected according to the light-time (Durech et al., 2010). So we suppose lightcurves is processed in this way before applying our method.

2.1 The Scattering Law

The scattering behavior is an inevitable problem in the asteroid model. Lumme & Bowell (1981a,b) considered several physical parameters, such as the single-scattering albedo Ω_0 , the asymmetry factor g , the volume density of the surface material D , the roughness of the surface ρ etc. At last a sophisticated scattering model was built to simulate the reflection behavior of the light from Sun. Hapke (1984) took into account the opposition effect and the shadow in the particles of the surface. These scattering models can express the physical characteristics of the light reflection in a rational manner, but they are not efficient in reality due to the uncertain physical parameters. Kaasalainen et al. (2005) made a photometry research about an artificial asteroid in the laboratory experiments and confirms that the shape variation is the main cause for the variation of brightness, not the scattering law. Furthermore, they found that it is hard to distinguish the difference between the scattering law and the random error. In order to acquire the shape model in an efficient way, a simple scattering law is needed. Kaasalainen et al. (2001) presented an convenient method to simulate the scattering behavior by merging both the single scattering factor S_{LS} (Lommel-Seeliger) and the multiple scattering factor S_L (Lambert) in a linear combination. The scattering law can be expressed in

$$S(\mu, \mu_0, \alpha) = f(\alpha) \left(\frac{\mu\mu_0}{\mu + \mu_0} + \gamma\mu\mu_0 \right), \quad (1)$$

where the μ, μ_0 are defined as follows under the definition of $\eta(\theta, \phi)$ as the outward unit normal vector of the surface and ω, ω_0 as the directions to the earth and the sun observed from the asteroid respectively,

$$\mu = \tilde{\eta} \cdot \omega, \mu_0 = \tilde{\eta} \cdot \omega_0,$$

The phase function $f(\alpha)$ is a fitted function in the three-parameter form

$$f(\alpha) = A_0 \exp\left(-\frac{\alpha}{D}\right) + k\alpha + 1.$$

where A_0 and D are the amplitude and scale length of the opposition effect and k is the overall slope of the phase curve. The above scattering law with four parameters adopted in this article can perform efficiently in the shape inverse problem and simulate the opposition effect rationally.

2.2 The Photometric Integration

In order to reconstruct the shape model of asteroids, the synthetic brightness must be described in the direct problem. As mentioned above, the scattering law with four parameters can be adopted herein to generate the photometric brightness as a surface integral

$$L(\omega, \omega_0) = \iint_{E_+} S(\mu, \mu_0, \alpha) d\sigma \quad (2)$$

where E_+ is the part of the asteroid shape which is both illuminated by the sun and visible from the earth, i.e. $\mu, \mu_0 > 0$. As assuming that the shape model of asteroids is tri-axial ellipsoid, the integral (2) can be calculated numerically by the traditional triangulation, tiling the approximately equal triangular facets on the surface, which is a linear algorithm as the number of tessellated facets. In Fig 2 it is shown that an error level of 10^{-4} needs more than 10^4 triangular facets tessellated on the surface of the ellipsoid.

Lebedev & Laikov (1999) presented a fast method to calculate the surface integral

on the unit sphere S by tiling the triangular facets not equally. Kaasalainen et al. (2012) applied this technic into their method and confirmed the lebedev quadrature is efficient in the surface integration. The different distributions of triangular facets of the traditional triangularization and lebedev quadrature are shown in Fig 1.

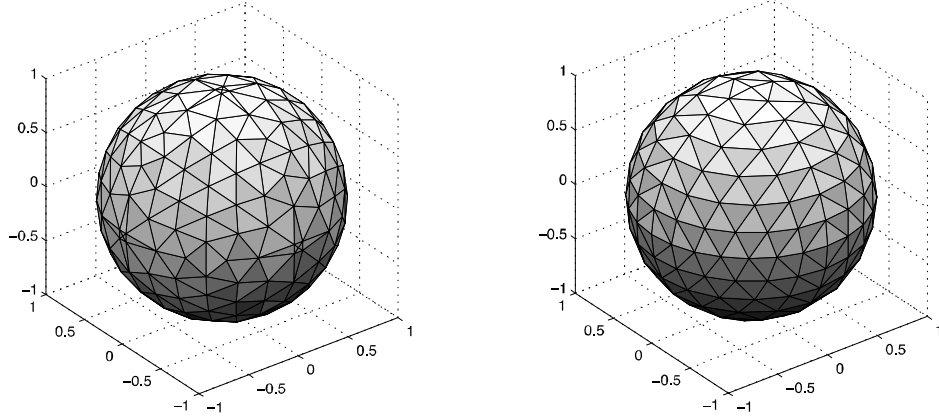


Figure 1. The comparison of two different tessellation methods (Left: Triangulation Right: Lebedev)

Due to that the lebedev quadrature is based on the unit sphere, in our method a curvature function from the surface of ellipsoid E to the unit sphere S is built with the format.

$$G(\theta, \varphi) = \frac{\left| \frac{\partial r}{\partial \theta} \times \frac{\partial r}{\partial \varphi} \right|}{\sin \theta}, r(\theta, \varphi) \in E.$$

With the curvature function $G(\theta, \varphi)$ the brightness integral (2) can be transformed to the surface integral on the unit sphere S ,

$$L(\omega, \omega_0) = \iint_{S_+} S(\mu, \mu_0, \alpha) G(\theta, \varphi) d\sigma \quad (3)$$

where S_+ is the similar part of unit sphere with $\mu, \mu_0 > 0$.

The curvature function under the standard parametrization of the ellipsoidal surface E

$$x_1 = a \sin \theta \cos \varphi, x_2 = b \sin \theta \sin \varphi, x_3 = c \cos \theta$$

has the form

$$G(\theta, \varphi) = abc \sqrt{\left(\frac{\sin \theta \cos \varphi}{a} \right)^2 + \left(\frac{\sin \theta \sin \varphi}{b} \right)^2 + \left(\frac{\cos \theta}{c} \right)^2}$$

while Kaasalainen & Lamberg (1992b) also presented the other curvature function with the form

$$G(\theta, \varphi) = \left(\frac{abc}{(a \sin \theta \cos \varphi)^2 + (b \sin \theta \sin \varphi)^2 + (c \cos \theta)^2} \right)^2$$

under the definition of (θ, φ) denoting the spherical coordinates of the normal vectors of the ellipsoidal surface.

Both of two curvature functions can perform well in computing the brightness

integral (2). But the first one mentioned and adopted in our method is more efficient for the extreme situations, such as the ellipsoid model with a large difference between its three semi axes. The ‘Dog-Bone’ shaped asteroid (216) Kleopatra has been found that its shape is close to an elongated ellipsoid (Descamps et al., 2011). Fig 2 shows the comparison of our curvature function(‘*’) and Kaasalainen’s curvature function(‘o’) to compute the surface area of ellipsoids with different semi axes with the following formula easily letting the scattering function $S(\mu, \mu_0, \alpha) = 1$ in the integral (2).

Apparently our curvature can obtain lower error lever than Kaasalainen’s curvature, especially in the case of elongated ellipsoids. Besides, the difference between the triangulation(‘◊’) and lebedev quadrature(‘*’ or ‘o’) is also compared in Fig 2. The dominant lebedev quadrature can guarantee the efficiency of our fast method.

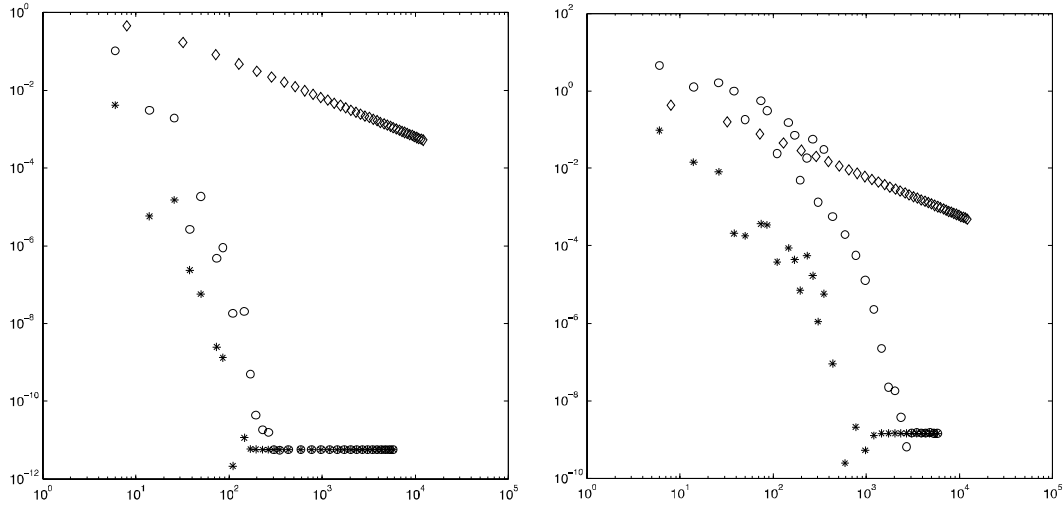


Figure. 2 The comparison of Triangulation(‘◊’) and Lebedev Quadratures with our Curvature(‘*’) and Kaasalainen’s Curvature(‘o’) respectively for computing the surface area of ellipsoids with various semi axes (Left: $a=8, b=7, c=6$ Right: $a=10, b=2, c=1.5$)

2.3 The Inverse Problem

With the definitions of both the scattering function and the brightness integration the inverse problem of the shape model of asteroids can be illustrated totally as follows.

Assuming that all lightcurves in this article are formatted in the same way of DAMIT(Durech et al., 2010), the relative brightness (L) with respect to a Julian Day (t) and the positions of the earth and sun (ω, ω_0) in ecliptic asteroid-centric coordinate system can be obtained directly from lightcurves.

According to the aforementioned brightness integration, all required parameters are three semi axes (a, b, c), the spherical coordinate (λ, β) of the spin axis in ecliptic system, the period (P), the four parameters (A_0, D, k, γ) of the scattering function and the initial phase angle (Φ_0) at the beginning epoch (t_0). So there are 11 parameters in all as t_0 is generally set to be the first Julian date of all lightcurves.

The observed brightness will vary periodically as the rotation of the asteroid around its spin axis, which seems that the sun and earth spin around the stationary asteroid. Assuming the asteroid coordinate system is the Cartesian frame with the spin axis as z-axis and the long semi-axis as x-axis, the origins of ecliptic and asteroid coordinate

system are located at the same point of the center of the asteroid. Denoting $\tilde{\omega}, \tilde{\omega}_0$ as the coordinate of the earth and sun in the asteroid coordinate system, the transformation between ecliptic system and asteroid system can be given as

$$\tilde{\omega} = R_3(\Phi)R_2(\beta)R_3(\lambda)\omega, \quad \tilde{\omega}_0 = R_3(\Phi)R_2(\beta)R_3(\lambda)\omega_0$$

where R_2, R_3 are the rotation matrices rotated as the y and z axis respectively with the forms

$$R_2(\theta) = \begin{pmatrix} \cos\theta & 0 & -\sin\theta \\ 0 & 1 & 0 \\ \sin\theta & 0 & \cos\theta \end{pmatrix} \quad R_3(\theta) = \begin{pmatrix} \cos\theta & \sin\theta & 0 \\ -\sin\theta & \cos\theta & 0 \\ 0 & 0 & 1 \end{pmatrix}$$

As the asteroid rotates in an angular speed $2\pi/P$, phase angle Φ varies with respect to the epoch t (Julian Day) in the form

$$\Phi = \Phi_0 + (t - t_0) \frac{2\pi}{P}$$

Let (θ, φ) be the discretized points of Lebedev quadrature with the total number of facets N , tessellating on the surface of unit sphere with a corresponding weight w , which can be also treated as the area of small facets. With the normal vector of any small facet of the ellipsoid shape

$$\eta = \left(\frac{\sin\theta \cos\varphi}{a}, \frac{\sin\theta \sin\varphi}{b}, \frac{\cos\theta}{c} \right)$$

the brightness integral (2) can be discretized.

Furthermore, under the definition of normal vector, the curvature function can be simplified in the form

$$G(\theta, \varphi) = abc|\eta|.$$

Finally merging the scattering function $S(\mu, \mu_0, \alpha)$ in the formula the discretized brightness integral will be

$$L(\omega, \omega_0) \approx \sum_{i=1}^N f(\alpha)(\tilde{\omega} \cdot \eta_i)(\tilde{\omega}_0 \cdot \eta_i) \left[\frac{1}{(\tilde{\omega} \cdot \eta_i) + (\tilde{\omega}_0 \cdot \eta_i)} + \frac{\gamma}{|\eta_i|} \right] abc w_i$$

where $(x \cdot y)$ is the inner product of two vectors x, y .

The inverse problem of the ellipsoid model can be described to find the 11 parameters mentioned above to minimize the

$$\chi^2 = \sum_i \left\| \frac{L^{(i)}}{\langle L^{(i)} \rangle} - \frac{\tilde{L}^{(i)}}{\langle \tilde{L}^{(i)} \rangle} \right\|^2$$

where $L(i), \tilde{L}(i)$ denote the brightness vectors of observed data and the synthetic data containing all points in the i-th lightcurve, while $\langle L(i) \rangle$ denotes the mean brightness.

3 Numerical Application

Firstly a simple numerical test for the fast method is present in Fig 3. With the assumption that the shape of the asteroid is an ellipsoid with three semi axes $a = 5$, $b = 4.5$, $c = 4$ and the spin axis coordinate $(220^\circ, 30^\circ)$ in ecliptic system with a spin period $P = 5.5$ hours, we simulated the rotation of asteroid in an observable night about 6 hours to generate the synthetic lightcurve denoted as '*' in Fig 3. The other parameters mentioned are set as $\Phi_0 = 30^\circ$, $\gamma = 0.1$, $A0 = 0.5$, $D = 0.1$, $k = -0.5$. By

applying our fast method to the synthetic lightcurve, the result denoted as the solid line in the left of Fig 3 apparently fits the original lightcurve very well and the best solution is $a = 5.296324$, $b = 4.781588$, $c = 4.247322$, $\lambda = 221.197010$, $\beta = 29.350023$, $P = 5.5010621$ with a $\chi^2 = 0.000024$. Although the fitted result of three axes is not close to the initial value, the ratios of $a/c = 1.246979$, $b/c = 1.125789$ is enough similar to the ones of the initial value, i.e. $a/c = 1.25$, $b/c = 1.125$. Comparison between the initial values and the fitted results confirms the efficiency of the fast method.

In reality the observed brightness commonly is affected by various causes, such as atmosphere and the instruments, which means we can not expect the observed lightcurves are enough accuracy as the previous test data. In the right of Fig 3 we adopt the fast method to the identical lightcurve by adding a 2% Gaussian noise and the fitted lightcurve denoted as the solid line rationally approaches the data points with a $\chi^2 = 0.001186$. The corresponding fitted parameters are $a = 5.536739$, $b = 5.060379$, $c = 4.278168$, $\lambda = 215.259798$, $\beta = 37.575509$, $P = 5.535496$, which is consistent with the initial ones.

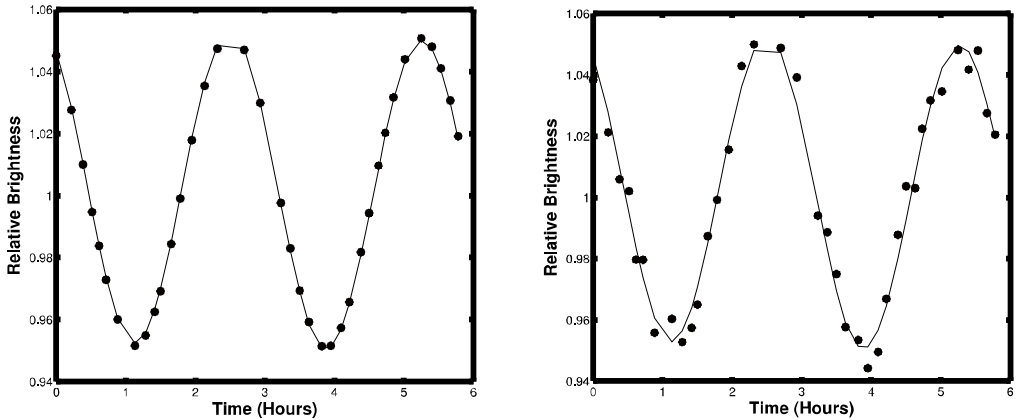


Figure. 3 The comparison of the synthetic lightcurve ('*') and the fitting lightcurve (solid line) assuming the ellipsoidal shape with three semi axes $a = 5, b = 4.5, c = 4$ and the spin axis ($220^\circ, 30^\circ$) with a spin period 5.5 hours(Left: Inverse with the original brightness data Right: Inverse with the corrupted brightness data adding 2% Gaussian Noise)

From the previous test to an ideal ellipsoidal asteroid some important experiences are obtained to guild the inversion for real asteroids. As the shape of (3)Juno is not irregular and close to an ellipsoid overall, we take it for example to make the illustration how to apply the fast method to get the shape model of a real asteroid step by step. Generally the variation of the position of both the earth and the sun in one observed lightcurve is very small for most of asteroids resulting in the small variation of the solar phase angle α . Consequently the solar phase function $f(\alpha)$ in scattering function can be neglected to search the required parameters in an efficient way. Due to the total 11 parameters in the fast method only few lightcurves observed in a good accuracy can deduce the fitted result. Here in the following inversion about (3)Juno we select two lightcurves with 88 points observed on the days of April 19th and 20th in 1985 (Birch & Taylor, 1989).

3.1 Searching Spin Period

The spin period is the first one parameter obtained in the fast method. As the

adopted optimal method is a local optimal algorithm, the method will search the best fitted result with various initial test values. Fortunately the period of most of asteroids is about several hours. We select the initial period values varying from 5 to 10 with a small increment $\Delta P = 0.02$ and the distribution of the fitted period by the fast method is shown in Fig 4. The best solution with a lowest $\chi^2 = 0.0093$ is the period $P = 7.1983$ where the dash line lies.

In the fast method the Lebedev quadrature is employed for the integration computation. The facets number N is taken into account to adjust the accuracy and the computing cost. In the experiments for a rough search $N = 230$ is a good choice with a very fast speed and $N = 350$ can be used to search a more accurate solution. Due to the Gaussian noise in lightcurves and the simple shape model it is no need to adopt a large facets number in the quadrature.

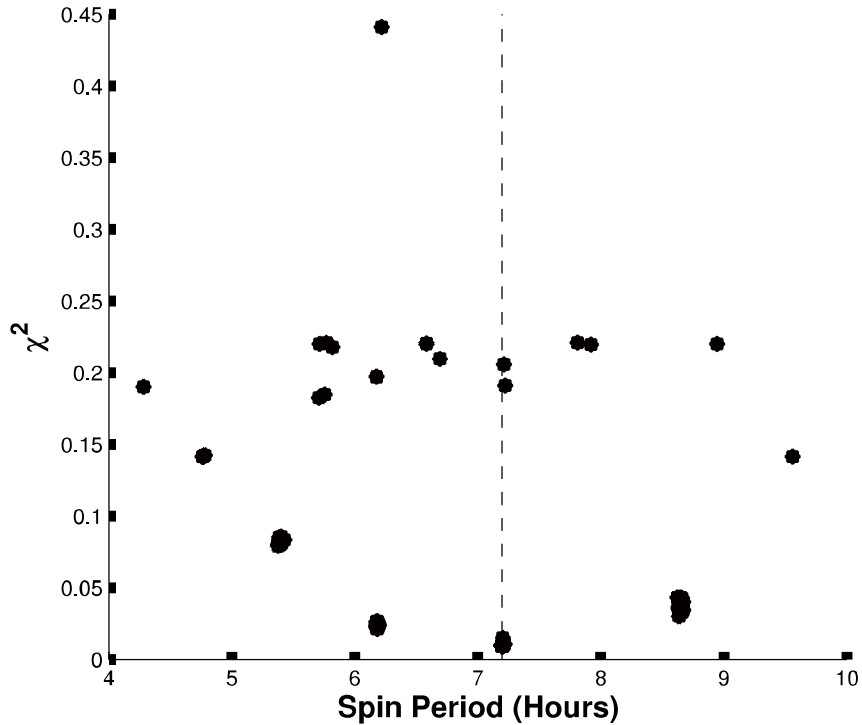


Figure. 4 Distribution of the fitted period with various initial period values from 5 to 10 ($\Delta P = 0.02$)

3.2 Searching Spinning Axis

After getting the fitted period the spin axis can be searched in the same way by fixing the period and the Φ_0 . A mesh-grid discretizing the λ on $[0^\circ, 360^\circ]$ and the β on $[0^\circ, 180^\circ]$ respectively with an increment about 10° , can be used as the initial test values of pole orientation (λ, β) in the fast method. The distribution of fitted pole orientation is show in Fig 5. It should be noted that the polar angle β in the fast method can be simply transformed to latitude $90^\circ - \beta$, which is more common in astronomy and geography fields. There are two best fitted longitudes(λ) located near 100° and 275° shown in Fig 5. Nevertheless the latitude is not concentrating on some special values like the longitude, but the three possible values with three smallest χ^2 are located near -30° and 20° . Furthermore test can be done for a more accuracy latitude to confirm that the 20° is the best choice.

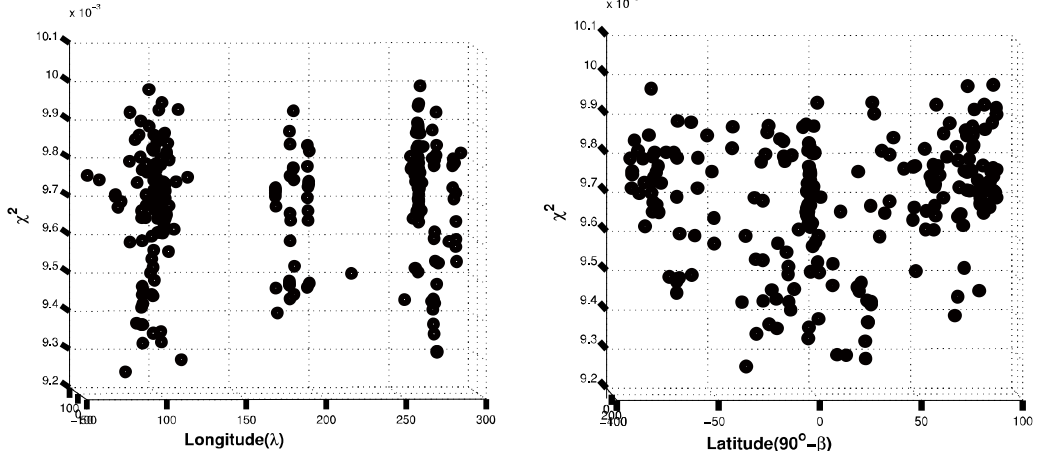


Figure.5 Distribution of the fitted pole orientation with various initial values discretizing in $[0^\circ, 360^\circ] \times [0^\circ, 180^\circ]$ (Left: Longitude of spinning axis: λ Right: Latitude of spinning axis: $90^\circ - \beta$)

3.3 Computing Ellipsoid Shape Model

At last the fast method can be adopted again with a higher accuracy of facets number $N = 350$ to search the best fitted semi axes with the initial other obtained parameters, such as the period $P = 7.1983$, orientation of pole $\lambda = 100^\circ$ or 275° and $\beta = 70^\circ$. Not only the semi axes will be found, but the period and pole orientation will also be refined ultimately. The best fitted parameter set is $a = 1.280042$, $b = 1.021712$, $c = 0.977137$, $\lambda = 275.3713^\circ$, $\beta = 78.4534^\circ$, $P = 7.199157$, $\Phi_0 = -50.21^\circ$, $\gamma = 0.3217$ with a $\chi^2 = 0.009230$, which is consistent with the result of $a/c = 1.3698$, $b/c = 1.0411$, $\lambda = 282^\circ$, $\beta = -21^\circ$, $P = 7.2055$ deduced by Cellino et al. (2009). The two fitted lightcurves denoted by the solid line are shown in Fig 6 to compare with the observed lightcurves denoted as '*'.

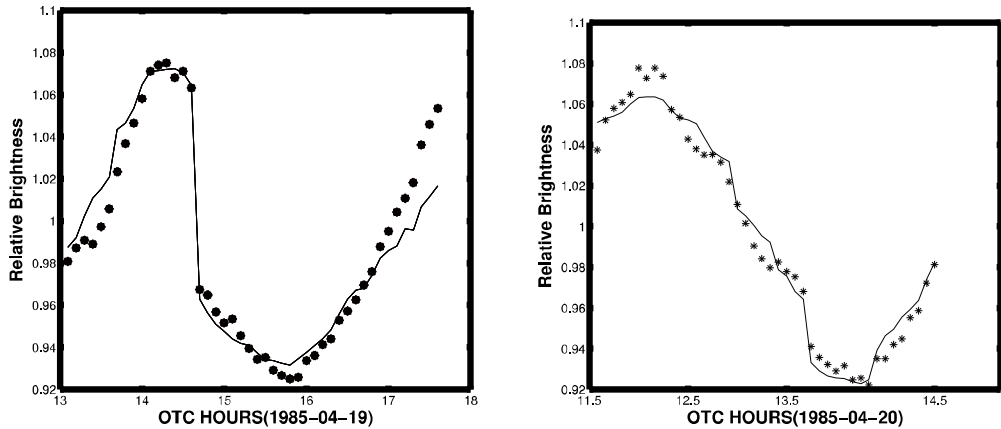


Figure. 6 Fitted Lightcurves(solid line) and observed lightcurves('*)' (Left: Lightcurve observed in 1985-04-19 Right: Lightcurve observed in 1985-04-20)

4 Conclusions

We have described a fast method to obtain the physical parameters and the shape models of asteroids basing on the ellipsoidal shape. This method adopted the Lebedev quadrature to discretize the surface integral on the unit sphere, which can decrease the computational cost largely with a high accuracy. In the section of numerical applications we take the asteroid (3) juno for example to show how to reconstruct the

shape model of asteroids step by step and the encouraging numerical results are consistent with those published ones. In addition now that this method can compute the period and the orientation of the spin axis in an efficient way, we can rely on its result to refine the shape of asteroids, such as adopting Kaasalainen's method.

Acknowledgements

This work is funded by the grant No. 019/2010/A2 from Science and Technology Development Fund, MSAR.

References

- Birch, P., & Taylor, R. 1989, Astron. Astrophys. Suppl. Ser., 81, 409
- Cellino, A., Hestroffer, D., Tanga, P., Mottola, S., & Dell'Oro, A. 2009, A&A, 506, 935
- Cellino, A., Zappalà V., & Farinella, P. 1989, Icarus, 78, 298
- Descamps, P., Marchis, F., Berthier, J., et al. 2011, Icarus, 211, 1022
- Hapke, B. 1984, Icarus, 59, 41
- Jordi, C., Gebran, M., Carrasco, J. M., et al. 2010, A&A, 523, 1
- Kaasalainen, M., & Lamberg, L. 1992a, A&A, 259, 318
- Kaasalainen, M., & Lamberg, L. 1992b, A&A, 259, 333
- Kaasalainen, M., Lu, X., & Vänttinen, A. 2012, A&A, 539
- Kaasalainen, M., Mottola, S., & Fulchignoni, M. 2002, Asteroids III, 139–150, Space Science Series(Univ. of Arizona Press)
- Kaasalainen, M., Torppa, J., & Muinonen, K. 2001, Icarus, 153, 37
- Kaasalainen, S., Kaasalainen, M., & Piironen, J. 2005, A&A, 440, 1177
- Karttunen, H. 1989, A&A, 208, 314
- Karttunen, H., & Bowell, E. 1989, A&A, 208, 320
- Lebedev, V., & Laikov, D. 1999, Doklady Mathematics, 59, 477
- Lumme, K., & Bowell, E. 1981a, Astron. J, 86, 1694
- Lumme, K., & Bowell, E. 1981b, Astron. J, 86, 1705
- Lumme, K., Karttunen, H., & Bowell, E. 1990, A&A, 229, 228
- Marquardt, D. 1963, J. Soc. Indust. Appl. Math., 11, 431
- Press, W. H., Flannery, B. P., Teukolsky, S. A., & Vetterling, W. T. 1992, Numerical recipes: the art of scientific computing; 2nd ed. (Cambridge: Cambridge Univ. Press)
- Rubincam, P. Icarus, 2000, 148, 2
- Russell, H. 1906, Astron. J, 24, 1
- Ďurech,J.,Sidorin,V.,&Kaasalainen,M.2010,A&A,513,46
- Ďurech,J.,Vokrouhlický,D.,Kaasalainen,M.,etal.2008,A&A,488,345

The shape inversion of asteroids and error estimates of spin parameters in Yunnan Observatory

Xiaobin Wang

*Yunnan Observatory, CAS
P.O.Box 110, Kunming, Yunnan Province China
wangxb@ynao.ac.cn*

Abstract — Asteroids are thought to be the remnants of planetesimals in the solar system. The physical parameters can provide important constrains on the formation and evolution of the entire Solar System as well as the individual small bodies themselves.

Using an 1.0m and a 2.4m optical telescope of Yunnan Observatory, some physical studies of asteroids were done. Here, we'll present the shape and spin parameters of the two C-type main belt asteroid (171) Ophelia and (360) Carlova which are obtained by using a convex inverse method. We also estimated uncertainties of spin parameters using the virtual photometric Monte Carlo method.

1. Introduction

Yunnan observatory is one of the major astronomical observatories in China, consists of three sites: Kunming, Lijiang and Fuxian lake (see the Figure 1). an 1.0m telescope in Kunming site and a 2.4m telescope in Lijiang site are often used in the asteroids' study. the low latitude (25° North) of the two telescopes makes for the observation for the objects in the solar system.

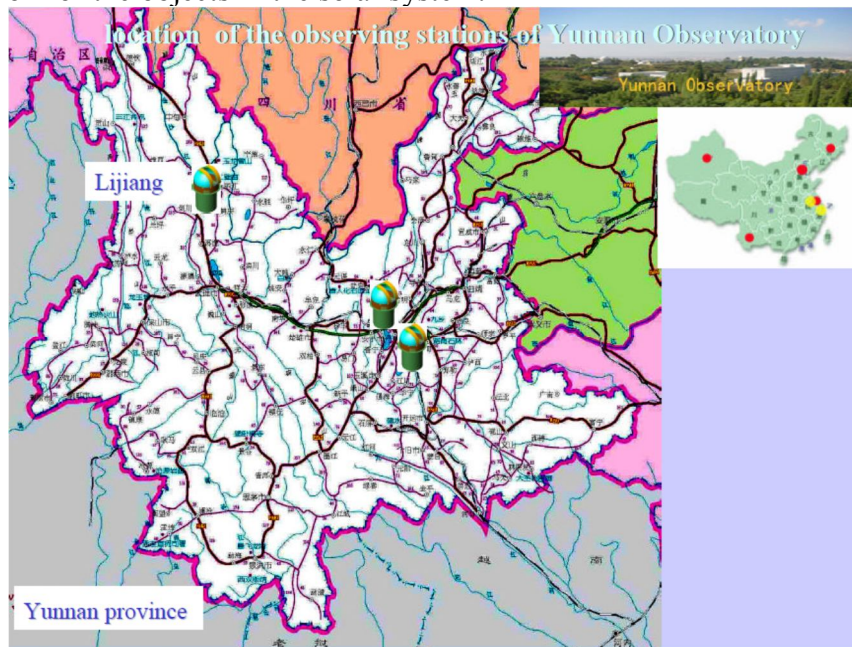


Figure 1. The location of three sites of Yunnan Observatory, CAS.

The 1.0 m RCC optical telescope in Kunming site has a 2k*2K CCD detector in Cassegrain focus and a spectral system installed in the Coude focus. The 2.4 m robotic telescope in Lijiang site has three instruments: a 1K CCD detector, YFOSC (Yunnan Faint Object Spectrograph & Camera) and LiJET (Li jiang Exoplanet Tracker). The left picture of Figure 2 is the dome of the 1.0 m telescope, and the right one is the 2.4 m telescope. The coordinates of two telescopes are listed in Table 1.

Table 1. The coordinates of two optical telescopes.

| Telescope | 1.0m | 2.4m |
|--------------|-------------|-------------|
| Located Site | Kunming | Lijiang |
| Coordinates | | |
| Longitude: | 102°51'24"E | 100°01'51"E |
| Latitude: | 25°01'45"N | 26°42'32"N |
| Altitude: | 1948.5m | 3193 m |

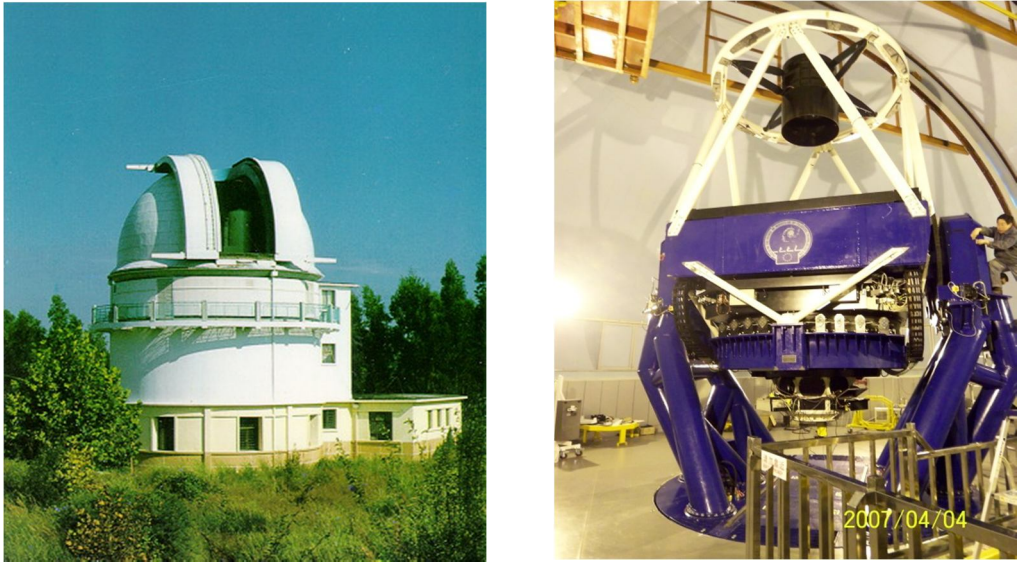


Figure 2. Left: The 1.0 m telescope in Kunming site; Right: The 2.4m telescope in Lijiang site.

Most of asteroids have a shape of aspherical, or even irregular, the observed brightness of asteroid will vary due to the rotation. Therefore the rotation period can be inferred from the brightness variation (or says light-curve). In the early time, the tri-axial ellipsoid model was often used to descript the shape of asteroids. Based on the assumption of a tri-axial ellipsoid shape, the spin orientation of asteroid was inferred from the light-curves obtained at different apparitions. For the asteroid of rubble-pile structure, the tri-axial ellipsoid model can represent the shape reasonable. While for the asteroids of irregular shape, the assumption of tri-axial ellipsoid model may introduce model errors in the determination of pole due to the large deviation of the model shape from its real shape. That is the main reason for dispersion in pole determination. Fortunately, a remedy was offered by numerous researchers (Russell (1906), Muinonen (1988), Muinonen & Lagerros (1988), Cellino et al. (1989), Karttunen & Bowell (1989), Kaasalainen et al. (1992a), Kaasalainen et al. (1992b), Kaasalainen & Torppa (2001a), and Kaasalainen et al. (2001b)).

Now, several inversion methods are developed to determine the shape and spin parameters of asteroids, e.g., the convex inversion method (Kaasalainen & Torppa(2001a) and Kaasalainen et al. (2001b)). The convex inversion method has

been applied successfully in the shape determination for more than one hundred asteroids in recent years.

Recent studies on the shape determination (e.g., Kaasalainen et al.(2002a), Torppa et al. (2003), Kaasalainen et al. (2004), Durech et al. (2009)) have demonstrated that the convex inversion method can give reliable globe shape and accurate spin parameters for main-belt asteroids (MBAs), near-Earth asteroids (NEAs), and Trojan asteroids from a varying combination of dense and sparse photometric data. However, error estimation for the convex inversion solution still constitutes a challenge. Kaasalainen et al. (2001b) and Torppa et al. (2003) estimated the errors for the pole orientation by the longitude and latitude distributions generated by varying the initial values of parameters of the scattering model. They derived steep distributions with a dispersion of about 2 degree, even though such distributions can be considered unrealistic. Hanus et al. (2011) also estimated uncertainties of pole and spin-period determinations. Hanus et al. (2011) gave a typical uncertainty value of ± 10 degree for pole by investigating the pole distribution derived from what they called “mock” objects. For spin period, Both of above two works gave an uncertainty of $0.01 \sim 0.1$ times the ‘basic resolution interval’ (see the definition in Kaasalainen et al. (2001b)). Here, a novel virtual photometric Monte Carlo method (Muinonen et al. (2012)) will be applied to estimate the uncertainties of pole and spin period of two asteroid (171) Ophelia and (360) Carlova.

2. The shape inversion of asteroids: (171) Ophelia and (360) Carlova

(171) Ophelia is one of core members of the Themis family, taken as a candidate of binary asteroid for the eclipse features in the lightcurve. In Themis family, one binary system (90) Antiope and one multiple system (379) Huenna have been confirmed till now. We observed (171) Ophelia for four nights using 1m telescope in Kunming. The photometric data were gathered by a 1K CCD camera through a Kron-cousins R filter. Additionally, another 35 light curves were collected from the database – Asteroids and Comets Rotation Curves, CdR⁸. As a whole, 39 unpublished light curves of (171) Ophelia are used in the analysis of its shape and spin parameters.

(360) Carlova is a C-type main-belt asteroid with a diameter of 138 km. We observed (360) Carlova for nine nights using 1m telescope of Yunnan Observatory in 2011 and 2012. The photometric data were gathered by a $2k \times 2k$ pixels Andor DW436 CCD. 9 lightcurves were obtained through R-filter or Clear filter depending on the weather conditions. Another 15 published lightcurves between 1977 and 2000 are also involved in the determination of the shape and spin parameters.

The aspect data for all photometric data of (171) Ophelia and (360) Carlova involved are listed in Table 2.

Table 2. Observational aspect data of (171) Ophelia and (360) Carlova

| UTC date | r | Δ | Phase | Ecliptic coordinates | Filter | Note |
|---------------|-------|----------|-------|----------------------|--------|---------------|
| | AU | AU | Deg. | in J2000.0 code | | |
| (171) Ophelia | | | | | | |
| 1977 01 16.30 | 2.835 | 1.858 | 2.86 | (121.717, 0.907) | V | Tedesco(1979) |
| 2003 11 25.63 | 3.210 | 2.256 | 5.37 | (50.693, -1.948) | R | Xiaobin Wang |
| 2003 11 30.67 | 3.204 | 2.277 | 7.09 | (51.541, -1.923) | R | Xiaobin Wang |

⁸ http://obswww.unige.ch/~behrend/page_cou.html

| | | | | | | |
|---------------|-------|-------|-------|-------------------|-------|-----------------------|
| 2003 12 01.57 | 3.203 | 2.281 | 7.39 | (51.693, -1.919) | R | Xiaobin Wang |
| 2003 12 02.63 | 3.202 | 2.286 | 7.74 | (51.872, -1.914) | R | Xiaobin Wang |
| 2005 03 17.94 | 2.739 | 1.944 | 14.92 | (147.223, 1.850) | Clear | Rui Goncalves |
| 2005 04 07.89 | 2.735 | 2.163 | 19.47 | (152.064, 1.991) | Clear | Rui Goncalves |
| 2005 04 08.88 | 2.734 | 2.175 | 19.62 | (152.294, 1.997) | Clear | Rui Goncalves |
| 2005 04 22.90 | 2.733 | 2.347 | 21.12 | (155.540, 2.083) | Clear | Rui Goncalves |
| 2005 04 24.91 | 2.733 | 2.372 | 21.26 | (156.007, 2.095) | Clear | Rui Goncalves |
| 2005 03 16.94 | 2.739 | 1.935 | 14.64 | (146.992, 1.843) | R | Pierre Antonini |
| 2005 03 17.92 | 2.739 | 1.944 | 14.92 | (147.219, 1.850) | R | Pierre Antonini |
| 2005 04 05.91 | 2.735 | 2.140 | 19.16 | (151.606, 1.978) | R | Pierre Antonini |
| 2005 04 12.84 | 2.734 | 2.222 | 20.15 | (153.210, 2.022) | R | Pierre Antonini |
| 2005 04 21.90 | 2.733 | 2.334 | 21.05 | (155.309, 2.077) | R | Pierre Antonini |
| 2005 04 13.83 | 2.734 | 2.234 | 20.27 | (153.439, 2.028) | R | Federico Manzini |
| 2005 04 17.83 | 2.733 | 2.283 | 20.70 | (154.366, 2.053) | R | Federico Manzini |
| 2006 03 09.62 | 2.938 | 2.548 | 19.21 | (226.425, 2.063) | R | Julian Oey |
| 2006 03 12.65 | 2.942 | 2.511 | 18.97 | (227.033, 2.047) | R | Julian Oey |
| 2006 03 26.61 | 2.958 | 2.347 | 17.21 | (229.811, 1.972) | R | Julian Oey |
| 2006 03 27.57 | 2.959 | 2.336 | 17.05 | (230.000, 1.966) | R | Julian Oey |
| 2006 04 01.61 | 2.965 | 2.282 | 16.13 | (230.994, 1.938) | R | Julian Oey |
| 2006 04 05.58 | 2.970 | 2.243 | 15.29 | (231.775, 1.915) | R | Julian Oey |
| 2005 04 20.88 | 2.733 | 2.321 | 20.97 | (155.073, 2.071) | R | Yassine Damerdji |
| 2005 04 21.89 | 2.733 | 2.334 | 21.05 | (155.307, 2.077) | R | Yassine Damerdji |
| 2005 05 01.87 | 2.732 | 2.462 | 21.57 | (157.621, 2.135) | R | Alain K. & Raoul B. |
| 2006 04 29.11 | 2.999 | 2.063 | 8.60 | (236.348, 1.776) | V | Arnand L. & Giller G. |
| 2006 04 28.07 | 2.997 | 2.069 | 8.96 | (236.146, 1.782) | Clear | Rui Goncalves |
| 2006 04 29.06 | 2.999 | 2.064 | 8.62 | (236.338, 1.776) | Clear | Rui Goncalves |
| 2006 04 30.03 | 3.000 | 2.059 | 8.29 | (236.525, 1.770) | Clear | Rui Goncalves |
| 2006 05 01.07 | 3.001 | 2.054 | 7.93 | (236.723, 1.763) | Clear | Rui Goncalves |
| 2006 05 25.00 | 3.031 | 2.020 | 1.41 | (241.277, 1.612) | R | Rui Goncalves |
| 2006 07 19.89 | 3.102 | 2.496 | 16.86 | (251.560, 1.235) | R | Rui Goncalves |
| 2011 04 09.98 | 2.778 | 1.794 | 4.88 | (191.236, 2.546) | V | Jacques Montier |
| 2011 04 22.94 | 2.787 | 1.860 | 9.79 | (194.134, 2.541) | V | Jacques Montier |
| 2011 04 20.91 | 2.786 | 1.847 | 9.06 | (193.680, 2.543) | B | Charistophe D. |
| 2011 04 21.94 | 2.786 | 1.853 | 9.43 | (193.911, 2.542) | B | Charistophe D. |
| 2011 04 22.92 | 2.787 | 1.860 | 9.78 | (194.129, 2.541) | B | Charistophe D. |
| 2011 04 25.95 | 2.789 | 1.881 | 10.84 | (194.804, 2.539) | V | Charistophe D. |
| 2011 04 26.84 | 2.790 | 1.888 | 11.14 | (195.001, 2.539) | V | Charistophe D. |

| | | | | | | | |
|---------------|-------|-------|-------|---------------------|-------|-------------------|--|
| (360) Carlova | | | | | | | |
| 1979 10 25.24 | 2.613 | 1.735 | 12.61 | (11.352, -9.954) | V | Harris(1983) | |
| 1979 10 26.13 | 2.612 | 1.740 | 12.91 | (11.573, -9.977) | V | Harris(1983) | |
| 1979 10 27.24 | 2.610 | 1.747 | 13.25 | (11.849, -10.006) | V | Harris(1983) | |
| 1979 10 28.27 | 2.609 | 1.754 | 13.58 | (12.107, -10.033) | V | Harris(1983) | |
| 1984 09 21.18 | 2.797 | 1.846 | 8.13 | (344.861, -6.267) | V | Di Martino(1987) | |
| 1984 09 22.21 | 2.795 | 1.850 | 8.50 | (345.079, -6.305) | V | Di Martino(1987) | |
| 1986 01 09.95 | 2.588 | 1.611 | 3.15 | (108.151, -4.949) | V | Dotto(1995) | |
| 1996 01 19.91 | 2.463 | 1.951 | 22.10 | (71.781, -10.265) | R | Michalowski(2000) | |
| 1997 03 03.01 | 3.038 | 2.058 | 3.50 | (165.885, 6.463) | V | Michalowski(2000) | |
| 1997 03 04.01 | 3.040 | 2.059 | 3.35 | (166.067, 6.494) | V | Michalowski(2000) | |
| 1997 03 10.99 | 3.052 | 2.071 | 3.55 | (167.320, 6.706) | Clear | Michalowski(2000) | |
| 1998 04 27.98 | 3.527 | 2.583 | 6.69 | (230.594, 11.597) | Clear | Michalowski(2000) | |
| 1998 04 30.98 | 3.528 | 2.572 | 6.05 | (231.007, 11.586) | Clear | Michalowski(2000) | |
| 1998 05 02.96 | 3.528 | 2.565 | 5.67 | (231.280, 11.578) | Clear | Michalowski(2000) | |
| 2000 11 15.63 | 2.496 | 1.629 | 13.54 | (33.903, -11.570) | R | Wang(2004) | |
| 2011 11 02.82 | 2.522 | 2.091 | 22.45 | (93.097, -7.500) | Clear | Wang Xiaobin | |
| 2011 11 26.81 | 2.547 | 1.840 | 18.30 | (99.334, -6.476) | Clear | Wang Xiaobin | |
| 2011 11 27.85 | 2.548 | 1.830 | 18.04 | (99.601, -6.431) | Clear | Wang Xiaobin | |
| 2011 12 17.73 | 2.572 | 1.683 | 11.62 | (104.646, -5.540) | Clear | Wang Xiaobin | |
| 2011 12 18.77 | 2.573 | 1.677 | 11.22 | (104.906, -5.493) | Clear | Wang Xiaobin | |
| 2012 01 23.78 | 2.622 | 1.662 | 5.90 | (113.745, -3.824) | Clear | Wang Xiaobin | |
| 2012 03 11.59 | 2.696 | 2.135 | 19.68 | (124.902, -1.585) | R | Wang Xiaobin | |
| 2012 03 12.55 | 2.698 | 2.148 | 19.81 | (125.118, -1.540) | R | Wang Xiaobin | |
| 2012 03 17.58 | 2.706 | 2.218 | 20.39 | (126.251, -1.317) | R | Wang Xiaobin | |

The convex inversion method (Source code from the DAMIT database <http://astro.troja.mff.cuni.cz/projects/asteroids3D/web.php>) was applied to determine the spin parameters and shape of the two asteroids. Before the procedure of the shape inversion, the absolute magnitudes and/or relative magnitudes of asteroid are converted into intensities. The absolute magnitude through different filters is transferred into the V band magnitude based on the color index of the asteroid. Then the V band magnitude is converted into the intensities along the Vega's flux in the V band (see equation (1)).

$$L_{obs_v} = 10^{-\frac{M_v}{2.5}} * L_{Vega_v},$$

$$L_{Vega_v} = 3631 \text{ Jy} \quad (1)$$

M_v represents the absolute magnitude in V band. L_{Vega_v} is the flux of Vega in V band (corresponding to the zero point of the visible magnitude system). For the case of relative magnitudes, the relative intensities of asteroids are computed with equation (2).

$$L_{rel} = 10^{\frac{m-\bar{m}}{2.5}} \quad (2)$$

Here, m and \bar{m} represent the individual magnitude and the mean of all magnitudes in each night, respectively.

The convex inversion method finds a shape and spin parameters for an asteroid by minimizing the RMS of model brightness comparing with observed ones.

$$RMS = \sqrt{\frac{\sum_{j=1}^n \|L_{obs}^j - L_{mod}^j\|^2}{n}} \quad (3)$$

L_{obs}^j is the individual observed brightness of an asteroid; L_{mod}^j is the modeled integrated brightness reflected by those visible and illuminated surface area. The modeled brightness of the asteroid is associated with the scatter law of surface, as well as the size of visual cross section for an observer.

$$\begin{aligned} L_{mod} &= \sum_i S(\mu, \mu_0) G(\vartheta_i, \psi_i) \sigma_i \\ S(\mu, \mu_0) &= f(\alpha) \mu \mu_0 \left(\frac{1}{\mu + \mu_0} + c \right) \\ f(\alpha) &= a \exp(-\alpha/d) + k \alpha \\ G(\vartheta_i, \psi_i) &= \exp \sum_{lm} a_{lm} Y_l^m(\vartheta_i, \psi_i) \end{aligned} \quad (4)$$

The $S(\mu, \mu_0)$ represents the scattering law of asteroid's surface, here the combination of the Lommel-seeliger law and the Lambert law with c as the weight factor is used. The μ and μ_0 are the cosine of angles from the i th facet's normal to the line of sight and the source of light. The $G(\vartheta_i, \psi_i)$ represents the Gaussian surface density of asteroid at the normal direction (ϑ_i, ψ_i) , which is represented by a truncated series of spherical harmonics. The $G(\vartheta_i, \psi_i) \sigma_i$ is the facet area on the asteroid surface, and σ_i is the facet area on a triangulated unit sphere.

By the damped least-squares (DLS) method (or called the Levenberg–Marquardt algorithm), the unknown parameters (coefficients of spherical harmonics, spin period, pole orientation and parameters of the scattering law) are solved by minimizing the RMS of model brightness.

With adding another published lightcurves (Tedesco(1979)) to our observations, 40 lightcurves of (171) Ophelia were used to determine the spin parameters and the shape with the convex inversion method. The whole data set spans 32 years, the solar phase angle of asteroid for the data set covers the range of $1^\circ.4$ to 21° .

As a result, a pair of pole solutions ($152^\circ, +36^\circ$) and ($317^\circ, +28^\circ$) in J2000 ecliptic coordinates was found with the RMS of 0.012. The pair of pole's orientations predicted the same spin period of 6.665429 hour. The shapes corresponding to the pair of pole's orientation are the mirror images of each other (see figure 3). Like the characteristic shape of (41) Daphne and (44) Nysa (Kaasalainen et al. (2002b)), the shape of (171) also shows a binary structure. It can be a contact binary or a "compound asteroid" consisting of two components of unequal size.

Parts of lightcurves of (171) Ophelia are presented in the figure 4, the red lines are the modeled lightcurves, and the black crosses are the observed ones.

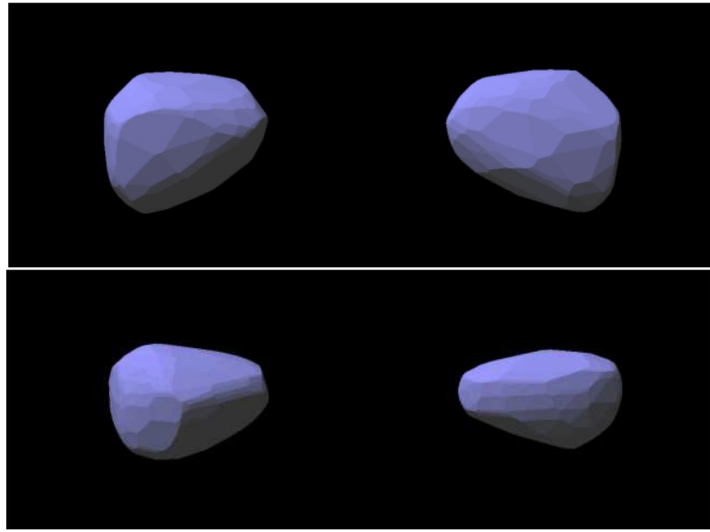


Figure 3. Obtained convex shapes of (171) Ophelia. The upper panel shows the pole-on view and the bottom panel shows the edge-on view. The left shape in each panel is corresponding to the pole of (152°, 36°), and the right one is corresponding to the pole of (317°, 28°).

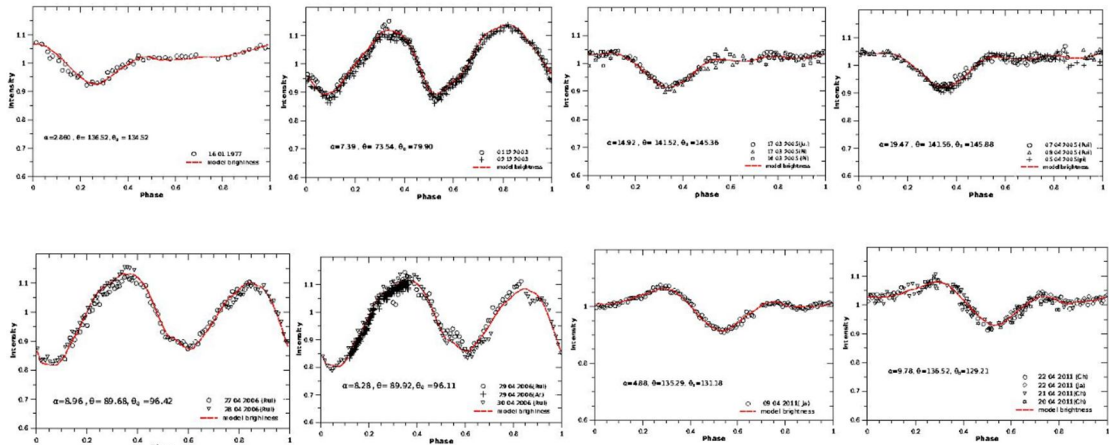


Figure 4. Light curves of (171) Ophelia.

23 lightcurves of (360) Carlova were used for the convex shape inversion. Among those, 9 lightcurves were obtained from the observations in 2011 and 2012, and the rest of them was collected from literatures (Harris & Young (1983), Di Marino et al. (1987), Dotto et al. (1995), Michalowski et al. (2000)). The whole data set spans 34 years (from 1979 to 2012), and the solar phase angle of asteroid corresponding to these lightcurves covers the range of 5° to 22°.

A pair of pole solutions: (105°, 61°) and (338°, 60°) was found for (360) Carlova. The spin periods derived from the both poles solutions were 6.189593 hours. Figure 5 shows the convex shapes of (360) Carlova. The left two are for the pole of (105°, 61°); and the right two are for the pole of (338°, 60°). The upper shapes are the pole-on view, and lower ones are the edge-on view. When comparing two projected shapes of pole-on view (the upper plots of Figure 5), they shows mirror images of each other. The images of the edge-on view for two poles are roughly mirror, except some length diverge along the shortest axis. That is due to large uncertainties in those facets near the pole.

The figure 6 shows the lightcurves of (360) Carlova.

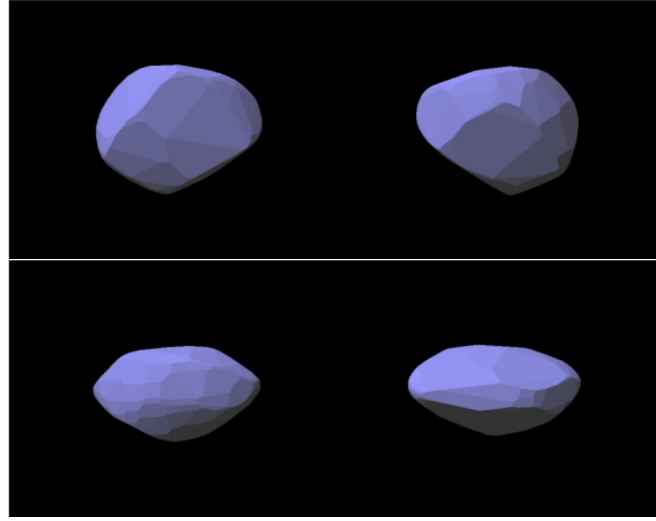


Figure 5. The convex shape of (360) Carlova. The left shapes are the pole for $(105^\circ, 61^\circ)$; the right shapes are the pole for $(338^\circ, 60^\circ)$.

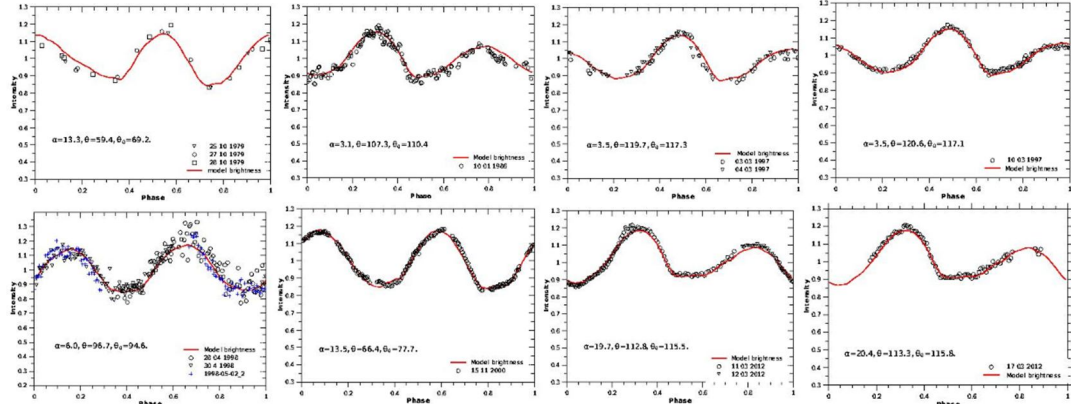


Figure 6. Lightcurves of (360) Carlova.

3. Error estimate for the spin parameters

Although the best way for the error estimate for the convex inversion solution has been in debate, in here, we applied a novel virtual photometric Monte Carlo method developed by Muinonen et al. (2012) to estimate the uncertainties of the pole and spin period. This new method estimates the error for the solution of convex inversion by the distribution of unknown parameters. In detail, the procedure of errors estimate contains the following steps. (1) The virtual photometric data set is generated by adding a Gaussian random noise into individual observed photometric data; (2) The virtual least-squares solution of the convex inversion is computed from the virtual photometric data set. Above two steps are repeated numerous times, the respective virtual least-squares solutions of convex inversion constitute a certain distribution of the unknown parameters.

For (171) Ophelia, 1000 virtual photometric data sets were generated by adding a Gaussian random noise of a standard deviation of 0.05 mag. The respective virtual least-squares solutions of the convex inversion were computed. Figure 7 shows the distributions of spin parameters (period rate and pole orientation) for (171) Ophelia. The upper-left plot shows the distribution of spin period versus the RMS, the upper-right plot is the distribution of pole orientation; the lower plots are the longitude (left) and latitude (right) distributions versus the RMS.

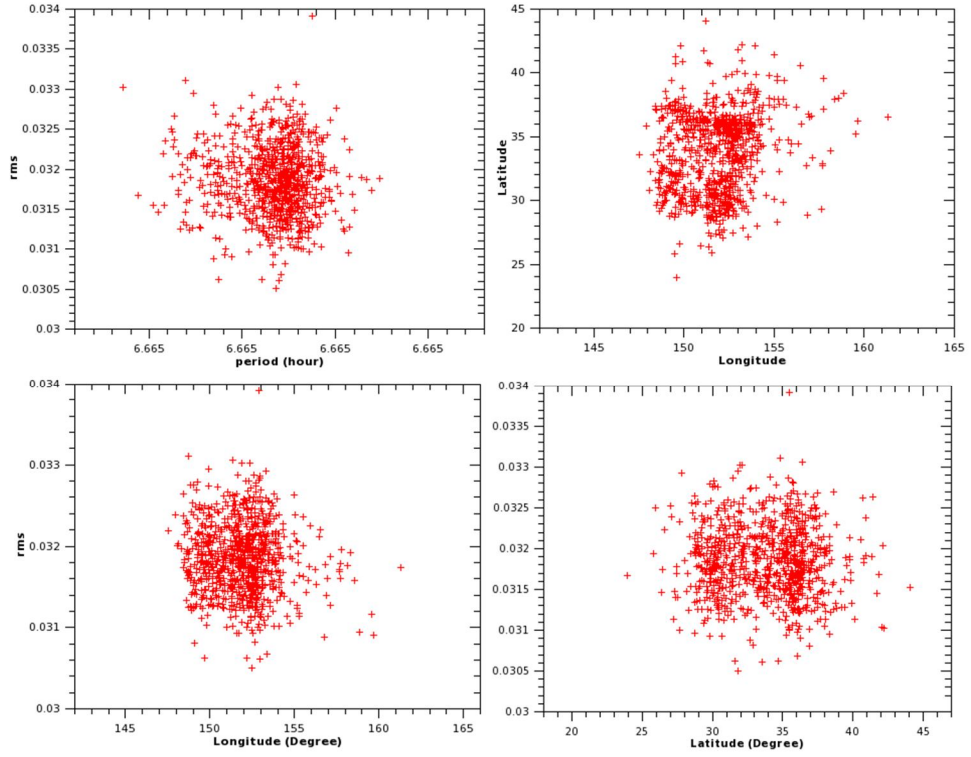


Figure 7. The distributions of the spin parameters of (171) Ophelia.

In the same way, the distributions of spin parameters of (360) Carlova were derived. Figure 8 shows the distributions of spin parameters of (360) Carlova. The upper-left plot shows the distribution of the spin period versus the RMS, the upper-right plot shows the pole distribution, the lower plots are the longitude (left) and latitude (right) distributions versus the RMS.

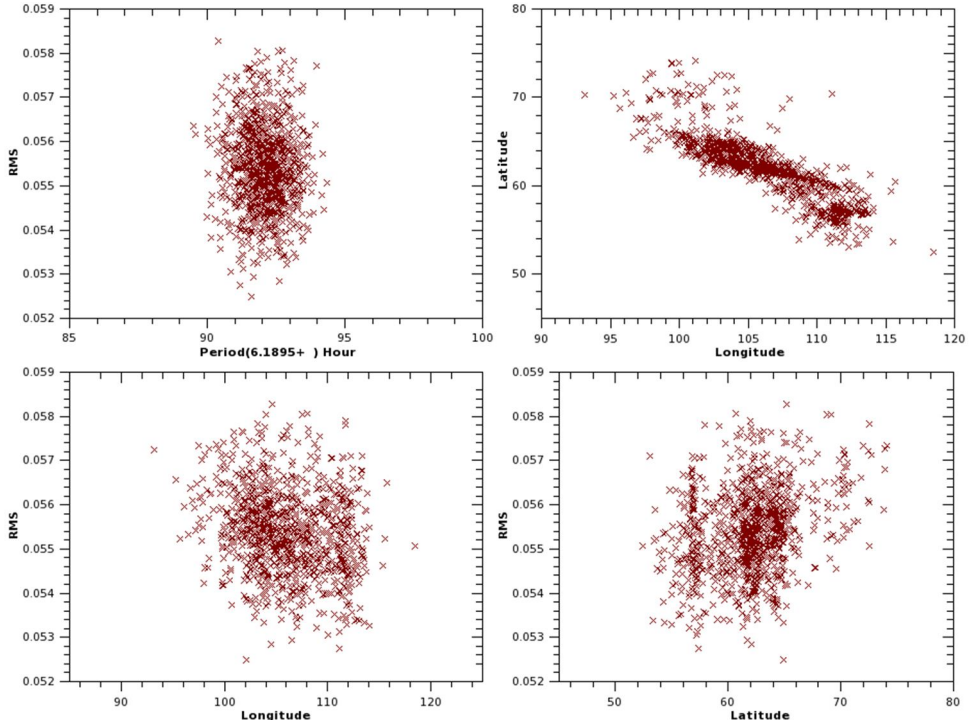


Figure 8. The distributions of the spin parameters of (360) Carlova,

In order to estimate the uncertainties of parameters, we also plotted the histograms for the spin parameters of the two asteroids (see figure 9 and 10). Based on these histograms, the uncertainties of spin period and pole orientation were estimated with statistical methods. For a standard normal distribution, the center value ‘ Xc ’ and the half of width ‘ w ’ of the distribution can be taken as the most likely value and the uncertainty for a parameter. But as the distribution can be an asymmetric, we take the mode value as the most likely value for the unknown parameter and give the $1-\sigma$ limit (the 15.85 and 84.15 percentage bounds) as the uncertainty of parameter.

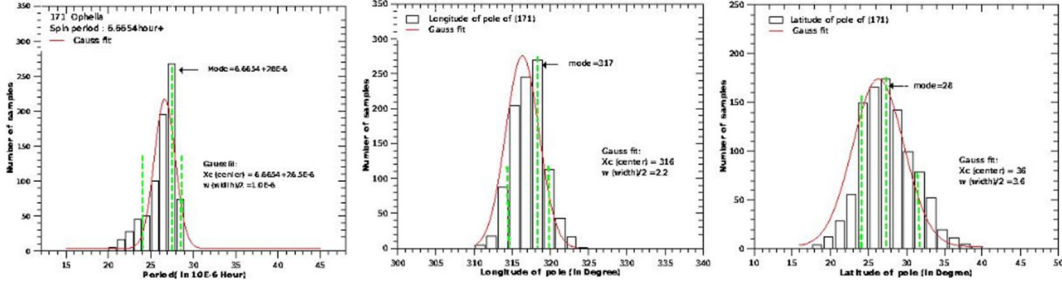


Figure 9. The histograms of spin rate spin parameters of (171) Ophelia. From left to right, they are the distribution of spin rate, longitude and latitude.

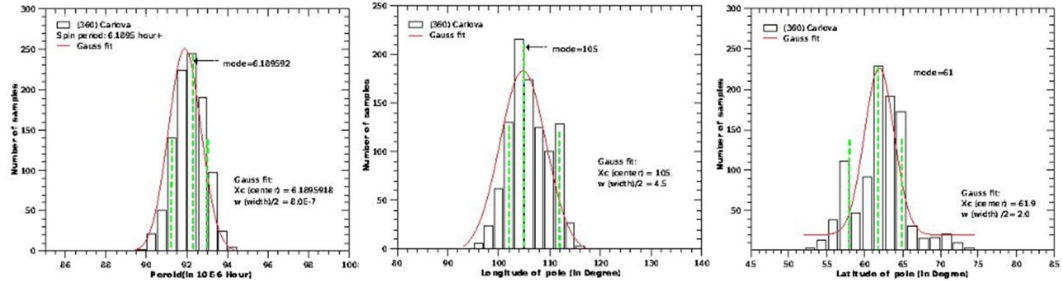


Figure 10. The histogram of spin parameters of (360)Carlova. From left to right, they are the distribution of spin rate, longitude and latitude.

As seen in Figure 9 and 10, the distributions of spin parameters are asymmetric. Therefore we used the $1-\sigma$ limit of distribution for the error estimates. Table 3 lists the estimates of spin parameters for the two asteroids

Table 3. The spin parameters of asteroids (171) Ophelia and (360) Carlova

| (171) Ophelia | Pole | Period |
|---------------|--|--------------------------------|
| | $(152^{+1.3}_{-2.2}, +36^{+0.6}_{-5.8})$ | $6.665429^{+7.7E-7}_{-4.1E-6}$ |
| | $(317^{+2.2}_{-2.1}, +28^{+4.1}_{-2.9})$ | $6.665429^{+3.2E-6}_{-1.5E-6}$ |
| (360)Carlova | | |
| | $(105^{+6.0}_{-2.7}, +61^{+3.7}_{-3.2})$ | $6.189592^{+8.5E-7}_{-6.8E-7}$ |
| | $(338^{+8.1}_{-4.7}, +60^{+4.5}_{-5.2})$ | $6.189592^{+8.6E-7}_{-1.5E-6}$ |

For the virtual shapes derived with the virtual photometric data, we investigated the size distribution of each facet, and found the size distribution of the facets near the equatorial region have a narrow Gaussian distribution, while the distribution of the facets near the pole region have a relatively wide distribution and sometime with some outliers. The wide distributions in the polar region are the reason for the large shape uncertainties of along the shortest axis dimension.

4. Summary

(1) The convex inversion method is used to determine the spin parameters and the shape of two asteroids (171) Ophelia and (360) Carlova. We derived a pair of poles for (171) Ophelia. The spin period corresponding to two poles are the same. The shapes of (171) Ophelia for two poles show a binary structure, like the situations of (41) Daphne and (44) Nysa. For (360) Carlova, we found the best spin period and a pair of poles. The shapes of (360) for the two poles are roughly a triaxial ellipsoid.

(2) A virtual Monte Carlo method is applied to estimate the uncertainties of spin parameters. By this method, we estimate the uncertainties of spin parameters. For the two asteroids, we found an uncertainty of around 5° for pole, and 0.000005 hours for the spin periods. The slight larger uncertainty of pole of (360) Carlova is due to the large scatter of photometric data.

5. Acknowledgements

This work was supported by National natural Sciences foundations of China No.11073051 and No.10933004.

References

- Bessell M.S., Castelli F., & Plez B. 1998, A&A, 333, 231
Collier Cameron A., and 24 colleagues 2006, MNRAS, 373, 799
Cellino A., Zappala V., & Farinella P. 1989, Icarus, 78, 298
Durech J., Kaasalainen M., Warner B. D., Fauerbach M., Marks S. A., Fauvaud S., Fauvaud M., Vugnon J.-M., Pilcher F., Bernasconi L., & Behrend R. 2009, A&A, 493, 291
Russell H. N. 1906, APJ, 24, 1.
Muinonen K. 1988, A&A, 332, 1087
Muinonen K. & Lagerros, J.S.V. 1988, A&A, 333, 753
Muinonen K., Granvika M., Oszkiewicza D., Pieniluomaa T., & Pentikinen H. 2012, Planetary and space science, 73, 15.
Karttunen H. & Bowell E. 1989, A&A, 208, 314
Kaasalainen M., Lamberg L., Lumme K., Bowell E. 1992, A&A 259, 318
Kaasalainen M., Lamberg, L. & Lumme K. 1992, A&A, 259, 333
Kaasalainen M., Torppa J. 2001 Icarus, 153, 24
Kaasalainen M., Torppa J. & Muinonen K. 2001, Icarus, 153, 37
Kaasalainen M., Torppa J. & Piironen J. 2002, Icarus, 159, 369
Kaasalainen M., Torppa J. & Piironen J. 2002, A&A, 383, L19
Kaasalainen M., Pravec P., Krugly N., Åarounov L., Torppa Virtanen J., Kaasalainen S., Erikson A., Nathues A., Urech J. and 12 coauthors 2004, Icarus, 167 178
Hanus, J., urech, J., BroÅ, M., Warner, B. D., Pilcher, F., Stephens, R., Oey, J., Bernasconi, L., Casulli, S., Behrend, R. and 5 coauthors 2011, A&A, 530, 134
Harris A.W., Young J.W. 1983, Icarus, 54, 59
Tedesco, E.F. 1979, Science, vol. 203, 905
Di Martino M., Zappala V., de Campos J. A., Debehogne H., Lagerkvist C.-I. 1987, A&A Suppl. Ser., 67, 95
Dotto E., de Angelis G., di Martino M., Barucci M. A., Fulchignoni M., de Sanctis G., Burchi R. 1995, Icarus, 117, 313
Michałowski et al. 2000, Astron. Astrophys. Suppl. Ser., 146, 471
Torppa J., Kaasalainen M., Michałowski T., Kwiatkowski T., KryszczyÅska A.,

- Denchev P., Kowalski R. 2003, Icarus, 164, 346
- Torppa J., Hentunen V.-P., Paakkonen, P., Kehusmaa P., Muinonen K. 2008, Icarus, 198, 91
- Tamuz O., Mazeh T., & Zucher S. 2005, MNRAS, 356, 1466
- Wang X-b. & Zhang X-l 2004, CAA
- Wang Xiao-bin & Gu Sheng-hong 2010, EM&P, 106, 97

Current Knowledge of Jupiter Trojans – toward the Solar Power Sail mission

Fumi Yoshida

*National Astronomical Observatory of Japan
2-21-1, Osawa, Mitaka, Tokyo 181-8588, JAPAN
fumi.yoshida@nao.ac.jp*

Abstract — JAXA is planning the Solar Power Sail mission heading to Jupiter Trojans (JTs) in 2020s. Main scientific purposes are the dust collection from the orbits of Earth to Jupiter, the dust-free infrared astronomy beyond the main belt, and the exploration of JTJs. The mission targets (the L4 or L5 swarm of JTJs) are not yet fixed.

This paper summarized a current knowledge of JTJs based on the latest JT's database. The following properties of JTJs were described herein: orbital, size, spin rate, and taxonomic distributions, total numbers, dynamical and collisional evolution, families, binary system and density, and space weathering on their surfaces.

1. Introduction

Jupiter Trojans (JTJs) are very interesting group because of their origin and absence of water. About their origin, there are two competing hypotheses: (1) Classical Model: current JTJs are remnants of planetesimals located near Jupiter during the formation of Jupiter. (e.g., Marzari & Scholl 1998a,b), and (2) Nice Model: the present JTJs are captured Trans-Neptunian Objects (TNOs) by Jupiter, which orbits were scattered and intruded inward during the giant planet migration (e.g., Morbidelli, et al., 2005).

The both possible origins suggest that the JTJs must have water, because they formed beyond the snow line at the early stage of the Solar System. However, so far, spectral studies did not find clear evidences of water ice on JT's surfaces. Most scientists strongly believe that JTJs have been hiding some materials related to water under their surfaces. The spacecraft mission may be able to find the water by taking close up images with high resolution, or digging the surface up by a rover.

The JTJs are ideal mission targets. Because no one has visited so far and it's likely that JTJs supply an important key for understanding a stage of planetary formation at the early Solar System. They excite our frontier spirit.

2. The Solar Power Sail mission

2.1 What is the Solar Power Sail ?

A solar sail is a form of spacecraft propulsion using the solar radiation pressure to push large ultrathin membrane. The first idea of solar sail was suggested by Johannes Kepler. He got this idea from cometary tail which extends toward the opposite direction from the Sun. The Solar Power Sail is a combination of the solar sail and ion engine generated by a thin membrane solar cell. This is the Japanese original concept of a form of spacecraft.

The development of the Solar Power Sail needs to overcome the following three

technical challenges: establishing the huge solar sail (~50m, 2000m²), developing the ultra light and large area thin film solar cell, and innovating the ultra high Isp (specific Impulse) electric propulsion system that is able to stand up to the long operation time (5-10 years). The developing history of the Solar Power Sail was summarized in Table 1.

Table 1. Development of Solar Power Sail in Japan

| Date | Development | Sail | Launch |
|---------------|---|--|--|
| 2003. Aug. | Balloon test (B30-71) at 36km alt. - Active deployment of sail (4m) |  |  |
| 2004. Aug. | Sounding rocket (S310-34) at >100km alt. - Active deployment of Sail (10m) - Modeling of sail dynamics |  |  |
| 2006. Sep. | M-V-7 rocket sub-payload (SSSAT) in LEO - Deployment demo of a Small Power Sail (5m) |  |  |
| 2010. May | H-IIA-17 piggy-back (IKAROS) in deep space (This is the first Solar Sail in interplanetary space) - Deployment of sail membrane (20 m) |  |  |
| 2020s | Solar Power Sail mission - Sail membrane (50 m) with ion engines - Sample return from the Jupiter Trojans |  | |

2.2 Mission Scenario and Targets

Technical demonstration of the Solar Power Sail was successful in 2010. Science and technical teams began detailed planning for the mission. The launch was estimated to be in early 2020s. The current mission plan includes flyby of a few JTs, rendezvous with a JT, and sample return from the JTs.

After launching, the spacecraft will swing-by the Earth. It will arrive at the main asteroid belt within 3 years. Then through Jupiter's swing-by, it will reach one of the JT swarms 8.5 years after launch. The sample return will take about 5 years or so to deliver the sample capsule back to the Earth.

The mission targets are not yet fixed. Detailed investigations of physical parameters of known JTs will be carried out with ground-based facilities over the next several years. At the same time, surveys (e.g. Pan-STARRS, Hyper Suprime-Cam (HSC) survey) will increase target candidates in order to broaden the range of flyby targets with different material composition and launch period.

The science team is considering many science cases as follows. During the cruising phase between Earth and JTs, (1) interplanetary dust collection and (2) the dust-free infrared astronomy (look out across the deeper universe with less interplanetary dust) beyond the main asteroid belt. And when the spacecraft arrives at the JT, the following measurements would be done: 3D-shape, albedo and color maps of the entire surface, crater distribution, geological feature, dust flux around the JT,

composition of the surface and/or subsurface and so on.

3. Our current knowledge of Jupiter Trojans

3.1 Size distribution

So far, Jewitt et al. (2000), Yoshida & Nakamura (the Subaru Main Belt Asteroid Survey (SMBAS), 2005, 2008), Szabo et al. (SDSS, 2007) have investigated the size distributions of JTs by optical surveys. The survey by Jewitt et al. is probably the first survey of the size distribution of JTs. They conducted the sky survey using the UH 2.2 m telescope. Although their main purpose was to search for new Kuiper belt objects, they detected 93 L4 JTs on their images. The slopes of cumulative size distribution are 4.5 for H (absolute magnitude) <9.5 and 2.0 for $11 < H < 14$, respectively. They found that the slope of size distribution varies around $H=10$ mag.

The SDSS produced the largest dataset of JTs (Szabo et al. 2007). They observed both L4 and L5 swarms and detected 1187 JTs in total. The SDSS obtained the following three important results. (1) all JTs brighter than $H=12.3$ mag are already discovered and listed in the MPC catalogue, (2) the slopes of size distribution of L4 and L5 groups are not different within the size range of SDSS, (3) significantly more asteroids exist in L4 swarm than in L5 swarm ($N(L4)/N(L5) = 1.6 \pm 0.1$).

So far the deepest survey of JTs is the SMBAS. These survey series have been conducted by Subaru telescope with the wide field camera: Suprime-Cam. Thanks to the large telescope's aperture, many fainter objects were detected. Though the SMBAS is a series of survey for studying sub-km MBAs, it is also able to study JTs. Yoshida & Nakamura (YN in Table 2) investigated the JT's size distribution in the data of SMBAS. They found 51 L4 JTs and 62 L5 JTs. For L4 JTs, the slope of cumulative size distribution varies at $H \sim 16$ mag from 2.4 to 1.3. Meanwhile for L5 JTs, there is no significant sign of the slope's change in the size distribution. They concluded that L4 and L5 have the same size distributions for JTs brighter than $H=16$ mag. However, the slope gets shallower only in L4 swarm for the darker size range ($H > 16$ mag).

Fig.1 shows the cumulative size distribution of JTs that combined all surveys' results. Our current knowledge of size distribution of JTs is as follows.

- (1) all JTs brighter than $H=12.3$ have been discovered.
- (2) the slope of cumulative size distribution changes at $H=10$ in both swarms and at $H=16$ in L4 swarm.
- (3) meanwhile, in L5 group, the slope of 2.1 continues till $H=18$.
- (4) although there are more asteroids in L4 than L5 in the population of larger JTs, if we assume the slopes of cumulative size distributions continue till the smaller JTs, the population ($L4 > L5$) can be reversed. The reverse happens around $D=1\text{km}$.

Since the L4 and L5 populations of large JTs show the same size distribution, they may share the same origin. The difference of the size distribution for smaller JTs ($D < 5\text{km}$) may be caused by collisional evolution in each swarm. The fact that the L4 has robust large collisional families (see section of families of JTs), whereas the collisional families in L5 swarm are ambiguous, seems to suggest that the L4 population has experienced significant collisional evolution than the L5 cloud. Through collision, small collisional fragments might drop from the stable region around the L4 Lagrange point. A simulation study on the collisional and dynamical evolution of L4 JTs by Elia & Brunini (2007) found that the removed JTs from the L4 swarm by collisional evolution are smaller than 5km in size, while most of the large

JTs ($D > 5\text{ km}$) remained stable in the L4 swarm. This supports the shallower slope of the size distribution of small L4 JTAs ($D < 5\text{ km}$).

Table 2. Size distribution of JTAs obtained from different surveys. The data of known Trojans is from the catalogue of Minor Planet Center (MPC) (<http://www.minorplanetcenter.net/iau/lists/JupiterTrojans.html>). The b is an index of power law distribution fitted with the range of H (absolute magnitude). We assumed albedo of 0.04 and 0.07 for calculating diameter (D).

| Source | $b(N > D) \propto D^{-b}$ | H range | D(0.04) | D(0.07) |
|-------------------------|---------------------------|--------------------------|---------------|---------------|
| Known all | 2.10+/-0.03 | 10.0-12.5 | 21-67 | 16-51 |
| Known L4 | 2.14+/-0.02 | 10.0-12.5 | 21-67 | 16-51 |
| Known L5 | 2.05+/-0.05 | 10.0-12.5 | 21-67 | 16-51 |
| Jewitt et al. (2000) | 2.0+/-0.3 4.5+/-0.9 | 11-16 >9.5 | 4.4-40 >84 | 3.2-30 >64 |
| Szabo et al. (2007) | 2.2+/-0.25 | 9-13.5 | 14-107 | 10-81 |
| YN L4 (2008) | 2.4+/-0.1 1.3+/-0.1 | 14.1- 15.7 15.7- 17.9 | 5-10 2-5 | 4-8 1.5-4 |
| YN L5 (2008) | 2.1+/-0.3 | 15.7- 17.9 | 2-5 | 1.5-4 |

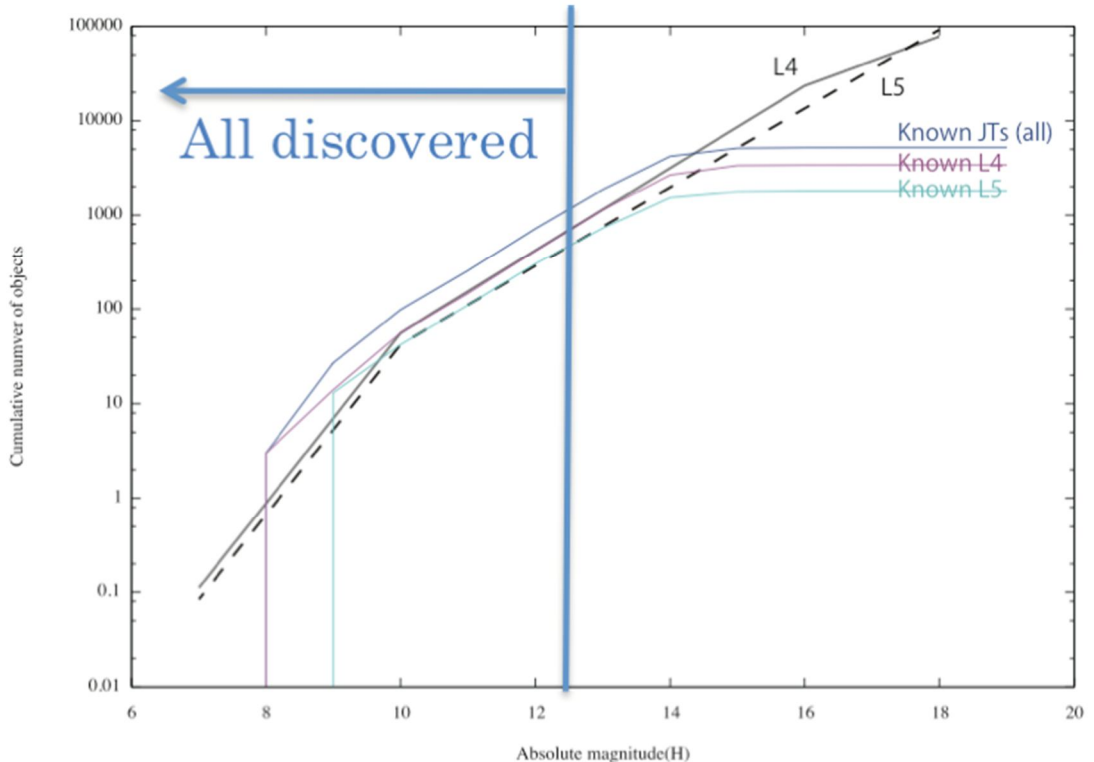


Figure 1. Cumulative size distribution of JTAs that combined MPC catalogue, Jewitte et al (2000), Szabo et al (2007) and Yoshida & Nakamura (2005, 2008) and connected slopes from each survey.

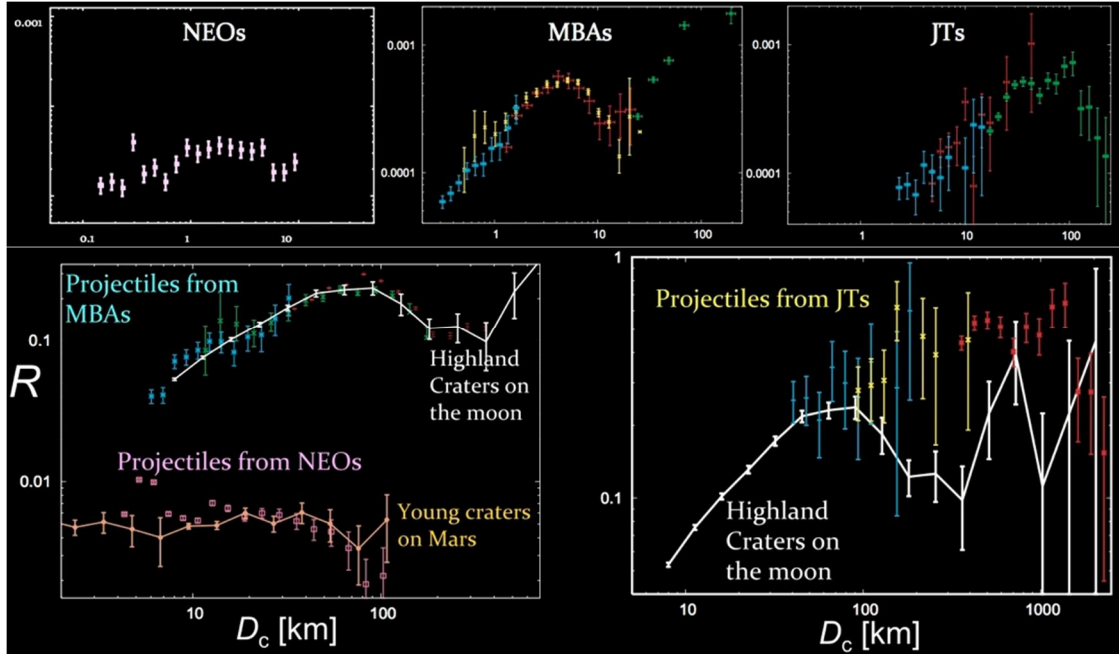


Figure 2. Comparison of the size distributions of NEOs, MBAs and JTAs on the R-plot (upper panels) and comparison of the size distributions of projectiles from NEOs, MBAs, JTAs groups to the Moon, highland craters on the Moon, and young craters on Mars on the R-plot (lower panels). The size of projectiles was converted with scaling law using typical impact velocities (these figures were modified from Ito et al. 2007, Strom et al. 2005a,b).

As shown in Fig.2, we compared the size distribution of JTAs with those of different dynamical groups (NEOs and MBAs) as well as crater size on the moon and Mars. It turned out that the distribution of JTAs is unique and it has different size distribution from those of inner planetary objects.

Fernandez et al. (2009) and Grav et al. (2011) investigated the albedo of the JTAs using Spitzer and WISE data, respectively. Fernandez et al. (2009) found a size dependency of albedo, which is the smaller JTAs have higher albedo. Then they proposed the size distribution with different slope from those of Jewitt et al.. However, Grav et al. (2011) reported that the size dependency of albedo founded by Fernandez et al. (2009) is not clear in WISE data. Therefore, the size dependence of the albedo still remains ambiguous.

3.2 Total number of JTAs and orbital distribution

The L4 population is slightly larger than L5. It has been known for a long time. Some scientists thought that this is caused by an observational bias because the surveys of JTAs have not made with the same area, instrument, and procedure of the L4 and L5 regions. However, the data of SDSS (Szabo et al. 2007), SMBAS (Yoshida & Nakamura 2008, Nakamura & Yoshida 2008) and WISE (Grav et al. 2012) included both the L4 and the L5 JTAs. It allows us to have unbiased dataset of JTAs of both swarms. The SDSS, SMBAS, and WISE surveys found that the number ratio L4 to L5 is 1.6+/-0.1, 1.8, and 1.34, respectively. Therefore, we can conclude that the L4 population is larger than L5 up to the detection limit of surveys ($D>2\text{km}$).

Using the catalogue supported by MPC (<http://www.minorplanetcenter.net/iau/lists/JupiterTrojans.html>), we can investigate the orbital distribution of L4 and L5 JTAs. Fig.3 shows the distribution of orbital inclination, eccentricity, and semi-major axis of both the swarms, separately. There is no significant difference in the mean eccentricity and mean semi-major axis

distributions of each swarm. Only mean inclination distribution shows a slight difference between L4 and L5.

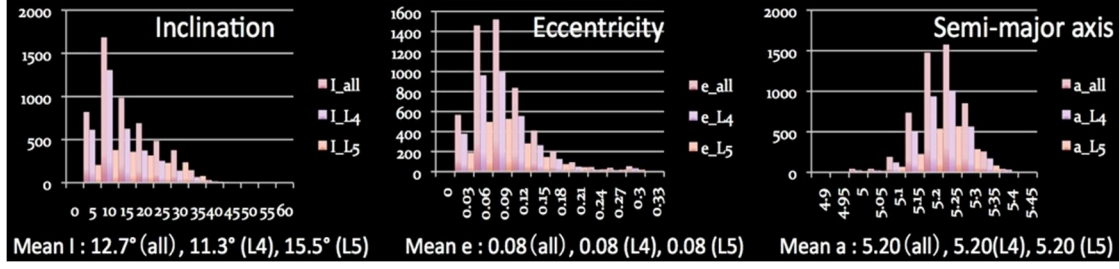


Figure 3. The inclination (left), eccentricity (middle), and semi-major axis (right) distributions of the L4, L5, and both swarms. Mean values of each swarm are also shown under each panel.

3.3 Dynamical and Orbital evolution and Origin

The JTs have attracted attentions of many scientists because of their special location. They have been studied from the dynamical and collisional aspects. So far, the two competing origins are proposed as following: (1) JTs are remnants of planetesimals near Jupiter during Jupiter's growing in the planetary gas (Peale 1993, Marzari & Scholl 1998). (2) JTs are captured objects by Jupiter, which were originated from the Kuiper belt region at the time of the late heavy bombardment (Nice model, Morbidelli et al. 2005).

There are several studies for stability of JTs. Schubart & Bien (1987) found that the amplitude of libration around the Lagrange points and proper eccentricity and proper inclination of each object is stable for a few 10^5 years. Levison et al. (1997), Giorgolli & Skokos (1997) suggested that about 3% of JTs are located in unstable orbits ($e>0.1$, $i>55^\circ$) and the erosion rate is about $\sim 6.2 \times 10^{-5} \text{ yr}^{-1}$ (for $D>1\text{km}$). Other objects are stable over the age of the Solar System.

Davis & Weidenshilling (1981) studied the collisional evolution of JT population and found that large JTs have survived for age of the Solar System without catastrophic disruption. Meanwhile, Milani (1993, 1994), Beauge & Roig (2001), Roig et al. (2008) identified collisional families in the L4 and L5 populations. This suggests that JTs have been experienced considerably collisional evolutions. Davis & Weidenshilling (1981), Marzari et al. (1997), Dell Oro et al. (1998) calculated average collisional velocities between JTs. Their results are $\sim 3.5 \text{ km/s}$, $\sim 5 \text{ km/s}$, $\sim 4.5 \text{ km/s}$, respectively.

The relationship between JTs and other dynamical groups was also studied. Marzari et al. (1995) suggested that about 20 % of collisional fragments created during family forming events acquired unstable orbits and then approached Jupiter. And they also suggested that a few tenth of observed short period comets (SPCs) were probably the fragments of JTs which were dropped from JT swarms by the family forming collision. Marzari et al. (1995) found that fragments from family forming events became Jupiter family comets (JFCs) first and then supplied 10% of SPCs and Centaurs.

de Elia & Brunini (2007) investigated the collisional and dynamical evolution of the L4 population with different collisional parameters. They estimated the size distribution, the mean collisional lifetime, and the ejection rate of Trojan fragments. They also studied possible contribution to the current Centaurs and JFCs populations. They found that almost no fragments with $D>5\text{km}$ were removed from the L4 swarm and only fragments with $D<5\text{km}$ were removed. This makes the shallow slope of cumulative size distribution for objects with $D<5\text{km}$. This is consistent with the observed shallow slope of L4 JTs with $D<5\text{km}$ (Yoshida & Nakamura 2005).

According to their simulation, the 70-250km sized JT_s are likely to have survived over the age of the Solar System. They also concluded that almost no JT_s become Centaurs or JFCs.

There is no investigation of the dynamical and collisional evolution for the L5 population so far. It should be done and compared with the evolutions of L4 population.

3.4 Family

Roig et al (2008) identified the JT_s families and investigated their taxonomic types by using available catalogues. The identified families are listed in Table 3. The L4 swarm has robust families. Meanwhile, in the L5 swarm, the borders of some families are ambiguous.

It has been thought that JT_s are quite homogeneous population in a standpoint of their composition (most of them are D-type). However, Roig et al. (2008) dealt with family members and background JT_s separately, then and found a slight inhomogeneity. They used photometric data of 250 JT_s obtained from moving object catalogue (MOC3; provided by SDSS) and spectroscopic data of 71 JT_s. According to them, two third of them seem to be red (D-type) and the rest of them are less red (C or P type). They confirmed a trend found by Szabo et al. (2007), which is that larger JT_s are red and with higher inclination in both swarms, for the background objects. In addition, a significant lack of large sized and less-red background JT_s was discovered. On the other hand, family members do not show any correlation between taxonomic type and size or inclination. The taxonomic types of L4 families are different from those of L5 families. In L4 swarm, there are C and P type families as well as D-type ones. However, families in L5 swarm are predominantly D-type.

Family members are generally considered to be younger than background asteroids and smaller JT_s (considered as collisional fragments) are younger than large JT_s (considered as survivors of collisional evolution). Therefore, it is natural to assume that the large background JT_s are more primordial than family members or smaller JT_s. The fact that large background JT_s are red (D-type) and have high inclination (excited) (founded by Szabo et al. (2007) and Roig et al. (2008)) may be conformable to a suggestion from of the Nice model "Jupiter captured JT_s which were originated from the Kuiper belt objects and intruded into inner region by planet migration".

Table 3. Families of JT_s in L4 swarm and L5 swarm. Identified by Roig et al. (2008).

| L4 | | | L5 | | |
|---------------|---|--|---------------|---|---|
| Menelaus Clan | | | Anchises Clan | | |
| Menelaus | For H<11(D>40km), a slight predominance of D-type. For H>11, dominated by P. | | Anchises | This is a tight family (5 members) inside of Anchises Clan. | |
| Eurybates | C, P | This is a tight family inside of Menelaus Clan. | Phathoos | P robust | Depends on the cut-off level, Phathoos, Polydoros, Sergestus families will be merged. |
| Epeios | Mostly P, especially at the large size. | | Polydoros | D robust | |
| 1986TS6 | P, D | | Sergestus | ? | |
| Kalchas | P | | Agelaos | P, D | The border between Agelaos and 1999RV165 families is ambiguous. |
| Makhaon | P, D | | 1999RV165 | P | |
| Euryalos | P, D | | Aneas | D | Depends on the cut-off level, these three families will be merged. |
| 1986WD | D, P, C | | Sarpedon | | |
| Laertes | All members (consisted of 15-20 JT _s) are small (H>11) and belonging to P-type. | | 1988RN10 | 1988RG10 | A quite homogeneous D-type family. |
| Demophon | P | | Asios | | |
| 1998XZ77 | P, D | | Phereclos | A quite homogeneous D-type family. | |
| Hektor | D | These are high-inclination families ($\sin I > 0.25$). They are dominated by D-type. | Misenus | P | |
| Teucer | | | | | |
| Sinon | | | | | |

3.5 Spin rate distribution

It has been known that lightcurves of JT s show larger amplitude than those of MBAs (Dunlop & Gehrels, 1969, Hartmann et al., 1988, Zappala et al., 1989, Binzel & Sauter, 1992). Recently, Melita et al. (2010) observed 6 JT s and investigated the characteristic of JT s lightcurves (a correlation of rotation period, or amplitude and asteroid size) with the data from their observations and available lightcurves database (<http://cfa-www.harvard.edu/iau/MPEph/MPEph.html>). They pointed out that the JT s with the same size range have various rotation periods. It seems that there is no correlation between asteroid size and rotation period. They also found a possible trend that fainter objects have smaller amplitude, namely small JT s are nearly spherical. Mottola et al. (2011) have observed 80 JT s with $H < 10$ ($D \sim 60$ km) for two decades. Their contribution increased lightcurves of JT s drastically.

Warner et al. (2009) provided the lightcurve database: <http://www.minorplanet.info/lightcurvedatabase.html>. This database updated to 2012 September at the time of writing this paper includes more than 5800 objects. Table 4 shows the numbers of dynamical group of NEA+MC, MBA, JT, and TNO with quality cord (QC) > 2 and with spin rate < 12 rev/day and their size range included in the database.

Table 4. Available Lightcurve data.

<http://www.minorplanet.info/lightcurvedatabase.html>.

| Group | Number (QC>2) | Spin rate < 12 | Size range (km) |
|----------|---------------|----------------|-------------------------------|
| NEA+MC | 692 | 575 | 0.003 - 42.63 |
| MBA | 3800 | 3797 | 0.08 - 848.4 |
| JT (all) | 117 | 117 | 21.16 - 233.23 |
| JT L4 | 65 | 65 | 21.16 - 233.23 (average 72.9) |
| JT L5 | 52 | 52 | 33.54 - 142.82 (average 71.6) |
| TNO | 48 | 48 | 6.36 - 919.44 |

So far no fast rotator (spin rate < 12 rev/day) was found in JT group. Fortunately, since the lightcurve database includes the L4 and L5 JT s with the same size range, we can compare the spin rate between L4 and L5 JT s. The spin rate distribution of asteroids has been studied by comparing with the Maxwellian distribution (Salo 1987, Harris & Burns 1979, Farinella et al. 1981, Pravec et al. 2002). Therefore we fitted their spin rate distribution with the Maxwellian distribution and then calculated the average rate : Ω_M , while Ω is a simple average of the spin rate. The top three panels of Fig. 4 show the spin rate distribution of JT s, L4 and L5, separately. The other panels of Fig. 4 show the spin rate distribution of other groups.

For a statistical analysis, we must take into account the completeness of lightcurve database. Szabo et al. (2007) said that all asteroids with $H < 12.3$ mag had been already discovered and catalogued into the MPC database. On the other hand, based on the slope's change of the size distribution around $H = 10$ mag (Jewitt et al. 2000), we can assume that JT s that are brighter than $H = 10$ are primordial objects and the rest of JT s (fainter than $H = 10$ mag) are fragments occurred from collisional evolution in JT swarms. If it is true, the spin period distribution of JT s with $H < 10$ represents a nature of spin state of the primordial JT s. We found that there are 85 JT s with $H < 10$ in the MPC catalogue and 73 of them have been determined their rotation periods. We

investigated the spin rate distribution of JTJs brighter than $H=10$ and fainter than $H=10$, separately in Fig. 5. For the groups with $H<10$, the lightcurve data is almost completed. In the group of all JTJs with $H<10$, the data completeness is 86% (73 lightcurves/85 JTJs), the Ω_M is 2.7 and Ω is 2.1. In the L4 ($H<10$), the completeness is 82% (41 lightcurves/50 JTJs), the Ω_M is 2.6 and Ω is 2.0. In the L5 ($H<10$), the completeness is 91% (32 lightcurves/35 JTJs), the Ω_M is 2.8 and Ω is 2.2. The spin rate of larger JTJs ($H<10$) which seem to be primordial is about 2 rev/day (about 12 hours). There is no significant difference of the spin rate between L4 and L5 swarms at the range of $H<10$. Comparing with that of smaller L5 group, the spin rate distribution of smaller ($H>10$) L4 group seems to be scattered. It may be related to the catastrophic disruptions which reset the spin rate of the parent bodies when dynamical families formed in L4 swarm.

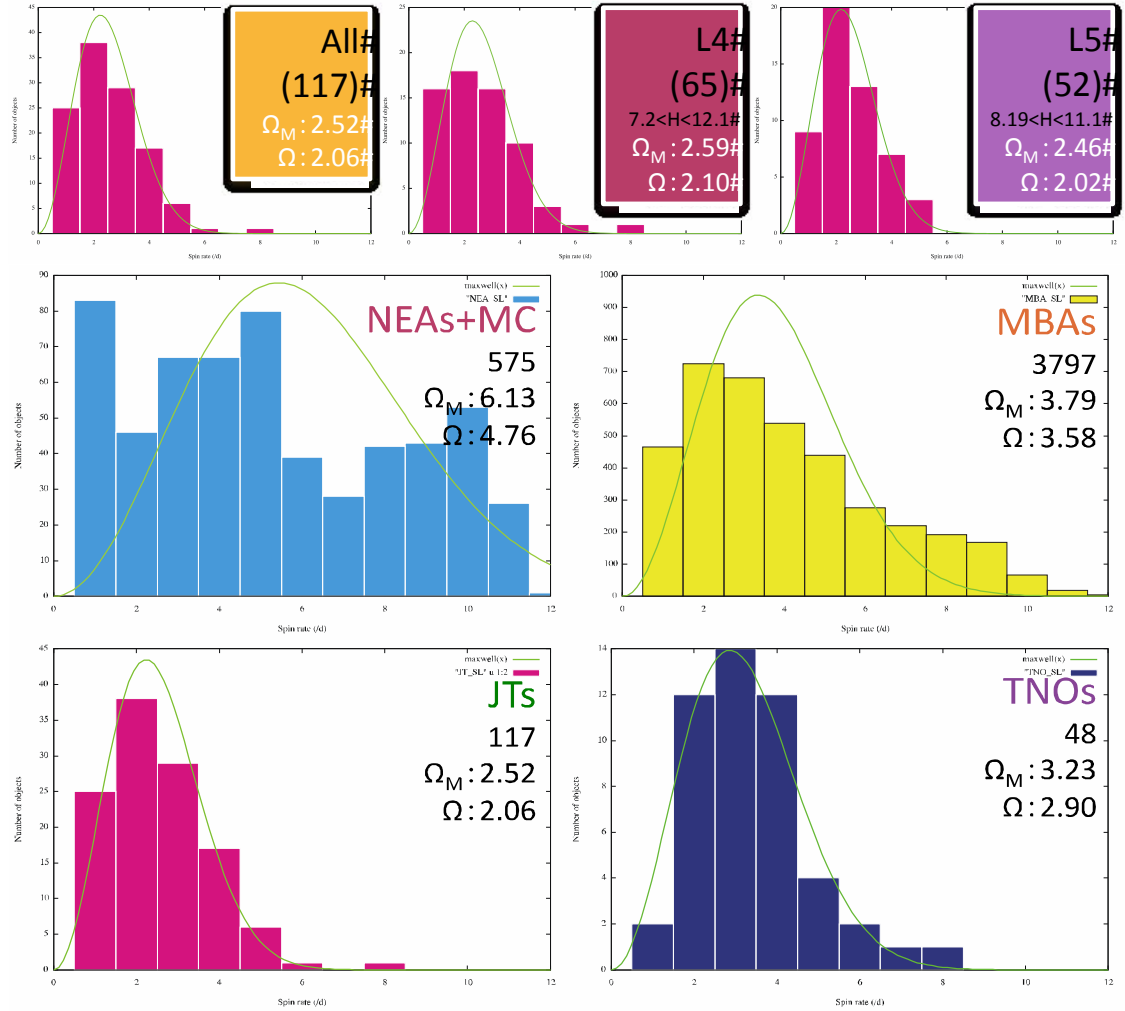


Figure 4. The spin rate distributions of JTJs (top left), L4 (top middle), and L5 (top right), MEAs + Mars crossing group (middle left), MBAs (middle right), and TNOs (bottom right). The Ω_M is average spin rate (rev/day) of fitted Maxwellian distribution (green lines). The Ω is a simple average of spin rate (rev/day).

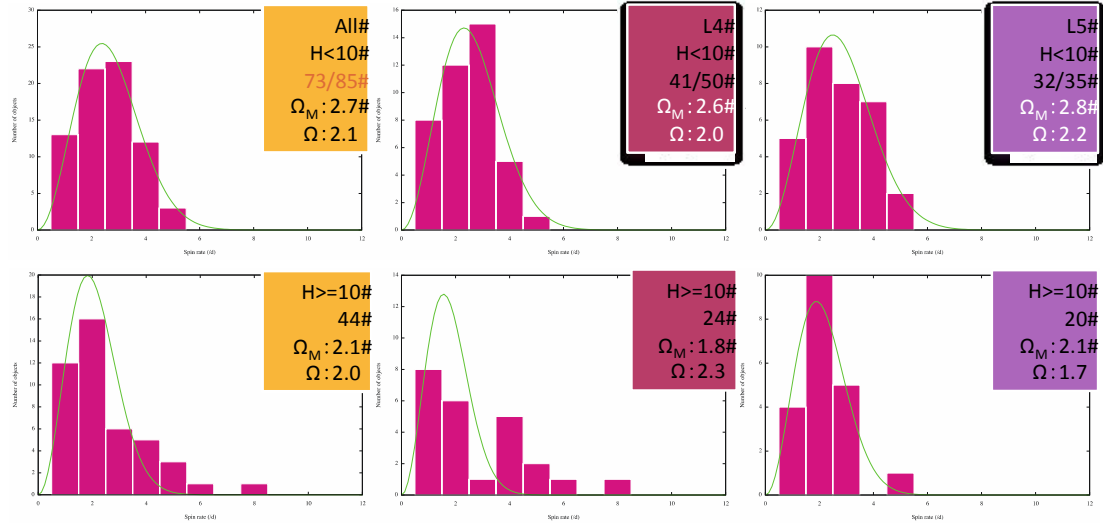


Figure 5. The spin rate distributions of all JTs (left), L4 (middle), and L5 (right) with $H < 10$ (upper row) and $H > 10$ (lower row).

3.6 Binary and Density

The data of binary system in the solar system is summarized at the following web page, which is organized by Wm. Robert Johnston: <http://www.johnstonsarchive.net/astro/asteroidmoons.html>. So far, four binary systems have been recognized in JT group, as shown in Table 5. (624) Hektor belongs in L4 swarm. It is a contact binary (363×207 km) having a small satellite ($D=15$ km). It is a D-type asteroid and its density is 2.4 g/cm^3 . (617) Patroclus is another large binary (the diameters of the primary and secondary are 121.8 ± 3.2 km and 112.6 ± 3.2 km, respectively) in L5 swarm. It is a P-type object and its density is 0.8 g/cm^3 . The densities of these two binary systems seem to be significantly different. This difference probably caused by porosity of asteroid or composition of asteroid related to taxonomic types. Other two contact binaries were identified by Mann et al. (2007) in the L5 group. Table 6 lists the range of densities of dynamical groups: MBAs, JTs, TNOs and cometary nucleus. The density range of JTs is similar to that of TNOs. Takahashi et al. (2013 in prep.) calculated the following four JT's densities by using approximation of Roche binary (Takahashi & Ip 2004). The densities of (20961) Arkesilaos (L4), (22008) 1999 XM₇₁ (L4), (11663) 1997 GO₂₄ (L5), and (32467) 2000 SL₁₇₄ (L5), are 0.73 g/cm^3 , 0.83 g/cm^3 , 0.33 g/cm^3 , and 0.55 g/cm^3 , respectively. The taxonomic types of them are unknown. The densities of (20961) Arkesilaos

Table 5. Binary systems in JT's group.

| | Name | Density (g/cm ³) | Type | Note |
|----|-----------------|------------------------------|------|---|
| L4 | (624) Hektor | 2.4 | D | Contact binary with a small satellite (Marchis et al. 2006). The density was measured by Lacerda & Jewitt (2007). |

| | | | | |
|----|------------------------------|------|---|---|
| L5 | (617) Patroclus | 0.8 | P | The primary and secondary are almost same size. (Merline et al. 2002, Noll 2006). The density was measured by Machis et al. (2006). |
| L5 | (17365) 1978VF ₁₁ | 0.78 | ? | This JT is a contact binary (Mann et al. 2007). |
| L5 | (29314) Eurydam as | 0.59 | ? | This JT is a contact binary (Mann et al. 2007). |

Table 6. Densities of other dynamical groups.

| Groups | Density | Note |
|---------------|---------------------------|---------------------|
| MBAs | 0.6-3.8 g/cm ³ | |
| JTs | 0.8-2.4 g/cm ³ | Mckinnon (2008) |
| TNOs | 0.6-2.5 g/cm ³ | Lowry et al. (2008) |
| Comet Nuclear | 0.1-1.5 g/cm ³ | Noll (2006) |

and (22008) 1999 XM₇₁ are close to that of (617) Patroclus. Other two seem to be low density.

3.7 Taxonomic types and Spectroscopic observations

There are many papers that investigated the taxonomy of JTs (e.g. Smith et al., 1981, Jewitte & Luu, 1990, Lagerkvist et al., 1993, Fitzsimmons et al., 1994, Xu et al., 1995, Carvano et al., 2003, 2010, Lazzaro et al., 2004, Bendjoya et al., 2004, Fornasier et al., 2004, 2007, Karlsson et al., 2009).

Main taxonomic types of JTs are D-, P-, C-types and B-, K-, T-types also exist. Generally, their spectra are featureless. So far no water's absorption was recognized even among family members (Dotto et al., 2006). It has been known that the JT population is quite homogeneous and there is no significant difference between L4 and L5 in taxonomy. However, recently Roig et al. (2008) studied family members and background objects (non-family member), separately, then they noticed some difference between families and background objects. For background objects, larger objects have higher inclinations. And larger objects are redder. These trends were seen in both swarms of L4 and L5. For family members, D-types dominate in L5 families. Meanwhile D-, C- and P-types families exist in L4. There is no correlation between size and orbital inclination or taxonomic types for family members.

Emery et al. (2011) investigated 68 JT's spectra obtained by the SpeX which can take spectra from the optical to the near infrared region: 0.7-2.5μm. All spectra of them were featureless. They found that the background JTs in both L4 and L5 are clearly distinguishable into two groups: "red" and "less red". Since there are no intermediate spectra, Emery et al. (2011) suggested that the difference between the red group and the less red group is caused by different intrinsic compositions rather than space weathering on their surfaces. They suggested that the red group were originated from the Kuiper belt region and migrated inward during the late heavy bombardment period. And, the less red group may be remnants of planetesimals around Jupiter. There is no albedo difference between red (0.055+/-0.016) and less red groups (0.051+/-0.016).

Grav et al. (2012) investigated taxonomic distribution of JTs using the WISE data. They pointed out that there is no significant size dependency of JT's albedo, which was found by Fernandez et al. (2009). They also reported that the taxonomic distribution of JTs is similar with that of irregular satellites of Jupiter. These two groups don't contain extremely red objects like Centaur or irregular satellites of Saturn. They also compared the taxonomic distribution of JTs with that of Hildas, then found that the taxonomic distributions of JTs and Hildas for larger objects ($D > 70\text{km}$) are different: D-type dominates in JTs and C/P-type dominates in Hildas. However the D-type objects increase in the size range of $D < 70\text{km}$ in Hildas. They suggested that the taxonomic distributions of JTs and Hildas in the smaller size ($D < 70\text{km}$) may be similar with each other. Grav et al. (2012) also found that the albedo of D-type JTs are higher than that of C/P-type at $3.4\mu\text{m}$ wavelength, though the visible albedos of D-, C-, P-type objects are similar.

Emery et al. (2006) observed (624) Hektor, (911) Agamemnon, and (1172) Aneas using the Spitzer telescope and obtained their spectra ranging of $5.2\text{-}38\mu\text{m}$. They found that each object shows emissivity plateau around $10\mu\text{m}$. An emission feature at $10\mu\text{m}$ can be interpreted as an existence of thin layer of fain silicate grains on the surface, which is may be linked to cometary activity which is going on or recently happened. They also pointed out that comets with $10\mu\text{m}$ emission were Mg-rich(=iron-poor).

Yang & Jewitt (2011) used the Spex and obtained spectra ($0.8\text{-}2.5\mu\text{m}$) of 7 JTs. They investigated $1\mu\text{m}$ absorption feature in their spectra and found that all spectra are featureless. The $1\mu\text{m}$ absorption appears in the case that the host silicate is iron-rich. Therefore, the lack of absorption feature at $1\mu\text{m}$ is consistent with the interpretation by Emery et al. (2006), namely JTs might be iron-poor. Yang & Jewitt (2011) also found that the NIR spectra of members of the Eurybates, which is a C-type family in L4, are similar with those of CM2 carbonaceous chondrite (hydrated mineral rich). The members of the Eurybates family may have experienced aqueous alteration.

Lagerkvist et al (2005) investigated the Cybele group, which lies at the heliocentric distances of $3.3\text{-}3.5$ AU and includes D-, C-, P-types as well as JT group. They found that D-type objects are smaller than C/P-type objects in the Cybele group and then suggested that D-type objects are collisional fragments from C/P-type parent bodies or C/P-type objects are robust than D-type because of different compositions.

de Leon et al. (2012) observed various B-type MBAs and got their NIR spectra. They found the various slope from red to blue consecutively in near infrared region. Most important finding is that the various slope illustrates various hydration level: redder spectra connect to wet material and bluer spectra connect to dry material. B-type members of Themis family show various slopes, it means that they have various hydration levels. Meanwhile B-type members of Pallas family show only bluer slopes, which mean their surfaces have dry material. Nesvorný et al. (2005) investigated SDSS data (optical data) and found that members of Veritas family (young C-type MBA family) show typical C-type spectra and averaged spectrum of members of Themis family (old C-type) is close to B-type, namely bluer spectrum. Ziffer et al. (2011) obtained NIR spectra of members of Themis and Veritas families, they found that Themis members show flat or rather red spectra and Veritas members show flat spectra. This means that the Themis members have different hydration level compared with the Veritas members. There are some C-type JTs. They must be related to carbonaceous chondrites as well as the C-type of MBAs. Therefore, we may find JTs with various hydration levels.

Based on the above findings, we may imagine a parent body of carbonaceous chondrite as shown in figure 6. The inside of parent body contains hydrated mineral and near surface region contains dehydrated mineral. Then a catastrophic impact can make fragments with different hydration levels.

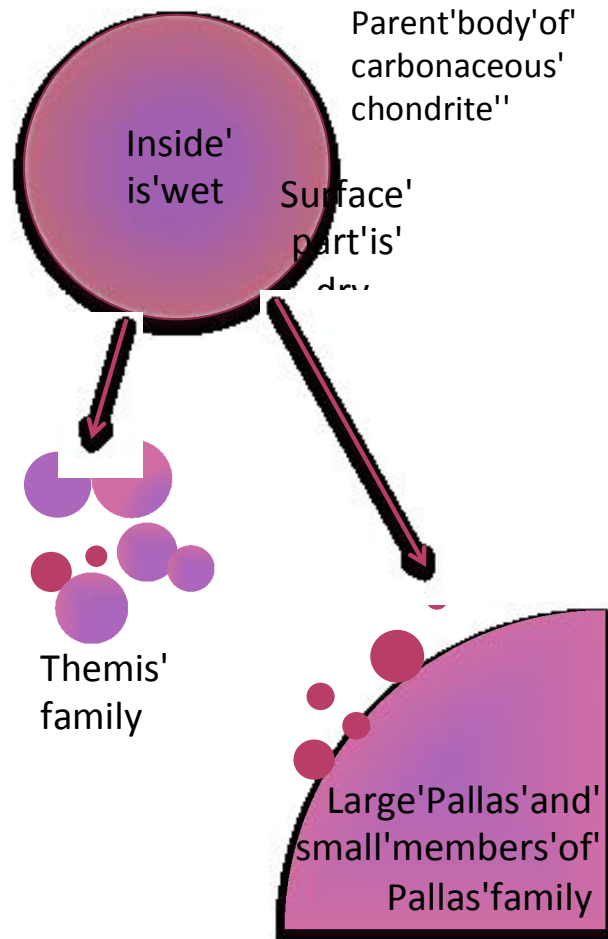


Figure 6. A possible parent body of carbonaceous chondrite with different hydration level. Disruption events for forming asteroid families can provide impact fragments with various hydration level. It is a possible explanation on C-type and B-type asteroids in the Themis family and the Pallas family.

3.8 Space weathering on Jupiter Trojans

It has been believed that JT's contain hydrocarbons and ice. Brunetto et al. (2006) performed ion irradiation experiments to ices of CH_3OH , CH_4 , and C_6H_6 , then they presented visible and near infrared ($0.65\text{-}2.7\mu\text{m}$) spectra. After the irradiation, the spectra of ices were significantly reddened and darkened because of the formation of an organic (C-rich) mantle.

Moroz et al. (2004) performed ion irradiation experiments onto Asphaltite and Kerite (both of them are natural complex hydrocarbons). Before the ion irradiation, the spectra of them were red with steep slope in the range of optical to $2.5\mu\text{m}$. After the irradiation, the spectra changed into shallow slope (moderately red), namely the spectra got bright in optical range and got dark in infrared range. This change seems to be because the surfaces of Asphaltite and Kerite were carbonized.

Based on those experiments, the ion irradiations on natural hydrocarbons or pure hydrocarbons ice change their spectra to the opposite direction, namely the space weathering varies the spectra of pure hydrocarbons ice to those of D-type (red)

because of formation of an organic refractory residue which is called irradiation mantle, while the spectra of natural complex-hydrocarbons change to those of P-type (less red) because of carbonization of their surfaces.

More experiments with different materials and different surface conditions are needed to understand the space weathering process on D-type and P-type asteroids, moreover a relationship between both types. From the investigations mentioned above, we may imagine that, at first, the space weathering changes icy bodies' surfaces into the D-types that are covered with irradiation mantle (equal to complex hydrocarbons). Further space weathering changes the D-type surfaces into the P-type by carbonization. Along this process, the P-type can be older than the D-type. This may explain that the inverse correlation between the size and the fraction of D-type (D-type asteroids are smaller than P-type ones) that is seen in Cybele and Hilda groups (Lagerkvist et al (2005), Grav et al. (2012)). Although the inverse correlation has been interpreted as following; since the P-type is more robust than the D-type, the P-type survives for longer time than the D-type.

4. Summary

- **Size distribution:** the size distribution of JT s has been determined down to 2 km in diameter so far. Comparing the distribution with those of NEAs or MBAs, it turned out that each group shows the intrinsic size distribution. In the size range of smaller than 5km in diameter, the size distribution of L4 JT s (the slope (b) of cumulative size distribution is ~ 1.3) is probably different from that of L5 JT s ($b \sim 2.1$).
- **Orbital distribution and total population:** there is no significant difference between L4 and L5 groups in orbital distribution. The L4 population is larger than L5 one. However, if we include smaller JT s, it may invert. The inversion would happen at about 1km in diameter.
- **Orbital and collisional evolutions:** Most of large JT s spend inside of JT swarms during entire age of the Solar System. The collision between JT s may remove small bodies with $D < 5\text{km}$ from the JT's stable area. Meanwhile the larger bodies ($> 70\text{km}$) survive collisional disruptions. There is almost no JT that become JFCs or Centaur.
- **Spin rate distribution:** there is no significant difference in the spin rate distribution between L4 and L5 groups. The average spin rate for the JT s with $H < 10$ (it has the almost complete database of rotation period) is about 2 rev/day, namely the average rotation period of them is about 12 hours.
- **Density:** although there is very few data about densities of JT s, there seems to be two groups: with high density (2.4g/cm^3) and low density ($< 1\text{g/cm}^3$).
- **Albedo:** the size dependency of albedo of JT s is still ambiguous. There is no difference of visible albedo between the red group and the less red group. However, the red group has higher albedo than less red group at $3.4\mu\text{m}$.
- **Taxonomic types:** in the non-family members, the L4 and L5 swarms show almost same taxonomic distributions. There is a trend that large objects are red and have high inclinations. In the family members have different taxonomic distributions between L4 and L5. The families in L4 swarm have D-, C- and P-type members, whereas the families in L5 swarm consist of almost D-type objects.
- **Space weathering:** the process of space weathering on JT surface is still unknown. We need more experiments and observations with the range of optical to infrared.
- **Surface of JT s:** the observation based on the $10\ \mu\text{m}$ feature of their spectra

suggested that JT_s might be covered with fine silicate grains as cometary nuclei.

Acknowledgements

The materials presented in section 2 “the Solar Power Sail mission” were provided from the presentation by Dr. Hajime Yano (JAXA) at COSPAR 2012 in India and Dr. Ryu Funase (Univ. of Tokyo) at Sail Science meeting in JAXA.

References

- Beaug & Roig (2001) A Semianalytical Model for the Motion of the Trojan Asteroids: Proper Elements and Families, *Icarus*, 153, 391-415.
- Bendjoya et al. (2004) Spectroscopic Observations of Jupiter Trojans, *Icarus*, 168, 374-384.
- Binzel & Sauter (1992) Trojan, Hilda, and Cybele Asteroids - New Lightcurve Observations and Analysis. *Icarus*, 95, 222-238.
- Brunetto et al. (2006) Ion Irradiation of Frozen Methanol, Methane, and Benzene: Linking to the Colors of Centaurs and Trans-Neptunian Objects, *ApJ*, 644, 646-650.
- Carvano et al. (2003) Search for Relations among a Sample of 460 Asteroids with Featureless Spectra. *Icarus*, 161, 356-382
- Carvano et al. (2010) SDSS-based Taxonomic Classification and Orbital Distribution of Main Belt Asteroids. *A&A*, 510, A43.
- Davis & Weidenschilling (1981) Avoiding Close Encounters: Collisional Evolution of Trojan Asteroids. *Lunar and Planetary Science XII*, 199-201.
- dell'Oro et al. (1998) Trojan Collision Probability: a Statistical Approach. *A&A*, 339, 272-277.
- Dotto et al., (2006) The Surface Composition of Jupiter Trojans: Visible and Near-infrared Survey of Dynamical Families. *Icarus*, 183, 420-434.
- Dunlap & Gehrels (1969) Minor Planets. III. Lightcurves of a Trojan Asteroid. *AJ*, 74, 796.
- de Elia & Brunini (2007) Collisional and Dynamical Evolution of the Main Belt and NEA Population. *A&A*, 466, 1159-1177.
- Emery et al. (2006) Thermal Emission Spectroscopy (5.2-38μm) of Three Trojan Asteroids with the Spitzer Space Telescope: Detection of Fine-grained Silicates, *Icarus*, 182, 496-512
- Emery et al. (2011) Near-infrared Spectroscopy of Trojan Asteroids: Evidence for Two Compositional Groups, *AJ*, 141, 25
- Farinella et al. (1981) Triaxial Equilibrium Ellipsoids among the Asteroids, *Icarus*, 46, 114-123
- Fernandez et al. (2009) Albedos of Small Jovian Trojans, *AJ*, 138, 240-250
- Fitzsimmons et al., (1994) A Spectroscopic Survey of D-type Asteroids, *A&A*, 282, 634-642
- Fornasier et al. (2004) Visible Spectroscopic and Photometric Survey of L5 Trojans: Investigation of Dynamical Families, *Icarus* 172, 221-232
- Fornasier et al. (2007) Visible Spectroscopic and Photometric Survey of Jupiter Trojans: Final Results on Dynamical Families, *Icarus* 190, 622-642
- Giorgolli & Skokos (1997) On the Stability of the Trojan Asteroids, *A&A*, 317, 254-261.
- Grav et al. (2011) ISE/NEOWISE Observations of the Jovian Trojans: Preliminary Results, *ApJ*. 731, 53-66.
- Grav et al. (2012) WISE/NEOWISE Observations of the Jovian Trojan Population: Taxonomy, *ApJ*, 759, 49

- Harris & Burns (1979) Asteroid Rotation Rates I. Tabulation and Analysis of the Data, *Icarus*, 40, 115-144.
- Hartmann et al., (1988) Trojan and Hilda Asteroid Lightcurves I. Anomalously Elongated Shapes among Trojans (and Hildas?), *Icarus*, 73, 487-498
- Ito et al. (2006) Size Distribution of Asteroids and Old Terrestrial Craters: Implications for Asteroidal Dynamics During LHB, *Advances in Geosciences, Volume 3: Planetary Science (PS)*. Editor-in-Chief: Wing-Huen Ip. Volume Editor-in-Chief: Anil Bhardwaj. ISBN: 981-256-983-8 (ISBN for the set of 5 volumes: 981-256-456-X). Published by World Scientific Co., Pte. Ltd., Singapore, p.337
- Jewitt et al. (2000) Population and Size Distribution of Small Jovian Trojan Asteroids, *AJ*, 120, 1140-1147
- Jewitt & Luu (1990) CCD Spectra of Asteroids II. The Trojans as Spectral Analogues of Cometary Nuclei, *AJ*, 100, 933-944
- Karlsson et al. (2009) (U)BVRI Photometry of Trojan L5 Asteroids, *Icarus*, 199, 106-118
- Lacerda & Jewitt (2007) Densities of Solar System Objects from Their Rotational Light Curves, *AJ*, 133, 1393-1408
- Lagerkvist et al. (1993) Investigations of D-type Asteroids, *Mon. Not. R. Astron. Soc.*, 260, 679-680
- Lagerkvist et al. (2005) A Study of Cybele Asteroids II. Spectral Properties of Cybele Asteroids, *A&A*, 432, 349-354
- Lazzaro et al. (2004) S3OS2: the Visible Spectroscopic Survey of 820 Asteroids, *Icarus*, 172, 179-220
- Leon et al. (2012) Near-infrared Spectroscopic Survey of B-type Asteroids: Compositional Analysis, *Icarus*, 218, 196-206
- Levison et al. (1997) Dynamical Evolution of Jupiter's Trojan Asteroids, *Nature* 385, 42-44
- Mann et al. (2007) Fraction of Contact Binary Trojan Asteroids, *AJ*, 134, 1133-1144
- Machis et al. (2006) A Low Density of 0.8 g cm^{-3} for the Trojan Binary asteroid 617 Patroclus, *Nature*, 439, 565-567
- Marchis et al. (2006) Search of Binary Jupiter-Trojan Asteroids with Laser Guide Star AO systems: a Moon around 624 Hektor, American Astronomical Society, DPS meeting #38, #65.07; *Bulletin of the American Astronomical Society*, Vol. 38, p.615
- Marzari & Scholl (1998a) Capture of Trojans by a Growing Proto Jupiter, *Icarus*, 131, 41-51.
- Marzari & Scholl (1998b) The Growth of Jupiter and Saturn and the Capture of Trojans, *A&A*, 339, 278-285
- Marzari et al. (1995) Are Trojan Collisional Families a Source for Short-period Comets?, *A&A*, 299, 267-276
- Marzari et al. (1997) Collisional Evolution of Trojan Asteroids, *Icarus*, 125, 39-49
- Merline et al. (2002) Asteroids do Have Satellites, in *Asteroids III*, 289-312
- Melita et al. (2010) Lightcurves of 6 Jupiter Trojan Asteroids, *Planetary and Space Science*, 58, 1035-1039
- Milani (1993), The Trojan Asteroid Belt: Proper Elements, Stability, Chaos and Families, *Celestial Mechanics*, 57, 59-94
- Milani (1994) Proper Elements and Stable Chaos, in *From Newton to Chaos: Modern Techniques for Understanding and Coping with Chaos in N-body Dynamical Systems*, A. E. Roy & B.A. Steves eds., Plenum, New York, 47-78
- Moroz et al. (2004) Optical Alteration of Complex Organics Induced by Ion

- Irradiation: 1. Laboratory Experiments Suggest Unusual Space Weathering Trend, *Icarus*, 170, 214-228
- Morbidelli et al. (2005) Chaotic Capture of Jupiter's Trojan Asteroids in the Early Solar System, *Nature*, 435, 462-465
- Mottola et al. (2011) Rotational Properties of Jupiter Trojans. I. Light Curves of 80 Objects, *AJ*, 141, 170
- Nakamura & Yoshida (2008) A New Surface Density Model of Jovian Trojans around Triangular Libration Points, *Publ. Astron. Soc. Japan*, 60, 293-296
- Nesvorný et al. (2005) Evidence for Asteroid Space Weathering from the Sloan Digital Sky Survey, *Icarus*, 173, 132-152
- Noll (2006) Solar System Binaries, in *Asteroids, Comets, Meteors*, in Proceedings of the 229th Symposium of the International Astronomical Union, ed. by L. Daniela et al., Cambridge Univ. Press (Cambridge, UK), 301-318
- Peale (1993) The Effect of the Nebula on the Trojan Precursors, *Icarus*, 106, 308-322
- Pravec et al. (2002) Asteroid Rotations, in *Asteroids III* (eds. Bottke et al.), 113-122
- Roig et al. (2008) Taxonomy of Asteroid Families among the Jupiter Trojans: Comparison between Spectroscopic Data and the Sloan Digital Sky Survey Colors, *A&A*, 483, 911-931
- Salo (1987) Numerical Simulations of Collisions between Rotating Particles, *Icarus*, 70, 37-51.
- Schubart & Bien, (1987) Trojan Asteroids - Relations between Dynamical Parameters. *A&A*, 175, 299-302.
- Smith et al., (1981) Spectrophotometry of J8, J9, and Four Trojan Asteroids from 0.32 to 1.05 μm , *Icarus*, 46, 108-113
- Strom et al. (2005a) The Origin of Planetary Impactors in the Inner Solar System, *Science*, 309, 1847-1850
- Strom et al. (2005b) The Origin of Impactors During the Inner Solar System Cataclysm, *Meteoritics & Planetary Science*, Vol. 40, Supplement, Proceedings of 68th Annual Meeting of the Meteoritical Society, held September 12-16, 2005 in Gatlinburg, Tennessee., p.5070
- Szabo et al. (2007) The Properties of Jovian Trojan Asteroids Listed in SDSS Moving Object Catalogue 3, *Mon. Not. R. Astron. Soc.*, 377, 1393-1406
- Takahashi & Ip (2004) A Shape-and-Density Model of the Putative Binary EKBO 2001 QG298, *Publ. Astron. Soc. Japan*, 56, 1099-1103, (2004)
- Warner et al. (2009) The Asteroid Lightcurve Database, *Icarus*, 202, 134-146
- Xu et al. (1995), Small Main-Belt Asteroid Spectroscopic Survey: Initial Results, *Icarus*, 115, 1-35
- Yang & Jewitt (2011) A Near-Infrared Search for Silicates in Jovian Trojan Asteroids, *AJ*, 141, 95-102.
- Yoshida & Nakamura (2005) Size Distribution of Faint Jovian L4 Trojan Asteroids, *AJ*, 130, 2900-2911
- Yoshida & Nakamura (2008) A Comparative Study of Size Distributions for Small L4 and L5 Jovian Trojans, *Publ. Astron. Soc. Japan*, 60, 297-301
- Zappala et al. (1989) An Analysis of the Amplitude-phase Relationship among Asteroids, *A&A*, 231, 548-560
- Ziffer et al. (2011) Near-Infrared Spectroscopy of Primitive Asteroid Families, *Icarus*, 213, 538-546

Overviews of Hayabusa2: The C-Class Asteroid Sample

Return Mission of Japan

Tatsuaki Okada

*Institute of Space and Astronautical Science, Japan Aerospace Exploration Agency
And JAXA Spece Exploration Center
3-1-1 Yoshinodai, Chuo-Ku, Sagamihara, 252-5210, Japan
Okada.tatsuaki@jaxa.jp*

Abstract — Hayabusa2, the next asteroid sample return mission, is now planned in Japan to visit a Near-Earth C-class asteroid 1999JU₃. The mission observes the asteroid in detail, collect samples from there and return them to Earth. The spacecraft and the mission design is based on the former Hayabsua. In scientific point of view, essential difference of target asteroid is its taxonomic class from S to C. We know little about an C-class asteroid but often associate it with a primitive carbonaceous chondrite. Key points to be investigated are aqueous alteration, reaction processes between organics and minerals, and physical properties of materials. In Hayabusa2, it needs the coverage of spectroscopy at 3 μm absorption band characteristic of hydrated minerals and the possible detection of unaltered fluffy material by thermo-physical properties. Optical telescopic and wide angle cameras and a laser altimeter are primarily mounted for guidance and navigation of spacecraft but also used for scientific purposes as in Hayabusa. Mobile robots will perform imaging, microscopy and radiometry of surface, complimentary to remote sensing. Impact experiment using a small-carry-on impactor (SCI) is added to excavate the surface to form a crater and surrounding ejecta. Its geometrical feature informs the surface physical properties, and the materials excavated or exposed by impact indicates the subsurface conditions. Maximum three samplings are conducted in Hayabusa2, possibly including the materials by the impact experiment. With all these experiments, Hayabusa2 will provide the data for investigation of the nature of the asteroid and its origin and evolution.

1. Introduction

Origin and evolution of the solar system has been investigated by theoretical and observational studies as well as analyses of meteorites or returned samples by space missions. Sample return provides most evident information on the past events or ancient environments preserved in each material or texture.

Hayabusa2 is the follow-on mission after Hayabusa, the first asteroid sample return in history, and also aims at investigating the nature of the asteroid and its origin and evolution processes by remote sensing and surface measurements as well as detailed analyses of returned samples.

Hayabusa was an engineering satellite to demonstrate technologies for sample return from near-earth asteroid 25143 Itokawa, and accomplished the first round trip to a body beyond the Moon. The seven years' trip started by the launch of Hayabusa by the 5th M-V launch vehicle in 2003, changed its trajectory to the asteroid by gravity assist during the Earth swing-by in 2004, arrived the asteroid after approach with optical navigation in 2005 followed by global mapping and observations of the asteroid, collected samples from there by autonomous descent and touchdown operation under micro-gravity condition, and finally returned to the Earth with the recovery of reentry capsule which has the sample container in 2010. The main technologies demonstrated are ion engine as the main thruster of spacecraft, optical autonomous navigation using imagers and laser instruments, sample collection under micro-gravity, and hypervelocity (12 km/s) direct Earth reentry from interplanetary orbit. Basically the same but some more optimized key technologies will be used in Hayabusa2.

Results of Hayabusa remote sensing experiments have been already reported, but it is summarized here that the small S(IV)-class asteroid Itokawa is less dense or porous with a low density of $1900 \pm 130 \text{ kg/m}^3$ and is found as a rubble-pile object¹⁾, must have experienced space-weathering processes on its surface^{2),3)}, has composition like an ordinary chondrite⁴⁾ and mineralogy most like an LL5-6 ordinary chondrite²⁾, has sedimentation of pebbles flown into the local gravity minimum area by gravitational force⁵⁾, and was formed by accretion of impact fragments from larger parent bodies¹⁾. High contrast of albedo, dichotomy of flat and rough terrains, and huge boulders with one tenth of the asteroid size are the important discoveries by asteroid imaging⁶⁾.

Hayabusa successfully returned a small amount of collected samples, although projectiles were not shot for sampling the surface materials. Most of samples are less than 100 μm in diameter and too small for petrology, but they are still important as the first and only intact samples from the uppermost surface of asteroid, which are lost in meteorites found on Earth. Results of returned sample analyses has been reported and summarized that most of stony particles originates from the extraterrestrial body⁷⁾⁻⁹⁾, and most of them are like an LL6 chondrite in mineralogy but some particles are less equilibrated like an LL4-5 chondrite⁷⁾. Elemental and isotopic composition shows extraterrestrial origin⁷⁾⁻⁹⁾ and similar to an LL or L chondrite^{7),10)}. Surface nano-phase FeS features show similarity to those by space weathering found in lunar regolith¹¹⁾.

After these discoveries of a S-class asteroid which is primitive and representative of inner region of solar system, the next mission to near-earth asteroid is planned to investigate a C-class asteroid, the other primitive but more enriched in volatiles and most existing type in the solar system. But there are only a few candidates in the near-earth region where a Hayabusa-class spacecraft can complete its go and return trip and retrieve samples from there to Earth. Actually the engineering is not yet matured even to conduct Hayabusa class missions so that the immediate follow-on

mission is essential to make the technology more robust and to keep the people involved in Hayabusa to continue working for the primitive body exploration. In addition, there is severe constraint on budget for space missions in Japan. Therefore, Hayabusa2 should be based on the same design concept as Hayabusa due to time and budgetary constraints. Hayabusa2 will be launched in 2014 (with backup in 2015) , cruise with iron engine as main thrusters, visit and start observation of C-class asteroid 1999JU₃ in 2018, collect samples as well as conduct experiments with surface mobile robots and a carry-on impactor, and return to the Earth for sample recovery on Earth in 2020. Basic design and characteristics of the spacecraft are shown in Fig.1 and Table 1, respectively.

The scientific aspect of Hayabusa2 is described in the following chapters. Purposes of the mission and the current knowledge of the target asteroid are shown. Specifications of science instruments and the observation plans are outlined. Surface robots and impact experiments are also introduced.

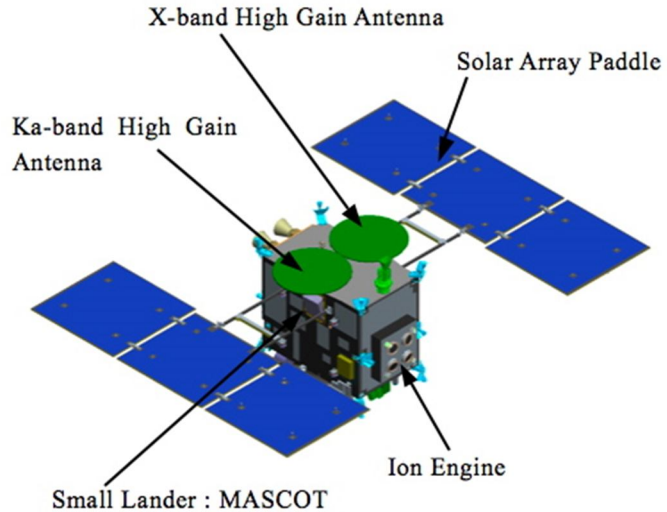


Figure 1(a). The outline of Hayabusa2 spacecraft is shown with the payloads mounted. The size of the main body is 1.6 m x 1.0 m x 1.25 m.

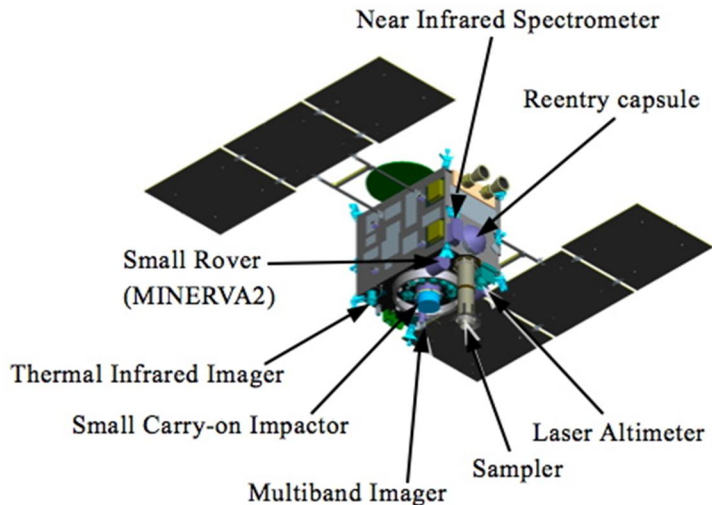


Figure 1(b). The same as in Figure 1a, but viewed from the opposite direction.

Table 1. Characteristics of Spacecraft and its schedule

| | | | |
|------------------|-----------------------------------|--------------------|---------------------|
| Size [m] | 1.6 x 1.0 x 1.25 | Target Asteroid | 1999JU ₃ |
| Mass [kg] | <600 | Trajectory [AU] | 0.96 – 1.42 |
| Attitude Control | 3 axis controlled | Schedule: | |
| Ion Thruster | 10 μ N x 4 x 1.5 yr | Launch | Dec, 2014 |
| Total Impulse | 2km/s | Earth Swing-by | Dec, 2015 |
| C ₃ | 21km ² /s ² | Asteroid Arrival | July, 2018 |
| Communication | X-band (up/down) | Asteroid Departure | Dec, 2019 |
| | Ka-band(n.a./down) | Return to Earth | Dec, 2020 |

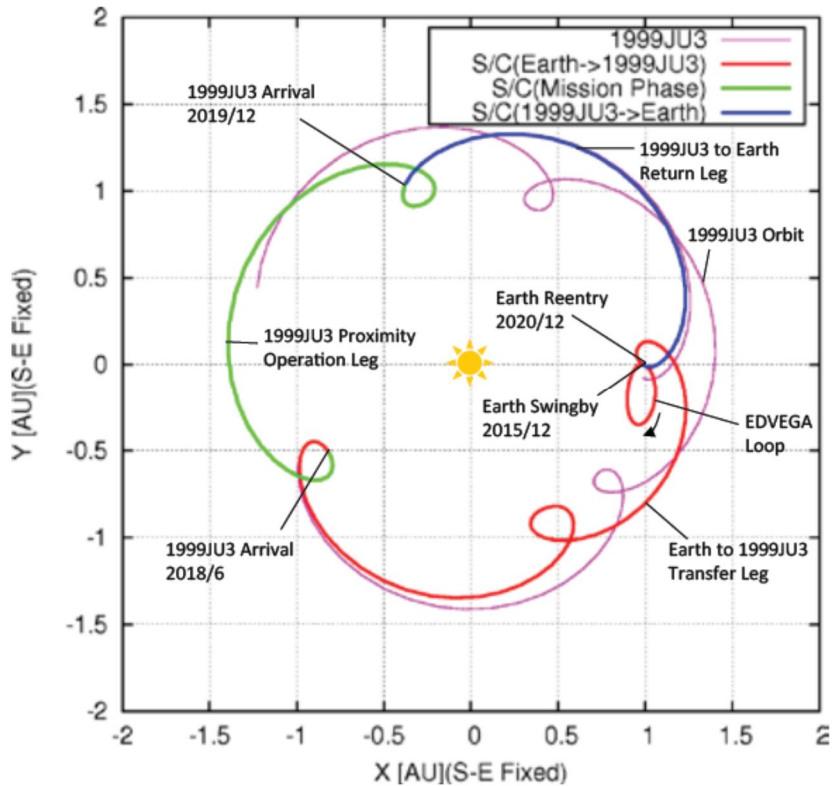


Figure 2. A trajectory of Hayabusa2 and 1999JU₃ in fixed Sun-Earth position

2. Purposes of Hayabusa2

Hayabusa2 is the follow-on mission of Hayabusa and it should have four goals for science of solar system, space technology, and exploration as well as space guard. For the science to search for a pristine clue to the origin and evolution of solar system, Earth and life, Hayabusa2 observes a primitive and volatile-rich C-class asteroid and collect samples from there to understand the nature of the primitive small body and investigate the early solar system origin and evolution. Key technologies demonstrated in Hayabusa should be made more robust, and new technical challenges such as Ka-band transponder and impact experiment are added. For the frontier exploring the new world, Hayabusa2 will visit a C-class asteroid, most representative of outer region of solar system primitive body, and land there for the first time of human history. For the space guard, the nature of most existing type of potentially hazardous body will be known.

The science targets aims at finding relics of solar system evolution to investigate the environments and interactions materials underwent from the solar nebula to an

asteroid, and at investigating the analogue to planetesimals to understand the formation and physical state of small bodies even if the body is primordial or rubble-piled.

In order to answer these targets, main science objectives of Hayabusa2 are described here and also shown in Fig.3. They are to investigate global heterogeneity of materials, mineral-ice-organics interaction in solar system, thermal evolution and surface processes on asteroid, and impact fragmentation and accretion processes of asteroid.

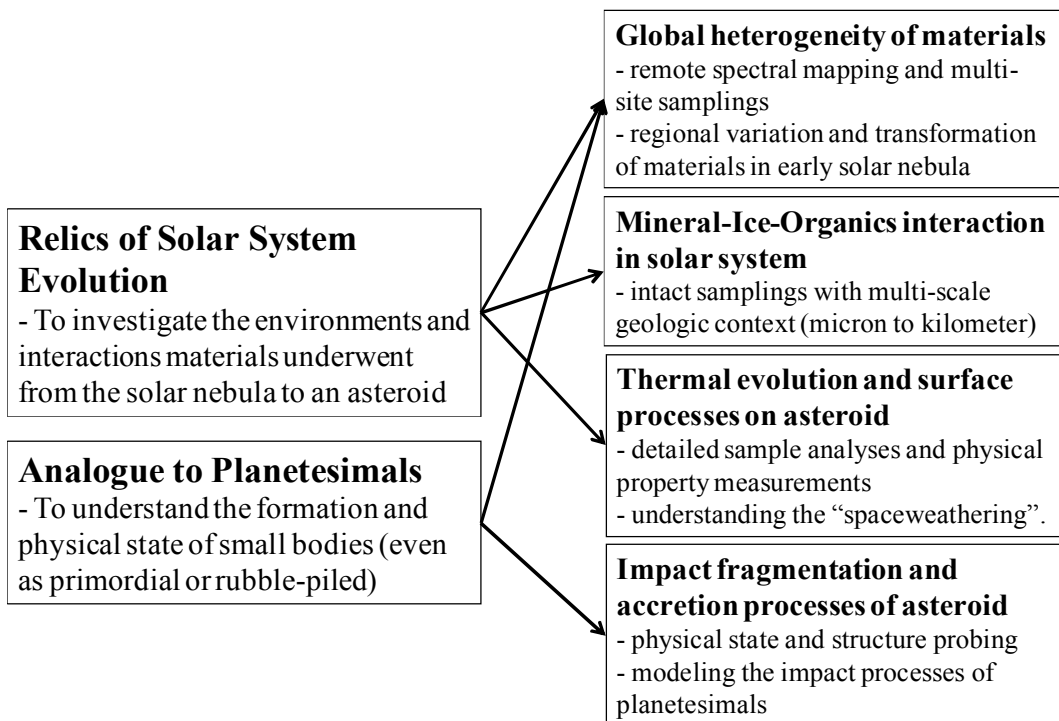


Figure 3. Science targets of Hayabusa2 with two main goals and four objectives to be investigated by remote sensing observations, surface experiments, and the analyses of returned samples

3. Target asteroid 1999JU₃

The target asteroid to be visited by Hayabusa2 is 1999JU₃, a near-earth and C-class asteroid. The characteristics ever obtained by ground-based observations are compiled in Table 2. The important points are the orbital elements accessible for sample return (a small inclination and near terrestrial heliocentric distance), and the low rotation rate sufficient for touchdown operation (longer than six hours). Rotation pole declination is also important but it is difficult to decide because 1999JU₃ is considered of relatively rounded shape and the aspect ratio is almost unity¹²⁾. The asteroid is classified as C-class but the signal-to-noise ratio is not enough to determine which type of meteorite is best suited to the spectrum or whether the asteroid has 0.7 μm absorption band or not. The band corresponds to hydrated minerals that is found for CM2 meteorite, whose existence in the spectrum of 1999JU₃ was once reported in the previous work¹³⁾. The asteroid has thermal inertia estimated 200-600 (latest data shows 200-300) Jm⁻²s^{-0.5}K⁻¹¹⁴⁾, which indicates the asteroid surface is covered mainly with pebbles, or relatively smoother than that of Itokawa. The shape model of 1999JU₃ is shown in Fig.4.

Now the main science targets of Hayabusa2 at 1999JU₃ are to observe the regional variation of visible-to-near-infrared absorption band and to search for the past aqueous alteration in parent body and thermal alteration during trajectory to the current near earth orbit.

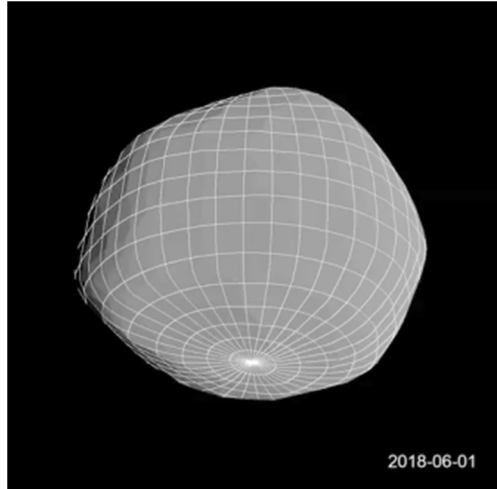


Figure 4 Shape model of 1999JU³¹⁴⁾.

Table 2. Compilation of 1999JU³ characteristics¹⁴⁾

| | |
|-------------------------------|--|
| Taxonomic Type ¹³⁾ | Cg |
| Diameter (D _{eff}) | 0.87±0.03 km |
| Axis ratio ¹²⁾ | 1.3 : 1.1 : 1.0 |
| Rotation period | 7.63±0.01 Hr |
| Pole axis(λ,β) | (73, -62) |
| Albedo (P _v) | 0.070 ± 0.006 |
| H ¹²⁾ | 18.82 ± 0.021 |
| G ¹²⁾ | -0.110 ± 0.007 |
| Thermal Inertia | 200 – 600 Jm ⁻² s ^{-0.5} K ⁻¹ |
| Orbit (solar distance) | 0.9633 – 1.4159 AU |

4. Science Instruments on Hayabusa2

Science instruments to be mounted on Hayabusa2 have been decided to achieve the above science targets and due to technical constraints. Their specifications are tabulated in Table 3

4.1 Optical Imagers:

Optical imagers are to map the whole shape and surface geomorphology of the asteroid, as well as to district the geologic units by albedo and color ratios. Three charge-coupled device based cameras ONC-T, -W1, and -W2 are primarily prepared and used for navigation and guidance of spacecraft, but also performed as scientific imagers. ONC-T is a telescopic camera of 1024 x 1024 pixels, 5.7° x 5.7° field of view and equipped with eight points filter wheel. ONC-T will be mainly used for asteroid shape model and geologic mapping. Its spatial resolution is expected about 2 m per pixel from Home Position at 20 km altitude from the asteroid, 50cm, 10cm, 1cm per pixel from 5 km, 1 km and 100 m altitude, respectively. So ONC-T can image both of the global shape and the regional high-resolved images. Color ratios could detect the regional distribution of differently altered materials, especially for

possible existence of hydrated minerals by 0.7 μm band, and for possible volatile loss due to the past heating process by lower ratio at $< 0.5 \mu\text{m}$ wavelength. ONC-W1 and W2 are the nadir- and side-looking wide angle imagers, respectively, to cover $60^\circ \times 60^\circ$ field of view. ONC-W1 is mainly used for navigation and guidance and could be also used as monitoring cameras for other instruments.

4.2 LIDAR

LIDAR (Light detection and ranging) based on YAG laser ($1.064 \mu\text{m}$) is prepared as the altimeter for navigation and guidance. It ranges 30 m to 25 km with high linearity with 1 m and 5 m uncertainty for low and high gain mode, respectively. It will be also used for science such as surface altitude distribution, reflectance mapping, and gravity measurement if doppler measurement of radar tracking with the ground station is performed at the same time. With the ONC images, the position of the spacecraft relative to asteroid will be determined. Time series detection mode are added for possible observation of dusts above the asteroid surface which are floating by natural electromagnetic forces or micro-meteoritic impacts or after impact experiments of Hayabusa2.

4.3 NIRS3

NIRS3 is a near-infrared spectrometer to observe asteroid surface from 1.9 to 3.2 μm , which can cover the 3 μm band of hydrated minerals. NIRS3 is expected to determine the existence and composition of hydrated minerals indicating the past aqueous alteration in the parent body. It is expected to map its regional distribution. NIRS3 is a point spectrometer so that scanning of spacecraft is necessary to map the whole surface of asteroid. The footprint is about 40 m and 2 m from Home Position at 20 km altitude and lower altitude at 1 km, respectively. More than 50 signal to noise ratio is required to distinguish between the different carbonaceous chondrite types such as CI and CM. To achieve this S/N ratio, 5 to 10 seconds of time integration is necessary which makes the spatial resolution worse by the accuracy of spacecraft attitude control.

4.4 TIR

TIR is a thermal infrared imager, based on an un-cooled bolometer array of 320×240 effective pixels, with $8\text{-}12 \mu\text{m}$ band. TIR has a field of view $16^\circ \times 12^\circ$ and the spatial resolution is 20 m, 1 m, and 10 cm from Home Position at 20 km altitude, 1 km and 0.1 km, respectively. TIR will map thermal emission and surface temperature of asteroid as well as thermo-physical properties there. Averaged thermal inertia of 1999JU³ is estimated 200 to $600 \text{ Jm}^{-2}\text{s}^{-0.5}\text{K}^{-1}$ ¹⁴⁾ and most like 200 to 300. Thermal inertia indicates physical conditions of regolith especially in particle size such as 50 (50-100 μm like lunar regolith), 100-200 (0.1-1 mm), 200-300 (1-10 mm), 300-500 (1-10 cm like Itokawa flat terrain), 500-1000 (0.1-1 m like Itokawa rough terrain). Thermal inertia indicates physical properties of rocks in porosity such as 1000-2000 (porous rock) and >2000 (dense rock). This indicates the altered materials are relatively dense but unaltered primordial materials are considered less dense, which could be distinguished each other. The surface condition will be determined even from Home Position.

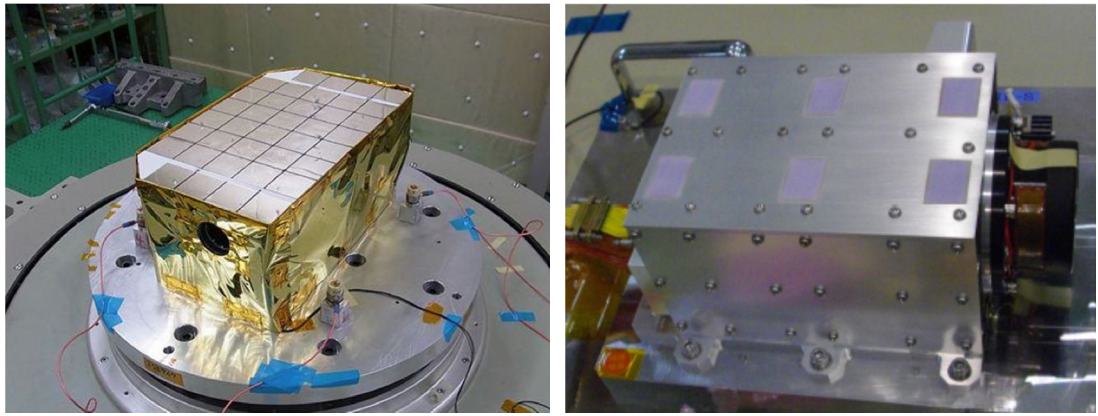


Figure 5. NIRS3-S proto-model (left) and TIR-S flight model (right).

4.5 Sampling Device

Hayabusa2 is an asteroid sample return mission and the sampling device is basically the same as that of Hayabusa¹⁵⁾. It is “Impact Sampling” device that consists of a gun unit that can shoot three tantalum projectiles at 300 m/s, one meter long extendable horn to collect materials excavated by impact, and the sample catcher placed at the focal point of the horn that has three rooms inside it to discriminate the samples collected at different sites. The catcher is moved into the reentry capsule and sealed with the lid of capsule to preserve volatile components and avoid contamination from terrestrial air. Contamination control is essential for sample return mission. Materials used for the sampling device is considered not to contaminate the samples as much as possible. Purified nitrogen purging during the flight model test is required as well as the clean of the device before its delivery.

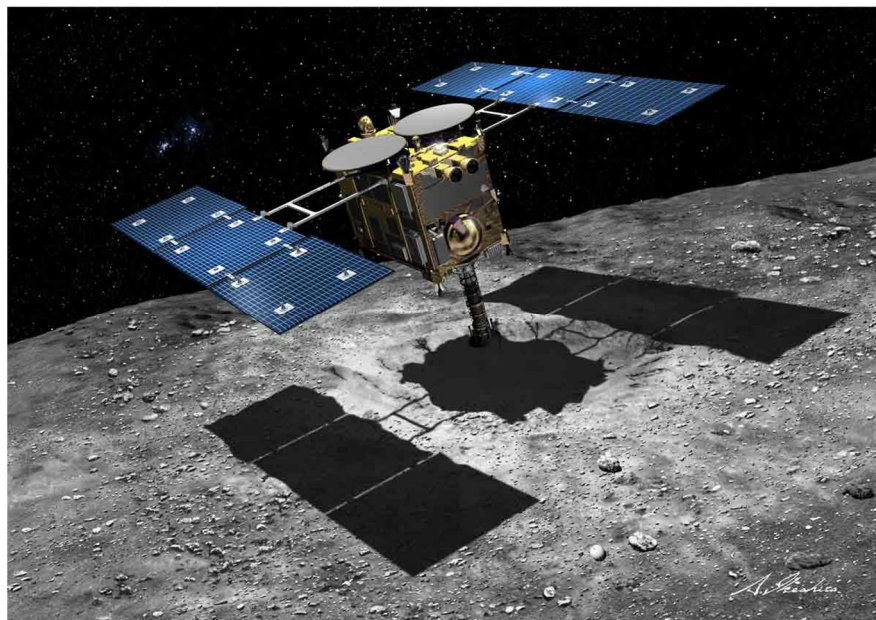


Figure 6. Schematic view of sampling by the horn shaped sampling device at the excavated crater impacted by SCI [courtesy of Akihiro Ikeshita]

4.6 Surface Robot Experiment (MINERVA-II, MASCOT)

Surface robotic experiments are planned by Japanese small robots named MINERVA-II-1A, MINERVA-II-1B, and MINERVA-II-2. The former two will be deployed simultaneously from the spacecraft. They are the same design concept as MINERVA on Hayabusa, with mobility by inside wheels and powered by solar

paddles. They will mount imagers for landscapes and surrounding geologic observations, visible spectrometer, and ultra-violet light emission diode to make fluorescence of organic matters if they exist. MINERVA-II-2 will be developed by the consortium of universities.

The other robotic experiment is planned by European community named MASCOT (Mobile Asteroid Surface Scout)¹⁶⁾. It is a 10 kg-class lander with mobility by inside rotating arms and powered by lithium primary battery. It works during the whole asteroid day, for the maximum life time of 16 hours (2 asteroid days). MASCOT will carry four science instruments: CAM (a wide angle imager), MARA (multi-band thermal radiometer), MAG (magnetometer), and MicrOmega (infrared hyper-spectral microscope). CAM images the surface and the landscape with 75° field of view during the day, and multi-color images using the light emission diode array with 470, 530, 640 and 870 nm for mineral information¹⁷⁾. MARA measures the radiation from the surface through the asteroid rotation and accurately determines surface thermal inertia, and obtain mineral information using six bands. MAG has three axis fluxgate magnetometer at 1nT accuracy and detect magnetism of asteroid if it exists. MicrOmega will image the surface by 20 μm spatial resolution and several mm area with spectrally scanning light from 0.9 to 3.5 μm by acousto-optical tunable filter (AOTF)¹⁸⁾. It is expected to detect hydrated minerals and organics particle to particle, as well as the surface condition directly (although some compaction is happened by this instrument). MASCOT is complimentary to the global scale observation by remote sensing and the micro scale analysis of returned samples.

4.7 Impact Experiment

Asteroid impact experiment is planned to investigate the excavated materials that might be free from space-weathering (uppermost surface), heating by solar radiation in history (several centimeter), or galactic cosmic ray radiation (one meter), as well as physical properties of asteroid surface constrained by crater dimension, ejecta sedimentation, and ejecta escaping velocity. Small Carry-on Impacter (SCI) will be mounted on Hayabusa2, which will be deployed from the spacecraft at 500 m altitude and from SCI a copper liner of 2 kg will be shot to the asteroid surface at 2 km/s. The crater and surrounding ejecta will be observed by remote sensing instruments, possibly followed by sampling from there. An optional small deployable imager DCAM will take the on-time images of the liner impacting the surface and ejecta materials escaping from the asteroid.

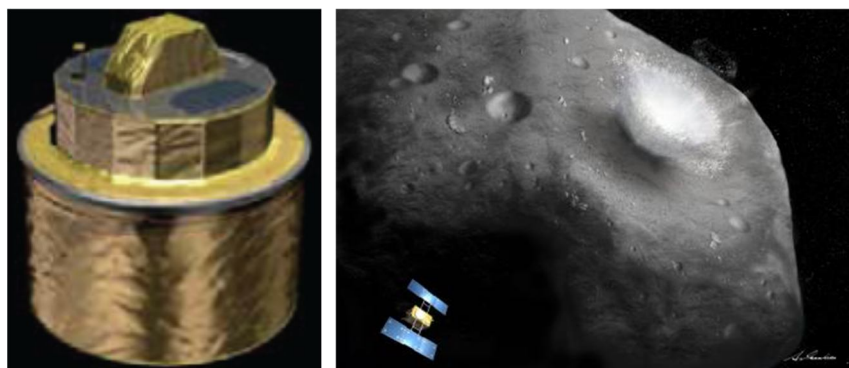


Figure 7. SCI and the impact experiments [courtesy of Akihiro Ikashita]

Table 3. Specifications of Science Instruments

| Payloads | Specifications |
|---------------------------------|--|
| Multiband Imager (ONC-T) | Wavelength: 0.4 – 1.0 mm, FOV: 5.7 deg x 5.7 deg, Detector: 1024 x 1024 px (e2v, Si-2D CCD) Filter (ul, b, v, w, x, p, 590nm, wide) (modified from Hayabusa) |
| Wide-angle Imager (ONC-W1 / W2) | Wavelength: 0.4-0.7 mm, FOV: 60 deg x 60 deg, Detector: 1024 x 1024 px (e2v, Si-2D CCD), (modified from Hayabusa) |
| Near IR Spectrometer (NIRS3) | Wavelength: 1.8 – 3.2 mm, FOV: 0.1 deg x 0.1 deg Detector: 128 pix, (Hamamatsu, InAs linear array) (New development) |
| Thermal IR Imager (TIR) | Wavelength: 8 -12 mm, FOV: 12 deg x 16 deg, Detector: 320 x 240 pix (NEC 320 uncooled bolometer) (Heritage: LIR on Akatsuki) |
| Laser Altimeter (LIDAR) | NdYAG laser: 1064 nm, Range: 30m – 30km, $\delta X=1m$ (Heritage: Hayabusa) |
| Sampler (SMP) | Sampling by projectile impacts, 3 shots (max) (Minor modification from Hayabusa) |
| Small Carry-on Impactor (SCI) | Impact of 2kg Cu projectile at 2km/s, an artificial crater formation on the asteroid surface (New development) |
| Small Rover (MINERVA-II) | Modified from MINERVA of Hayabusa, Totally 3 robots (1A, 1B, 2) with cameras and thermometers (Heritage: Hayabusa) |
| Small Lander (MASCOT) | Wide Angle Camera, MicrOmega(IR spectro-microscope), MARA (thermal emission), Magnetometer in 10kg package, Heritage of ROSETTA/Philae (DLR + CNES) |
| Radio Science | X-band (Ka-band) Doppler-shift measurement and ranging. |

5. Observation Plans of Hayabusa2

Hayabusa2 has a scenario for science observations of 1999JU₃. Just after the arrival at Gate Position just outside of Hill radius of the asteroid, performances of all the instruments are checked. Consequently the observation will start to understand the state of asteroid, select the landing sites, and plan the safe landing for sample collection. Figure 8 shows a scenario of observation plan of Hayabusa2.

5.1 Observation of the whole body to understand the state of asteroid

Before arrival of asteroid, ONC and TIR will observe the asteroid to compare with earth based observations. At Home Position, ONC and TIR will start observations for global mapping to construct shape model with rotation axis, albedo or color ratio map, or thermal model of the whole asteroid. Depending on the rotation axis of asteroid, it takes time to cover the whole surface, and the color ratio maps and thermal models are much improved using the data from different solar phase angles and at different solar distance. NIRS3 will start the surface spectroscopy by scanning the attitude of spacecraft.

5.2 Selection of candidate landing sites

After the initial models or maps are constructed for asteroid shape, geomorphology, albedo and color ratio, mineralogy and hydrated degree, and thermo-physical properties including temperature, several candidate landing site will be listed for sample collection or surface robot experiments. With lower altitude operation on the sub-Earth line, gravity of asteroid will be determined by LIDAR within a practical uncertainty. Gravity and the necessary fuel consumption for

operation could constrain the maximum numbers of descent operation during the mission.

In Hayabusa2, the priority of landing site is higher from unaltered pristine, hydrated, and dehydrated materials. They could be determined or constrained by spectroscopy at 3 μm band, but other information on geology, mineralogy, surface physical conditions should be provided by ONC and TIR. The target site must have a geologic unit of 50 to 100 m size if the error of navigation and guidance is considered, and the geologic unit is mapped by ONC. The most desired samples to be collected should have the size of several hundred microns to a few millimeters because they include all the necessary petrologic features. The typical size of surface materials is constrained from thermal inertia by TIR.

5.3 Final decision of landing sites

At low altitude 1-5 km, higher resolved imagery is conducted at some candidate sites. Not only the materials but also the surface conditions could be precisely observed at 1 m or less spatial resolution by ONC or TIR, and the safe descent operation is numerically simulated from the engineering point of view. Detailed local measurements are also performed for scientific point of view to investigate the nature of asteroid.

5.4 Descent operation for rehearsals, deployment of robots

At the lower altitude at 100m or lower the close-up images will be taken to understand the surface physical properties around the landing sites, especially by ONC and TIR. Surface robots will observe the materials, conditions, and physical properties directly on the surface. These data could be used for scouting the later landing sites for robots or sampling sites.

5.5 Touchdown operations and sample collections

For the samplings, the spacecraft will autonomously touch the surface and collect materials by impact sampling method and soon ascend to the safety altitude. During the low altitude, ONC-W1 and TIR will take images at a few centimeter resolution around the touchdown sites. In Hayabusa2, three samplings is planned if technically feasible in terms of asteroid surface condition, state of spacecraft, or fuel remained for Earth return.

5.6 Impact experiment

Since it is hazardous for Hayabusa2, impact experiment should be done after other operations finished such as global remote sensing, surface robot experiments, and at least one sampling. If successful, a crater will be formed with ejecta blanket surrounding it. It might be searched by TIR or ONC at Home Position or at 1 to 5 km altitude. If the ejecta is larger than 10 m, spectroscopy by NIRS3 could be done by scanning the spacecraft for excavated materials. Dimension of crater and ejecta will be measured to understand the physical properties of asteroid surface by ONC and TIR.

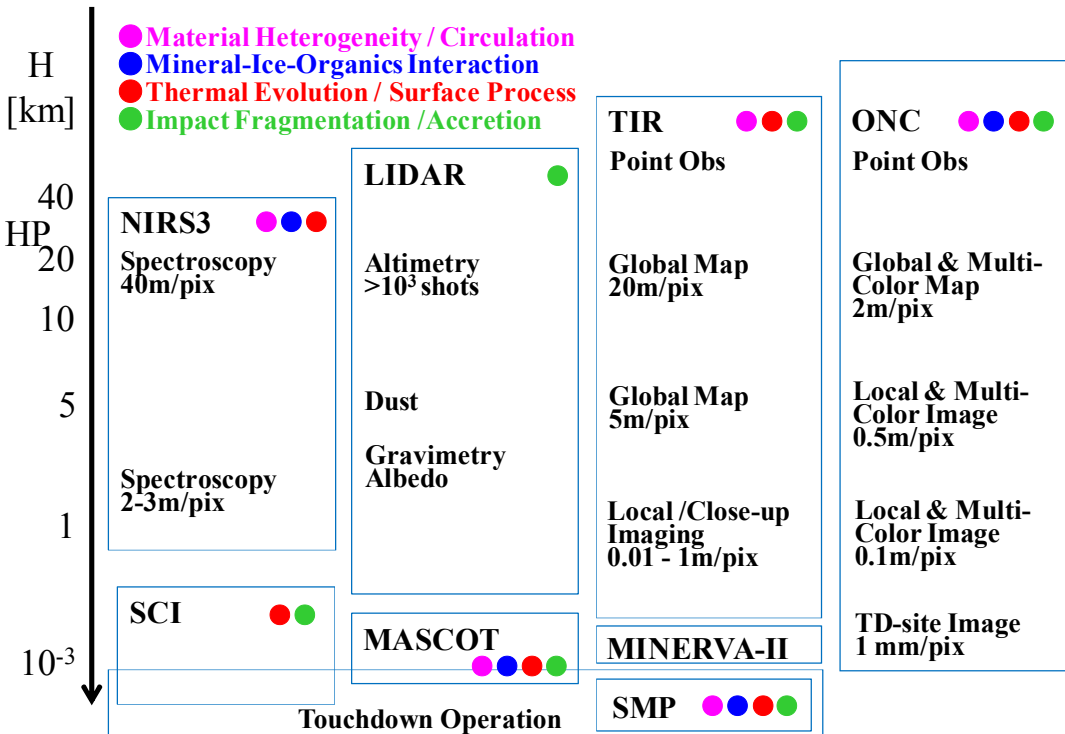


Figure 8. Observation plans of Hayabusa2 with remote sensing, surface robots, impact experiments, and samplings

6. Concluding Remarks

Hayabusa2 is the next near-earth asteroid sample return mission in Japan to visit a C-class asteroid 1999JU₃ and observes the asteroid, collects samples from its surface, and returns them to the Earth. The basic design of the spacecraft and the mission design as well as the key technology used in this mission is basically the same as those of Hayabusa. But the potential significance of science in Hayabusa2 is so strong enough to conduct another mission to a primitive asteroid. Thus Hayabusa2 is the immediate follow-on mission of Hayabusa, using the heritage of it.

The science targets are somewhat different from those of Hayabusa because the asteroid to be explored is a C-class, associated with more volatile-rich and primitive meteorites. Thus the main target is to find the clue to the origin and evolution of the solar system, Earth, and life. In addition, the asteroid is the new frontier which is the representative of outer region of the solar system and never visited so far.

Science instruments are different from Hayabusa to optimize the observation and sampling site selection of C-class asteroid. NIRS3 will cover 3 μ m absorption band indicating the hydrated minerals, and TIR will take thermograph images of asteroid that inform on the thermo-physical properties which are distinguishable between primordial fragile and altered dense materials, or determine surface physical condition. ONC and LIDAR are primarily prepared for navigation and guidance of spacecraft but also used as science instruments for shape modeling, geomorphology, geologic units by color ratios, indication of hydrated materials, and gravity measurements.

Sampling device is basically the same as that of Hayabusa with some minor optimization such as three individual rooms for samples collected at different sites, and more complete sealing of volatiles.

Surface experiments which failed to land in Hayabusa will be done in Hayabusa2

with three Japanese small robots and with European led 10 kg-class robots called MASCOT. They will conduct *in situ* measurements on the asteroid surface, and provide information on the geologic context and possibly for scouting the later samplings or the other rover missions.

Impact experiments will be done with SCI to excavate the surface by impact to form a crater with ejecta blanket. This will be another target of remote sensing to investigate the subsurface materials free from influences by space-weathering, past heating by sunlight, and GCR to investigate the surface processes experienced. Dimensions of crater and ejecta will indicate the surface physical properties.

With these experiments, Hayabusa2 could answer questions of origin and evolution of the early solar system and processes that happened on the small bodies. Ground-based observations help understanding the nature of asteroid and preparing the instruments and observation plans prior to arrival at the asteroid. Currently the knowledge of the asteroid is still incomplete and more supports of ground observations are expected especially in spectroscopy, rotation axis, and thermal models.

Acknowledgments

The author appreciates all the members of Hayabusa2 project to propose, design and develop the spacecraft and the onboard science instruments. The author would like to thank all the science members of Hayabusa2 to have many discussions and improve the science scenario and observation plans. The author would give special thanks to local organizing committee members to hold the meeting in Macau.

References

- 1) Fujiwara, A. et al. (2006), The rubble-pile asteroid Itokawa as observed by Hayabusa, *Science* 312, 1330-1334.
- 2) Abe, M. et al., (2006), Near-infrared spectral results of asteroid Itokawa from the Hayabusa Spacecraft, *Science* 312, 1334-1338.
- 3) Hiroi, T., et al. (2006), Developing space weathering on the asteroid 25143 Itokawa, *Nature* 433, 56-58.
- 4) Okada, T. et al., (2006), X-ray fluorescence spectrometry of asteroid Itokawa by Hayabusa, *Science* 312, 1338-1341.
- 5) Miyamoto, H. et al., (2007), Regolith migration and sorting on asteroid Itokawa, *Science* 316, 1011-1014.
- 6) Saito, J. et al., (2006), Detailed images of asteroid 25143 Itokawa from Hayabusa, *Science* 312, 1341-1344.
- 7) Nakamura, T. et al., (2011), Itokawa dust particles: a direct link between S-type asteroids and ordinary chondrites, *Science* 333, 1113-1116.
- 8) Nagao, K. et al, (2011), Irradiation history of Itokawa regolith material deduced from noble gases in the Hayabusa samples, *Science* 333, 1128-1131.
- 9) Yurimoto, M. et al, (2011), Oxygen isotopic compositions of asteroidal materials returned from Itokawa by the Hayabusa mission, *Science* 333, 1116-1118.
- 10) Tsuchiyama, A. et al, (2011), Three-dimensional structure of Hayabusa samples: origin and evolution of Itokawa regolith, *Science* 333, 1125-1128.
- 11) Noguchi, T., et al., (2011), Incipient space weathering observed on the surface of Itokawa dust particles, *Science* 333, 1121-1125.
- 12) Abe, M. et al. (2008), Ground-based observational campaign for asteroid 162173 1999JU₃, COSPAR Scientific Assembly, B04-0061-08.
- 13) Vilas, F. (2008), Spectral characteristics of Hayabusa2 near-earth asteroid targets

- 162173 1999JU₃ and 2001QC34, Astron. J., 135, 1101-1105.
- 14) Mueller, T.G. et al. (2011), Thermo-physical properties of 162173 (1999JU₃), a potential flyby and rendezvous target for interplanetary missions, A&A, 525, A145 (pp.6).
 - 15) Yano, H. et al., (2006), Touchdown of the Hayabusa spacecraft at the Muses See on Itokawa, Science 312, 1350-1353.
 - 16) Ho, T.M., et al., (2012), A mobile surface science package – MASCOT – for in situ characterization of asteroids, Asteroids, Comets, Meteors 2012, #6138.
 - 17) Schmitz, N. et al., (2012), Context for the MASCOT lander on Hayabusa-2 – the MASCOT-CAM, Asteroids, Comets, Meteors 2012, #6141.
 - 18) Bibring, J.-P., et al, (2012), MicrOmega: an hyper-spectral NIR microscope on board Hayabusa2, Asteroids, Comets, Meteors 2012, #6399.

Scientific Use Of LIDAR data Of Hayabusa-2 Mission

N. Namiki¹, T. Mizuno², N. Hirata³, H. Noda⁴, H. Senshu¹, R. Yamada⁴, H. Ikeda⁵, S. Abe⁶, K. Matsumoto⁴, S. Oshigami⁴, M. Shizugami⁴, F. Yoshida⁴, N. Hirata⁷, H. Miyamoto⁷, S. Sasaki⁸, H. Araki⁴, S. Tazawa⁴, Y. Ishihara⁹, M. Kobayashi¹, K. Wada¹, H. Demura³, J. Kimura¹⁰, M. Hayakawa², and N. Kobayashi²

¹Chiba Institute of Technology, Narashino, Japan 275-0016,

²The Institute of Space and Astronautical Science, JAXA, Sagamihara, Japan 252-5210,

³The University of Aizu, Aizu-Wakamatsu, Japan 965-8580,

⁴National Astronomical Observatory of Japan, Oshu, Japan 023-0861,

*⁵Aerospace Research and Development Directorate, JAXA, Tsukuba, Japan 305-8505,
⁶Nihon University, Funabashi, Japan 274-8501,*

⁷The University of Tokyo, Tokyo, Japan 113-0032,

⁸Osaka University, Suita, Japan 565-0871,

⁹National Institute of Advanced Industrial Science and Technology, Tsukuba, Japan 305-8568,

¹⁰Tokyo Institute of Technology, Tokyo, Japan 152-8550.

Abstract — LIDAR is one of four remote-sensing instruments onboard Hayabusa-2, and is used to measure altitudes of the spacecraft from a surface of the asteroid, 1999 JU₃, for not only secure navigation but also scientific investigation of a C-type asteroid. Hayabusa-2 LIDAR has been improved from that onboard Hayabusa which explored and returned samples from asteroid 25143 Itokawa. The wavelength of laser pulse is 1064 nm. The shortest and longest distances to be measured are 30 m and 25 km, respectively. An accuracy of range measurement is dependent on both random and bias errors, and are 0.845 m at 30-m altitude, and 2 m at 20-km altitude. The range resolution is 0.5 m and the fastest rate of data acquisition is 1 Hz. We plan to use LIDAR data for studies of 1999 JU₃, such as shape modeling, gravity measurement, albedo mapping, and detection of asteroid dust. The shape model will be developed from camera images and LIDAR range data. Non-dimensional shape is estimated using images taken from various configurations, and LIDAR range data determines its length scale. Mass is also essential for geodetic study of C-type asteroid. We let the spacecraft descend toward 1999 JU₃ from 20-km to 1-km altitudes without orbital maneuvers, and let the spacecraft ascend freely as well. Such experiments will be conducted 2 to 6 times to improve an accuracy of the estimate depending on the physical characteristics of the asteroid such as gravity, rotation axis and surface temperature. LIDAR is an active sensor unlike other instruments on Hayabusa-2. Ratio of transmitting and receiving powers can be directly translated to geometric albedo at the surface of 1999 JU₃. Further, we take an advantage of a wide dynamic range of Hayabusa-2 LIDAR for the first detection of dusts possibly levitating around the asteroid. A new function called dust count mode is implemented to Hayabusa-2 LIDAR to observe spatial distribution of dust number density in 8 levels with resolution of 20 m in bore sight direction.

1. Introduction

The Japanese first asteroid mission, Hayabusa, visited at the small asteroid 25143 Itokawa in September, 2005. Images taken by Hayabusa are combined with other remote sensing observations revealing that this asteroid as small as 500 m in the longest axis is the first rubble-pile body identified in our solar system [Fujiwara *et al.*, 2006]. Despite of several serious failures of the spacecraft occurred during and after rendezvous, Hayabusa successfully retrieved samples from the surface of 25143 Itokawa to the Earth in 2010 to reveal unpredicted nature of a very small asteroid [Abe *et al.*, 2006; Fujiwara *et al.*, 2006; Miyamoto *et al.*, 2007; Barnouin-Jha *et al.*, 2008; Hirata *et al.*, 2009].

JAXA and collaborating scientists are now developing the second asteroid mission named "Hayabusa-2". Hayabusa-2 is based on a heritage of the first Hayabusa. At the same time, Hayabusa-2 is improving engineering and scientific achievements of the first Hayabusa, and also challenging new technologies. Furthermore, target asteroid is different from that of the first Hayabusa. The asteroid 25143 Itokawa explored by Hayabusa is silicate-rich S-type. On the other hand, Hayabusa-2 is visiting a C-type asteroid, (162173) 1999 JU₃. The C-type asteroids are one of the most primordial types and are possible to contain organic matters and hydrated minerals. Thus an exploration of this type asteroid enables to study fundamental questions regarding the formation of our solar system and origin of life. Primordial organic matters and water existed in the solar system, and their relations to life and ocean water on the Earth are particularly important for planetary sciences.

The target asteroid 1999 JU₃ was discovered on 1999 May 10 by the Lincoln Near-Earth Asteroid Research survey at Socorro. It is one of the near-Earth asteroid whose orbit is suitable for the sample return mission by a small spacecraft (Table 1). The most important point is that 1999 JU₃ is the C-type asteroid which is rare in the near Earth region. The majority of the near-Earth asteroid are S-type. Thus this asteroid provides a unique opportunity for Hayabusa-like small asteroid missions. Physical parameters of this asteroid have been extensively examined during the close encounter with the Earth in 2009 (Table 2), and were updated by the most recent encounter [Moskovitz *et al.*, 2013].

Table 1. Orbital parameters of 1999 JU₃.

| Parameter | Value |
|---------------------|------------------------|
| Semi-major axis | 1.190 AU |
| Eccentricity | 0.190 |
| Inclination | 5.884 degree |
| Perihelion distance | 0.963 AU |
| Aphelion distance | 1.4159 AU |
| Orbital period | 473.9 days (1.30 year) |

An architecture of the Hayabusa-2 spacecraft is developed on the basis of the first Hayabusa, with some improvements and new challenges from the original design. For example, four ion engines of Hayabusa-2 are reinforced 25 % from old ones in order to travel farther distance than the orbit of 25143 Itokawa.

The launch windows to reach 1999 JU₃ are limited. Hayabusa-2 needs to depart from the Earth in 2014 in either early December 2014, or July 2015. After Earth swing-by in December 2015, Hayabusa-2 will arrive at the asteroid in June 2018. During rendezvous phase of about one and half year, the asteroid will be observed

carefully to reveal the shape and the surface properties by Multiband Imager (ONC-T), Near Infrared Spectrometer (NIRS3), Thermal Infrared Imager (TIR), and Laser Altimeter (LIDAR). In addition, Hayabusa-2 releases small rovers , MINERVA-II-1a, -1b and -2, and a lander named MASCOT which is developed and provided by ESA. Hayabusa-2 will touchdown on the surface of the asteroid twice to capture the surface materials in sampling device. Finally Small Carry-on Impactor (SCI) will be released to fire an impactor of approximately 2 kg in weight from 500 m above the surface to create a crater of several meters in diameter at the asteroid surface. SCI attempts to excavate fresh, less altered samples buried below the surface for remote-sensing observation and the third sampling, if possible. Hayabusa-2 leaves the asteroid in December 2019, and will come back to the Earth in December 2020 bringing back the samples in the capsule. Those samples will be distributed to scientists in the world for detailed analysis.

Table 2. Physical properties of 1999 JU₃.

| Parameter | <i>Kawakami et al.</i> [2010] | <i>Müller et al.</i> [2011] |
|--------------------------------|--|--|
| Rotation period | 7.63 ± 0.06 hours | 7.63 ± 0.01 hours |
| Spin axis (λ, β) | 331 ± 10 degree, 20 ± 10 degree | 73 degree, -62 degree |
| Aspect ratio | $1.3 : 1.1 : 1.0$ | |
| Diameter | 0.92 ± 0.12 km | 0.87 ± 0.03 km |
| Albedo | $0.063 + 0.020 / - 0.015$ | 0.070 ± 0.006 |
| Absolute magnitude | 18.82 ± 0.02 | |
| Thermal Inertia | $> 500 \text{ J m}^{-2} \text{ s}^{-0.5} \text{ K}^{-1}$ | $200 - 600 \text{ J m}^{-2} \text{ s}^{-0.5} \text{ K}^{-1}$ |
| Taxonomic type | C | |

LIDAR measures altitudes of the spacecraft from a surface of the asteroid by taking a time of flight of laser pulse. As a part of Attitude and Orbit Control System (AOCS), the LIDAR data are used for navigation of the spacecraft. The data are particularly important during touchdown operation. Besides, the LIDAR data are served for scientific analysis of the shape, mass, and surface properties of the asteroid in order to elucidate physical evolution of minor bodies such as impact fragmentation and coagulation. We also wish to expand outcomes of Itokawa exploration by examining uniformity and variation of porosity within rubble-pile body and detecting dusts levitating above the surface of asteroid. The remote sensing observations of Hayabusa-2 will be carried out from Home Position (HP), middle altitude, and low altitude whose distances from the asteroid surface are nominally 20 km, 5 km, and 1 km, respectively. We discuss in detail goals of scientific observations and operation plans of Hayabusa-2 LIDAR.

Design of Hayabusa-2 LIDAR is based on that of the first Hayabusa (Table 3) [*Mukai et al.*, 2007; *Mizuno et al.*, 2010]. The size and weight are 240 x 240 x 230 mm (Figure 1) and 3.7 kg, respectively. Gray part shown in Figure 1 is two telescopes for transmitting and receiving laser. Laser pulses of 10 mJ at 1064 nm wavelength are emitted from a passive Q switched Nd:YAG laser at 1 Hz at fastest. The 1-mrad

divergent beam corresponds to surface footprint diameter of 20 m at HP. A Cassegrain type telescope of 127 mm in diameter is used as a primary receiver to measure distance longer than 1 km. In addition, another receiver optics is implemented for range measurement shorter than 1 km and longer than 30 m. Light reflected from the surface is refocused onto a silicon avalanche photodiode through a narrow band-pass interference filter. All optics are aligned on optical bench shown by purple color (Figure 1). Detector and electronics are implemented in a chassis shown by green color in Figure 1. Telemetry and command are transferred between LIDAR and the ground station via AOCS. The range data passed to AOCS are used to keep the spacecraft in a safe distance from the asteroid or control touchdown approach. LIDAR has large radiator shown in light blue in Figure 1, because thermal environment at the time of touchdown is very severe commonly for all instruments onboard Hayabusa-2.

Table 3. Specification of Hayabusa-2 LIDAR.

| Parameter | Value |
|------------------------------|---|
| Altitude range | 30 m ~ 25 km or longer |
| Range resolution | 0.5 m |
| Range accuracy (1σ) | ± 1 m or less (at 30-m altitude) ± 5.5 m or less (at 25-km altitude) |
| Pulse repetition rate | 1 Hz |
| Receiver telescope | Cassegrain type |
| Telescope diameter | 127 mm |
| Pulse energy | 10 mJ or more |
| Pulse width | 10 nsec or less |
| Pulse divergence | 1 mrad |
| Field of view | 1.5 mrad |
| Receiver detector | Si-APD |
| Power consumption | 18.5 W (w/o survival heater) |

Hayabusa-2 LIDAR will provide a time resolution of less than 3 ns corresponding to 0.5-m range resolution (Table 3). LIDAR is expected to measure the distance from 30 m to 25 km above the surface of the asteroid. During mission phases, topographic data will be acquired constantly to cover entire surface of the asteroid. The experiment will provide the integrated intensity of the transmitted and returned pulses allowing an assessment of surface albedo including shadowed areas. Overall, Hayabusa-2 LIDAR is sufficient for spacecraft navigation, but is not as high-performance as the most recent instrument onboard OSIRIS-Rex [Barnouin *et al.*, 2012; Dickinson *et al.*, 2012]. To compensate for the performance of the instrument, we need to take most advantage of experiences of the first Hayabusa in operational planning.

2. Formation Processes of Small Asteroids

Finding of rubble-pile asteroid as small as 500 m in diameter is one of major achievements of Itokawa exploration [Abe *et al.*, 2006; Fujiwara *et al.*, 2006]. This

discovery has a significant implications on an evolution of size distribution of small asteroids [e. g., *Michel et al.*, 2003; 2004]. Needless to say, this finding was elucidated by incorporating various kinds of datasets derived from remote-sensing observations and analysis of returned samples. We consider it important to verify and possibly extend this achievement of the first Hayabusa in successive asteroid missions.

The rubble-pile body is generally regarded as an object that consists of numerous pieces of rock loosely bound under an influence of self-gravity and shows no tensile strength for collision process [*Richardson et al.*, 2001]. The idea of rubble pile asteroid has been proposed in as early as 1970's by *Chapman* [1978]. At first, a rubble-pile structure was argued as an outcome of successive destructive impacts or one nearly crushing event. Recently, however, it is widely accepted that a rubble-pile structure is formed by gravitational reaccumulation of fragments from a completely disrupted parent body. The latter scenario can bridge the discrepancy of size distribution between fragments derived from impact experiment and the largest members in collisional families [*Chapman et al.*, 1989]. This scenario is also traced in numerical studies on catastrophic disruption and reaccumulation [*Michel et al.*, 2003; 2004], although a computational ability at present constrains the smallest size of fragments in the numerical simulation to be larger than 1 km.

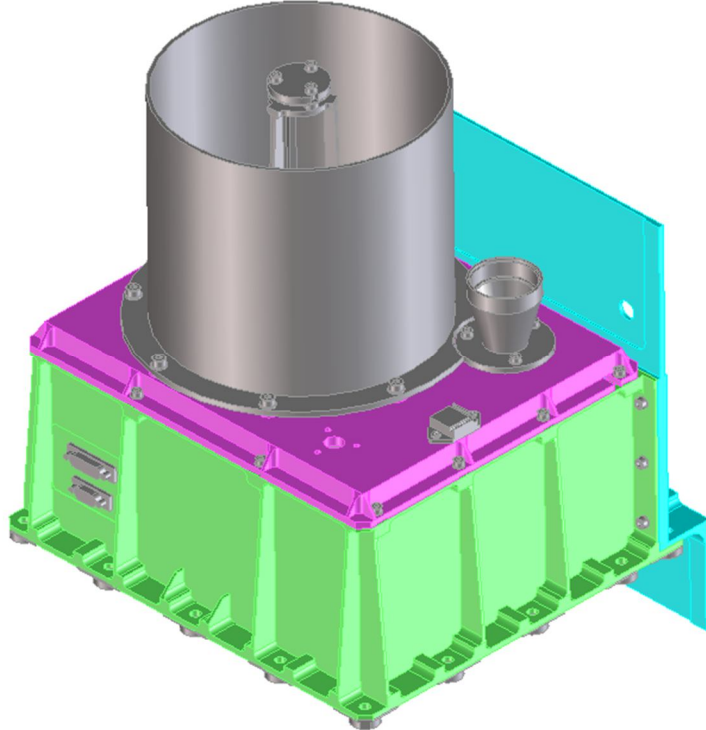


Figure 1. Engineering drawing of Hayabusa-2 LIDAR.

On the other hand, an observational evidence of rubble-pile body was absent before the exploration of 25143 Itokawa, 243 Ida, 433 Eros, and possibly 951 Gaspra and 253 Mathilde, are considered not to have a rubble-pile structure because of their low porosity and presence of global structures. While Dactyl, a small satellite of 243 Ida, is interpreted as a captured fragment of the Koronis parent body [*Greenburg et al.*, 1996] representing an accumulation process of collisional fragments, 243 Ida is generally regarded as a monolithic body. Thus 25143 Itokawa is the first and only rubble-pile body that has been confirmed by a spacecraft.

A paucity of explored asteroids can be compensated by ground-based observations. Baer *et al.* [2011] show mass and porosity of 26 asteroids by astrometric mass determination using mass and orbits of 300 large asteroids. Although their estimate is not as accurate as in-situ observation, a rough distinction of porosity can be made with additional estimates found in other literatures (Figure 2). Figure 2 shows that classification changes significantly with diameter. The porosity of asteroids larger than 500 km is smaller than 20 % indicating a compaction due to self-gravity. Asteroids whose diameter ranges between 100 and 500 km consist of two extremes of high and low bulk porosities. This observation could be inferred as coexistence of rubble-pile bodies and survived primordial asteroids. Alternatively, the high bulk porosity cluster which consists of mostly C-type asteroids and its affinity may imply presence of monolithic asteroids whose grain density is low or microscopic porosity is high. 253 Mathilde can be thought as an example of such asteroid. The estimates of bulk porosity of asteroids smaller than 50 km are few and are difficult to understand. Asteroids whose diameter is between 50 and 100 km show high porosity. In contrast, those larger than 5 km and smaller than 50 km show low porosity. And the smallest group, including 25143 Itokawa, again shows high porosity. In this point, the exploration of 1999 JU₃ that belongs to the smallest group is important to verify or deny this unresolved signature.

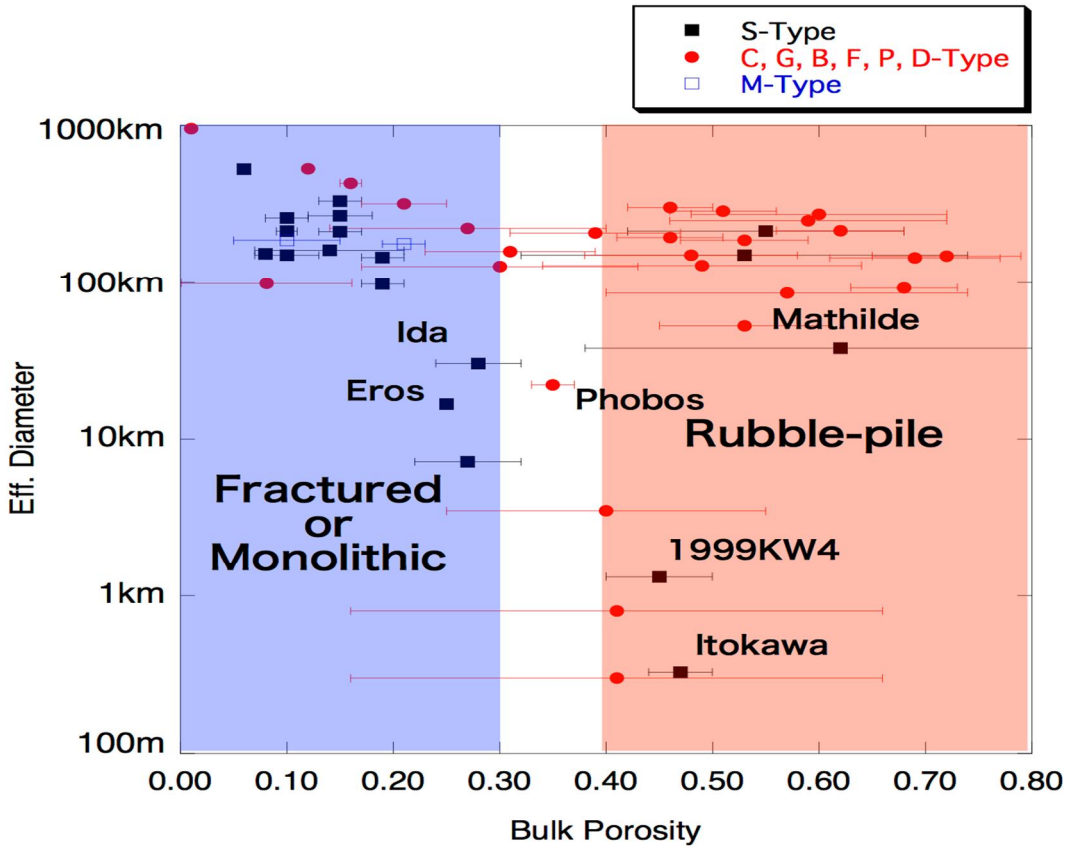


Figure 2. Relation of effective diameter and bulk porosity of asteroids. In addition to estimates by Baer *et al.* [2011], data taken from literatures are shown. Inferred internal structures such as fractured, monolithic and rubble-pile are based on classification by Britt *et al.* [2002]. Microscopic porosity is assumed to be 10 % that is a typical value of meteorites.

The estimate of bulk density is also important for the study of C-type asteroids. The C-type asteroids are often suggested to be highly porous even in a size range larger than 100 km as we discussed above. This inference, however, is challenged

by a wide variation of bulk density of carbonaceous chondrites that are likely natural samples from C-type asteroids. To answer this question, we probably need a comprehensive study on 1999 JU₃ by both remote sensing and sample analysis.

In Hayabusa-2 mission, not only average bulk density, but also its variation in the asteroid will be examined. Without the knowledge of density variation, internal structure of 25143 Itokawa has remained speculative even though its appearance seems suggesting an adhesion of two rubble-pile bodies (Figure 3). In case of Hayabusa-2, we aim to determine the difference between center of mass and center of figure of 1999 JU₃. Along with the difference between spin axis and principal axis of moment of inertia that is calculated from the shape model [Demura et al., 2006], crude idea of collision and accretion history of the asteroid can be argued.

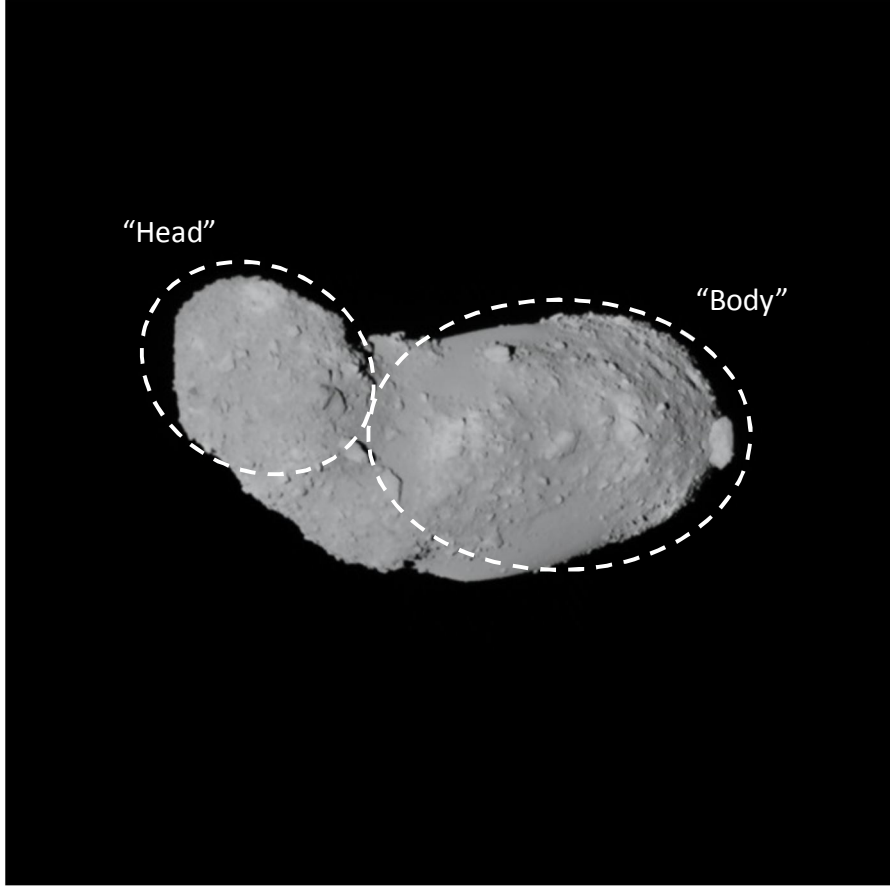


Figure 3. Image of 25143 Itokawa taken by the first Hayabusa (ST-2420855658).

Accuracy Requirement for Gravity and Volume Estimates.

The simple classification proposed by Britt et al. [2002] gives us an idea how accurate an estimate of bulk porosity needs to be. In Figure 2, fractured and rubble-pile bodies are distinguished by a 10% transition of bulk porosity. Therefore the accuracy less than 10% is required for remote sensing observation of 1999 JU₃. With a practice of Itokawa exploration [Demura et al., 2006], we fix the accuracy requirement of bulk porosity estimate to be 7%, and allocate 3% and 5% for gravity and volume estimates, respectively.

3. Gravity Measurement

In order to measure the mass of 1999 JU₃, we will have the spacecraft descend toward 1999 JU₃ from 20-km to 1-km altitude without orbital maneuvers, and have

the spacecraft ascend freely as well. An accuracy of mass estimate is evaluated by numerical simulation of tracking data during free flights assuming errors of LIDAR altimetry and X-band Doppler tracking to be 10 m and 0.2 mm s⁻¹, respectively (Figure 4). Sampling frequencies of LIDAR and integrated Doppler tracking are assumed to be 1 and 1/60 Hz, respectively. In addition, auxiliary navigation data are assumed to be available. A center of asteroid image will be determined with an accuracy of 0.1 degree for every 120 seconds, and position of the spacecraft with respect to the asteroid will be estimated with an accuracy of 10 m for every 10 to 30 minutes. Perturbations from planets and solar radiation pressure are taken into account in the numerical simulation. As we discuss below, an error of GM, universal gravitational constant times asteroid mass, is required to be less than 3% for the study of porosity estimate. Thus Figure 4 suggests that a free flight longer than 12 hours is sufficient for precise measurement of GM. And for secure touchdown operation, at least two free flight experiments are recommended before touchdown.

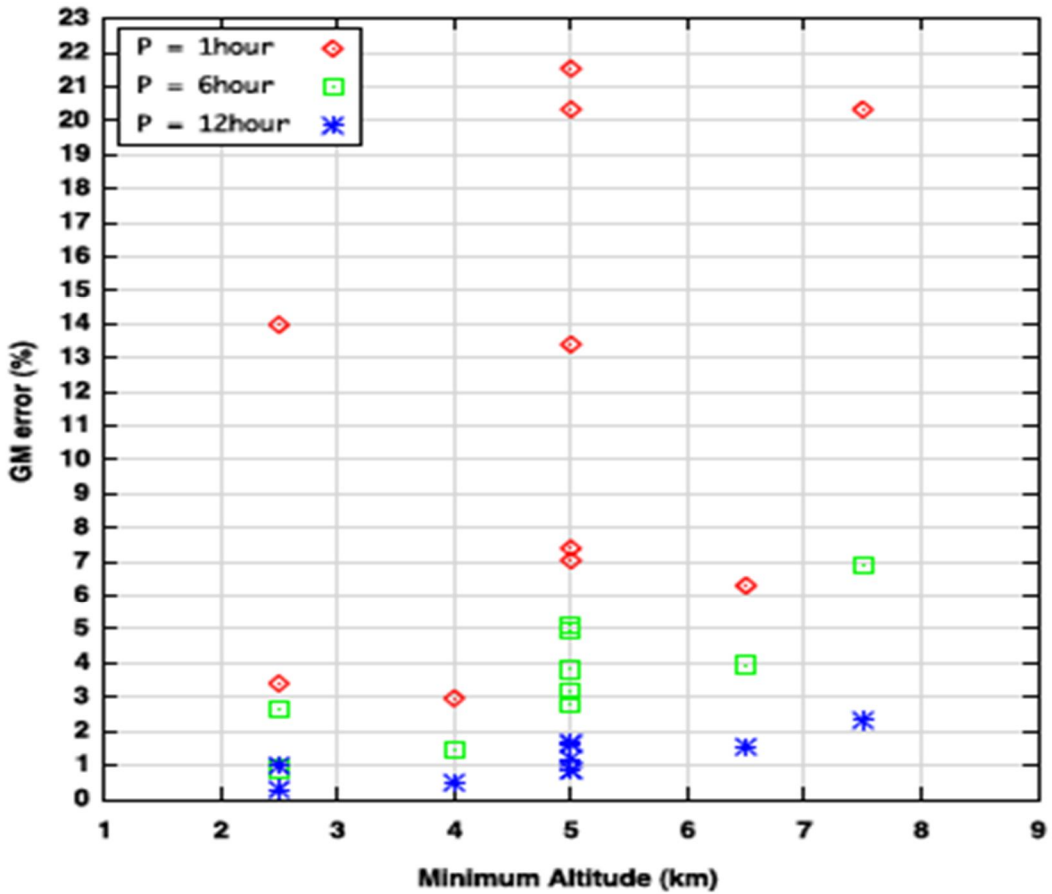


Figure 4. Errors of GM value depending on the lowest height of free flight pass. Durations of free flight shown by red diamond, green square, and blue asterisk are 1, 6, and 12 hours, respectively. Variation of symbols for given minimum altitude and duration results from different initial conditions such as velocity and altitude [Ikeda et al., 2013].

An accuracy of gravity estimate can be improved as the number of free flights increases. Because a free flight is not necessarily a descending track to an asteroid, but an ascending track from an asteroid is useful, too, the number of experiments increases by taking range data during passes escaping from close approach. We plan to take as many opportunities as possible so as to study a variation of density, namely that of porosity, inside of 1999 JU₃. For this purpose, we evaluate a requirement of

minimum number of the experiments by simply assuming a combination two spheres with different porosity. It is shown that if center of mass will be determined with accuracy of 10 m or less with respect to center of figure, porosity difference greater than 10 % can be estimated for two spheres of size ratio of 3 or less. And this requirement can be satisfied by tracking of 6 or more free flights.

4. Shape Model

Shape model of the target asteroid is necessary for spacecraft operation. For example, navigation of the Hayabusa spacecraft was performed by tracking ground control points at the surface of the asteroid. In principle, the shape model is developed from ONC images and LIDAR range data. Non-dimensional shape is estimated using images taken from various configurations. Then LIDAR range data determines its length scale.

Shape and topography are unarguably fundamental data set of geologic study of an asteroid. For example, the rubble-pile structure of 25143 Itokawa is strongly supported by boulders at the surface of the asteroid. Also, so-called head and body of 25143 Itokawa imply a coagulation of two independent bodies (Figure.3) , even though internal structure cannot be inferred uniquely from the shape only. Estimating surface slopes with respect to asteroid geoid (Figure.5) is not only critical for touchdown operation of the spacecraft, but also important for study of mass transport at the surface [Miyamoto *et al.*, 2007]. Further, formation of grabens and ridges, and crater distribution of 25143 Itokawa [Hirata *et al.*, 2009] have been argued within a context of entire shape of the asteroid [Gaskel *et al.*, 2008].

Shape modeling method and estimation of position of the spacecraft with respect to the asteroid.

The approach taken for asteroid shape modeling is different from that for geodetic measurement of large planetary bodies such as Moon and Venus [e. g., Araki *et al.*, 2009]. Because errors of orbit estimate of spacecraft and asteroid mass center are frequently greater than size of asteroid, these estimates are not taken as a reference in spatial coordinate. In case of 25143 Itokawa, the shape and spacecraft position have been solved simultaneously and iteratively [Barnouin-Jha *et al.*, 2008]. Once a global shape model of 25143 Itokawa has been fixed, small-scale topography is resolved using a method named Shape-from-Shading (SfS) method [Gaskel *et al.*, 2008].

For Hayabusa-2 project, new algorithm is considered by taking an advantage of recent improvement in the field of computer vision. This new algorithm is called Structure-from-Motion (SfM) method that retrieves feature points as well as positions and attitudes of the camera in three-dimensional space from multi-view images that vary in distance, signal-to-noise ratio, frame size, viewing geometry, and so on. The SfM method is a well-established technique, and several implementations have been released to public. For asteroid shape modeling of Hayabusa-2 project, we employ *Bundler* which is a popular SfM implementation developed by Snavely *et al.* [2006]. *Bundler* reconstructs a sparse point cloud, namely a low-resolution shape model. In order to obtain a high-resolution shape model, we apply second software package named *PMVS2* [Furukawa and Ponce, 2010] to the outcome from *Bundler*.

Non-dimensional shape of an asteroid determined by the SfM method needs to be scaled using LIDAR data. The size of an asteroid would be easily calculated if footprint location in an image is precisely determined. We use the estimates of optimized position and altitude of camera derived from sparse bundle adjustment.

By taking a position of LIDAR footprint in ONC image as a free parameter, a combination of non-dimensional shape model, estimated camera position and attitude, and LIDAR range data allows to scale the shape model in the manner of least-square approximation.

We examined Bundler and PMVS2 by using images of 25143 Itokawa taken by the first Hayabusa. The number of images is 167 and they cover full rotational phase of the asteroid. The high-resolution shape model was successfully reconstructed (Figure 5). The resolution of the shape model that is defined by the average distance of adjacent feature points is 3.92 m. For comparison, the resolution of the initial shape model of 25143 Itokawa [Demura et al., 2006] is 73.9 m. Thus a great improvement is achieved. We also evaluate accuracy of the model by comparing with the model by Gaskell et al. [2008]. The difference of two models is calculated as a root mean square of radial distances of feature points and is 4.87 m. In contrast, the RMS difference of the shape models by Demura et al. [2006] and Gaskell et al. [2008] is 12.8 m. This 4.87-m difference of the new model and that of Gaskell et al. [2008] is equivalent to 1.5% of the size of asteroid satisfying requirement on estimation of the volume of the asteroid (Section 2). We also note that the new algorithm takes only a several hours to reconstruct a shape model once the images of the asteroid are obtained. Such prompt reconstruction is very important for safe navigation of the spacecraft. And later in the mission phase, the rough initial model of asteroid shape will be fine-tuned by shape-from-shading and photometric stereo techniques [Gaskell et al., 2008].

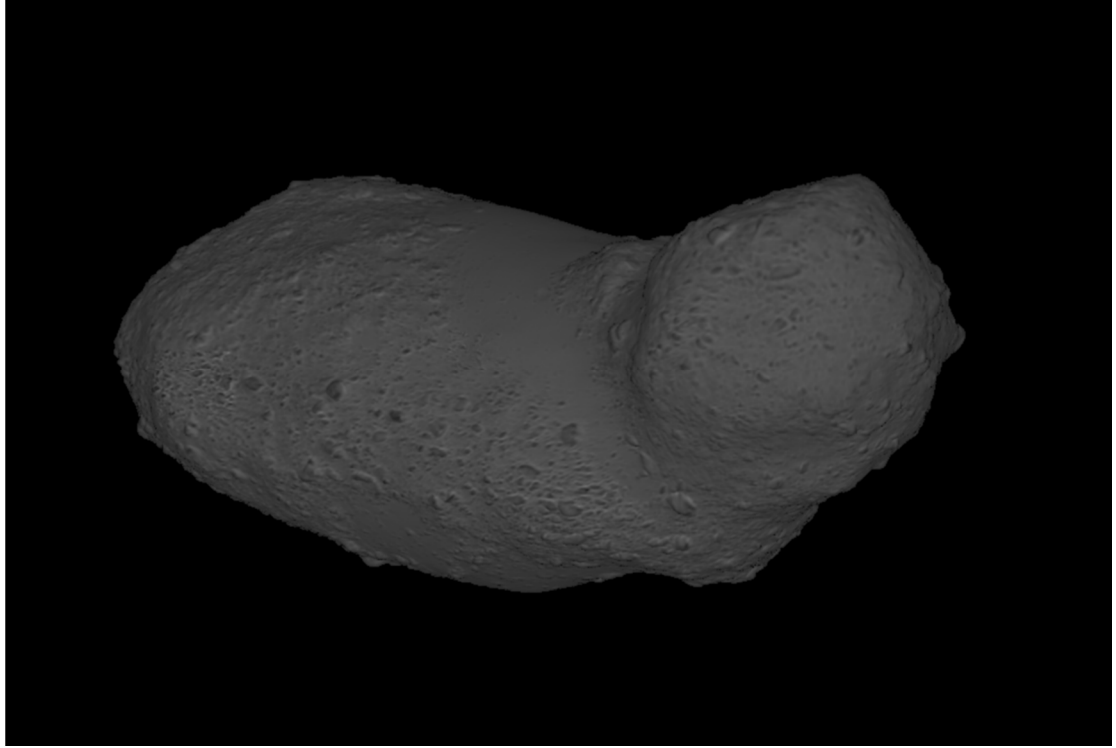


Figure 5. Itokawa shape model reconstructed by using *Bundler* [Snavely et al., 2006] and *PMVS2* [Furukawa and Ponce, 2010].

Cross verification among shape models obtained by independent methods and independent data sets is helpful to evaluate the accuracy of the models. Series of LIDAR observation during the orbit without thruster maneuver can be taken as a profile of topography. At a HP, the frequency of thruster maneuver is expected to be once in hours. In a period between thruster maneuvers, a propagation error of the orbit estimate is likely as small as $3\text{-}30 \text{ mm s}^{-1}$. Therefore an accuracy of position estimate

in an arc from 150 to 1500 sec is less than nominal error of altimetry of 5.5 m, making possible a direct comparison of topography profile and LIDAR range data. A cross-over analysis of altimetry data [Rowlands *et al.*, 1999] further improves an accuracy of position estimate and enables to construct mesh data of topography that is independent from ONC images.

Requirement of Range Accuracy.

The 5% requirement of volume estimate given in Section 2 corresponds to 1 to 2% accuracy of the shape model in radial direction. Thus for the asteroid of 500 m in diameter, the range accuracy needs to be less than 10 m. This requirement is satisfied by the current design of LIDAR specification (Table 3).

An accuracy of the asteroid volume is also dependent on lateral distribution of feature points. Because it is impossible to predict a roughness of the surface of 1999 JU₃ before an arrival of the spacecraft, we examine two end members of rough and smooth surface. The former is 25143 Itokawa, and the latter is laboratory model of an asteroid. As shown in Figure 3, the surface of 25143 Itokawa is characterized by numerous boulders. In contrast, the surface of the laboratory model is smooth simulating a thick veil of regolith (Figure 6). In both cases, a number of reconstructed feature points are between 5000 and 10,000. Then an average distance among the feature points uniformly distributed on an asteroid of 1000-m diameter is 25 m. If this average distance can be taken as a discrepancy between LIDAR footprint and the position of the feature point, an error of radial distance is 13 m assuming a typical slope of the surface of 30 degrees (Figure.5).

A simple sum of the range accuracy and the error of radial distance is 18 to 23 m and is greater than the 1 to 2 % requirement. However, because the asteroid shape is modeled by using many images, the random errors decrease in inverse proportion to the number of images as demonstrated by the examination of Itokawa images. We plan to take as many as 500 images at an altitude of 20 km during a period of global mapping. Therefore the accuracy of the shape model is probably dominated by the bias error of 1.7 m of LIDAR range measurement.

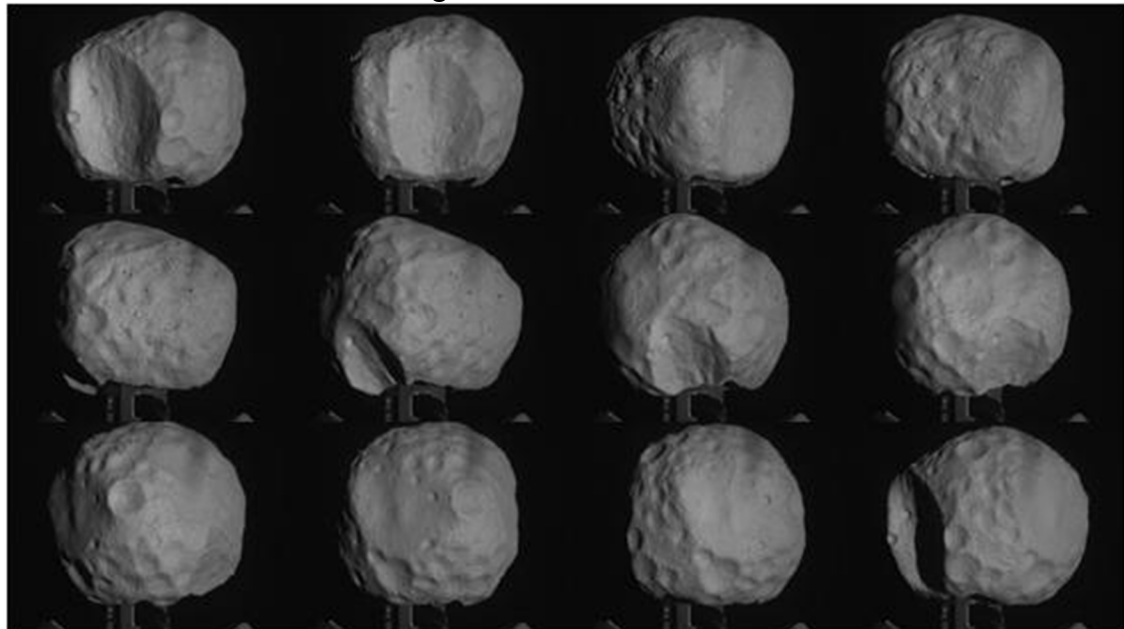


Figure 6. Laboratory model of an asteroid. Pictures of 73 equatorial views are taken for every 5 degrees under parallel lights whose solar angle is 29 degrees.

5. Roughness and Albedo

Roughness Observation.

The roughness is an important source of information about asteroid surface such as boulder size distribution and crater diameter and depth, as previously shown for 25143 Itokawa by *Barnouin-Jha et al.* [2008]. In principle, roughness within a footprint of LIDAR is calculated from an elongation in time of returned pulse relative to transmitted pulse. Hayabusa-2 LIDAR, however, is not designed to measure the elongation of the pulse. Instead, we plan to calculate the roughness directly from range data. As the footprint of LIDAR moves laterally on the surface of the asteroid, time sequence of range data represent local variation of topography independently of digital elevation model that is derived from camera images. By reducing regional slope and spacecraft motion from range data, roughness in scale of 1 to 100 m is extracted.

Accuracy requirement of roughness observation is dependent on the surface property of 1999 JU₃ which is hardly quantified by ground-based observations. An available analogue is only 25143 Itokawa. Therefore we again evaluate the results of 25143 Itokawa for this purpose. As shown by *Barnouin-Jha et al.* [2008], a standard deviation of height difference on rough terrain of 25143 Itokawa is greater than 2 m while that on smooth terrain is less than 1 m. The latter is likely dominated by range resolution of LIDAR onboard Hayabusa. Thus the range resolution of Hayabusa 2 (Table 3) is sufficiently low to distinguish the rough and smooth terrains of 1999 JU₃, if they were equivalent to those of 25143 Itokawa.

Location of footprint also needs to be determined precisely. An uncertainty on asteroid surface needs to be smaller than the footprint diameter, that is, 5 and 20 m at 5 and 20 km altitude, respectively. In order to meet this requirement, we examine an alignment between LIDAR and navigation camera in flight by comparing LIDAR range profile and a location of feature points such as boulder and small crater in the images.

Albedo Measurement.

LIDAR is an active sensor unlike other scientific instruments onboard Hayabusa-2. Ratio of transmitting and receiving powers can be translated into geometric albedo at the surface of 1999 JU₃ when the roughness within a footprint is adequately estimated. In case of the first Hayabusa, a power meter could not measure both transmitting and receiving power simultaneously. In contrast, a design of Hayabusa-2 LIDAR is modified so that both transmitting and receiving powers can be measured.

Albedo variation at the surface of C-type small bodies has not been understood well. 253 Mathilde is the first C-type asteroid that was investigated by a spacecraft, and shows an albedo variation of only $\pm 6\%$ [*Clark et al.*, 1999]. Another target for comparison is Phobos, a popular satellite of Mars. Observed spectrum of Phobos indicates that an origin of this satellite is a captured C-type asteroid from main belt while this inference has not been universally accepted yet. In contrast to Mathilde, Phobos shows the regional variation of albedo as great as $\pm 20\%$ [*Simonelli et al.*, 1998]. The variation of albedo on Phobos can be interpreted as a consequence of lateral transport of regolith and local variation of space weathering because the variation is related with small craters and topography. In case of 1999 JU₃, *Vilas* [2008] shows from ground-based observation that reflectance spectrum changes within a rotation period. This observation may be suggesting a regional variation of albedo, because the variation of reflectance spectrum of Phobos is correlated with that

of albedo. Interestingly, however, the extensive observations in the summer 2012 do not show similar change in reflectance spectrum.

Regional variation of albedo can occur due to ejecta distribution and seismic shaking of impacts. Furthermore, resurfacing and consecutive space weathering at steep slopes possibly play an important role for the surface variation of 1999 JU₃, whose morphology may be influenced by tidal force of the Earth as a potentially hazardous asteroid. Then in-situ observation of the albedo of 1999 JU₃ can promote our understanding about space weathering process of C-type small bodies that is still ambiguous compared with S-type asteroids.

The albedo observation also makes it possible to argue gardening process of asteroid regolith if lateral changes of mixing ratio of carbonaceous material to silicate is observed. In addition, because the wavelength of laser pulse is covered by the absorption band of olivine, a regional variation of olivine fraction and space weathering of olivine is possibly observed if 1999 JU₃ consists of as much olivine as Allende meteorites. However, because the albedo observation by LIDAR is restricted in a single band at 1064 nm, it is necessary to refer and examine spectral data taken by ONC and NIR3 onboard Hayabusa-2 to distinguish relative contributions from these processes.

Conversely, LIDAR can contribute to calibration of images taken by other instruments. In principle, the albedo measurements of LIDAR is always carried out with zero phase angle between incident and reflecting lights, namely, in a configuration of opposition. Usually the Hayabusa-2 spacecraft stays along a line between the Earth and the asteroid. As a consequence, the phase angle between the sun and imagers rarely becomes zero. Although there will be an operation dedicated for observations under opposition condition, a chance is few and the duration of time is short. Thus LIDAR albedo measurements provides an important information regarding optical scattering property that is otherwise difficult to obtain.

An accuracy of the albedo measurements of LIDAR is dependent on the altitude of the spacecraft. The power of return pulse is calculated from an output voltage from an amplifier. This output is 5.1 V at the highest and is quantized into 8 bits allocating 20 mV per bit. On the other hand, expected powers of return pulse are 560 mV and 140 mV for altitudes of 10 and 20 km, respectively. Thus the quantization becomes a significant source of errors depending on the altitude. Of course, the ratio of quantization error to the return pulse decreases as the altitude becomes lower. However, a gain of detector is switched to low value at the altitude lower than 8 km. And below 3-km altitude, the power meter will be saturated. Such performance is designed in order to enable a wide dynamic range of distance measurement from 30 m to 25 km (Table 3). In the case of observation at 20-km altitude, an accuracy of energy measurement is about 30% with respect to average of surface albedo of 0.07. In contrast, an expected variation of albedo at the surface of C-type asteroid is about 20% or less [Simonelli *et al.*, 1998; Clark *et al.*, 1999]. After all, the best altitude range for the albedo measurement is between 3 and 5 km, or 8 and 15 km. We therefore plan to carry out the albedo measurements at HP for initial mapping, and at 5-km altitude for nominal mapping.

A performance of receiver detector also influences the accuracy. For Hayabusa-2 LIDAR, Si avalanche photo diode is used (Table 3). A sensitivity of Si-APD is dependent on temperature and applied voltage. Hayabusa-2 LIDAR controls applying voltage to Si-APD onboard on the basis of monitored temperature so as to calibrate a gain of Si-APD automatically. The smallest scale of onboard thermometer is 1 K. In order to improve the accuracy of albedo measurement, we plan to measure the

temperature-dependent sensitivity curve for every 0.1 K during verification tests of the flight model.

6. Detection of Levitation Dust

Majority of returned samples from 25143 Itokawa are a few tens to 180 μm in diameter [Nakamura *et al.*, 2011; Tsuchiyama *et al.*, 2011]. Such fine particles are continuously produced at the surface of airless bodies like the Moon and asteroids by innumerable micro impacts and thermal stress related to large temperature difference between daytime and nighttime. On the other hand, it has not been clear how the first Hayabusa spacecraft captured those particles despite of a failure in shooting a bullet from the sampler horn [Fujiwara *et al.*, 2006; Yano *et al.*, 2006].

A motion of the particles on an asteroid is difficult to predict because an influence of surface forces such as radiation pressure and electrostatic force increases with respect to asteroid gravity as a size of particle decreases. However, a clue is provided from a similar behavior of dust on the Moon that has been intensively studied since Apollo era. The surface of the Moon is covered by fine particles known as regolith whose diameter is 70 μm on average and the thickness ranges from a few cm to several 10 m. A sooty appearance of Apollo astronauts is likely a consequence of dusts stirred up during an operation at the lunar surface indicating that dusts are easily flown and adhere to space suit by static electricity. Also discovered by Apollo mission is the horizontal glow that is a scattering of sunset light observed in images of camera placed at the lunar surface. The thickness of scattering layer is about 30 cm, and a characteristic size of the particles is estimated to be 3 μm [Criswell, 1973; McCoy and Criswell, 1974; Rennilson and Criswell, 1974]. A similar phenomenon is observed from orbiters. In this case, the thickness of the layer is 100 km and the characteristic size of dust is 0.1 μm . While a mechanism to levitate dusts on the Moon is not well understood, electric field at the surface and a charge of dust particle likely play important roles [Robinson *et al.*, 2001; Poppe and Horanyi, 2010].

Previous asteroid missions have revealed smooth appearance of topography on 951 Gaspra, 243 Ida, and 433 Eros [Carr *et al.*, 1994; Lee *et al.*, 1996; Sullivan *et al.*, 1996; Thomas *et al.*, 1996; Prockter *et al.*, 2002; Buczkowski *et al.*, 2008] suggesting that these asteroids are covered with particles smaller than resolution of camera images. Particularly, the exploration of Eros by NEAR Shoemaker has revealed as smooth surface as a liquid water at the base of craters whose diameter is between 20 and 300 m [Robinson *et al.*, 2001; Veverka *et al.*, 2001]. A bluish color of this “pond” is consistent with stagnant dusts of diameter smaller than 50 μm [Robinson *et al.*, 2001]. From this observation, Colwell *et al.* [2005] propose dust levitation occurring on Eros. According to their hypothesis, a photoelectric effect of solar UV positively charges both dust and the surface. Then a balance between electric repulsion and gravity causes 0.5- μm dusts to oscillate vertically over the surface of Eros long period of time. When a dust has a horizontal velocity, it transfers laterally until it reaches to a shadow of topography where electrostatic field is weaker than surroundings. Thus topographic depression such as a crater becomes a sink of levitating dusts. This hypothesis can be applied to a small satellite found in A ring of Saturn, too. A very smooth surface and an overall shape of this satellite can be explained consistently by a transfer of levitating dusts [Hirata and Miyamoto, 2012].

One major achievement of 25143 Itokawa sample analysis is a finding of short residence time of particles at the surface. An abundance of cosmic-ray-produced ^{21}Ne indicates that an average residence time of 25143 Itokawa samples is less than 8

million years [Nagao *et al.*, 2011]. On the other hand, the levitation hypothesis of Eros pond predicts that the electrostatic repulsion of a particle of a few μm is strong enough to escape from the gravity of 25143 Itokawa. Thus dust particles quickly depart from 25143 Itokawa to become an interplanetary dust particle (IDP). Both the dust levitation hypothesis and isotopic analysis of 25143 Itokawa sample are closely related with production and chemical evolution of IDPs.

The dust levitation hypothesis successfully explains the distribution of particles on the surface of small airless bodies, at least, qualitatively. In contrast, production rate of particles is hardly quantified by the hypothesis and is necessarily constrained by in-situ observation. Except for a detection of fast ejecta from micro impact [Krivov *et al.*, 2003], there has not been any direct observation even though lateral transport of dust particles is generally regarded important for formation of local topography of small body [e. g., Hirata and Miyamoto, 2012]. Also, vertical transport of dust is critical for interpretation of irradiation age of cosmic rays and implantation of solar wind elements found in IDPs and breccia meteorites [Kimura and Mann, 1998; Eugster *et al.*, 2006]. Thus an attempt of first detection of asteroid dust by Hayabusa-2 LIDAR is highly anticipated.

Both ground-based and space borne LIDAR instruments have been used to measure aerosol and clouds in the Earth's atmosphere [Fiocco and Smullin, 1963; Fernald *et al.*, 1972; Klett, 1981]. A pulse of laser transmitted from the LIDAR instrument is reflected by aerosol and clouds on a line of bore sight. Then an effective backscatter cross section can be measured from a profile of returned pulse. Unfortunately, however, Hayabusa-2 LIDAR is not capable of downlinking a profile of returned pulse. Instead, a new function called dust count mode is implemented by taking an advantage of a wide dynamic range of Hayabusa-2 LIDAR. The time range of the detector is divided into 50 bins corresponding to 20 m resolution along a line of bore sight, and each bin returns 1-bit telemetry indicating whether or not a reflection in the bin is higher than a threshold level. By changing threshold level in 8 steps, a rough profile of returned pulse is obtained. Then under an assumption that a size distribution of particles is similar to that of 25143 Itokawa samples [Tsuchiyama *et al.*, 2011], a spatial distribution of column density can be estimated. The range gate that delays the time of detection of the first bin can be changed arbitrary by a command from 0 to 126 μs , corresponding to an altitude from 0 to 19 km. Thus the spatial distribution of dust density between the asteroid surface to an altitude of 20 km can be roughly measured in 8 steps with 20-m resolution by a series of dust mode observation.

Dust count by LIDAR determines a distribution of dusts along a line of bore sight. In contrast, images taken by ONC and TIR onboard Hayabusa-2 reveal a reflection of sunlight integrated over the line of bore sight. Consequently, the reflection from dusts is overwhelmed by that from asteroid surface when a camera captures the asteroid within its view. On the other hand, LIDAR can hardly observe lateral distribution of dusts, but distinguish a weak reflection of thin dust cloud from that of the surface.

To plan an operation of the dust count mode observation is difficult because the number density of asteroid dust is not known at all. Instead, we evaluate the lower bound of number density that is geologically important for morphology of asteroid surface. For a given number density of dusts and under an assumption that a characteristic time of levitation is the rotation period of 1999 JU₃ (Table 2), the rate of embayment of craters is calculated. If this rate of embayment is greater than that of crater production, we need to take into account a modification process for the study of crater morphology and crater counts of 1999 JU₃. This lower bound is calculated to be 10^6 m^{-3} for a cloud of dusts whose radius is larger than a few μm . Then we set this

value as a target of the dust count mode observation.

A detectability of dust count mode is dependent on sensitivity of Hayabusa-2 LIDAR and an altitude of the spacecraft. We calculate a reflection from dusts using Mie scattering model [Bohren and Huffman, 1983; Liou, 2002] assuming that a diameter of dust particle is constant and is larger than the wavelength of laser, that is, 1064 nm. A characteristic distance between dusts is also assumed to be sufficiently larger than the wavelength so that interaction between dust particles is negligible. Instrument parameters and physical values of dusts adopted for the following calculation are listed in Tables 4 and 5, respectively. Returned pulse from dust particles is integrated over a column within a pulse divergence (Table 3) and vertical resolution of 20 m. Peak power of the returned pulse, $W(a)$, is calculated as

$$W(a) = P_0 T_T T_R \frac{c \Delta t}{2} \frac{\pi R_R^2}{4h^2} \frac{\beta}{4\pi} \quad (1)$$

where a is the radius of particle, P_0 is the peak power of laser transmission, T_T and T_R are the optical efficiencies of transmitter and receiver, respectively, c is the speed of light of $2.998 \times 10^8 \text{ m s}^{-1}$, Δt is the pulse width (Table 3), R_R is the effective radius of receiver telescope, and h is the distance. β is a multiple of the number density of particle, N , and the Mie backscatter cross section, S_b , and is given by

$$\beta = N S_b(a) \quad (2)$$

$$S_b(a) = \frac{\pi}{\kappa^2} \left| \sum_{n=1}^{\infty} (-1)^n (2n-1) (A_n(a) - B_n(a)) \right| \quad (3)$$

where κ is the wave number of $5.91 \times 10^6 \text{ m}^{-1}$. A_n and B_n are the Mie scattering coefficients and are defined using spherical Bessel function of the first kind, $j_n(x)$, and spherical Hankel function of the first kind, $h_n(x)$

$$A_n(a) = \frac{\left\{ \frac{\Psi_n'(\sqrt{\varepsilon} \kappa a)}{\sqrt{\varepsilon} \Psi_n(\sqrt{\varepsilon} \kappa a)} + \frac{n}{\sqrt{\varepsilon}} \right\} \Psi_n(\kappa a) - \Psi_{n-1}(\kappa a)}{\left\{ \frac{\Psi_n'(\sqrt{\varepsilon} \kappa a)}{\sqrt{\varepsilon} \Psi_n(\sqrt{\varepsilon} \kappa a)} + \frac{n}{\sqrt{\varepsilon}} \right\} \xi_n(\kappa a) - \xi_{n-1}(\kappa a)} \quad (4)$$

$$B_n(a) = \frac{\left\{ \frac{\sqrt{\varepsilon} \Psi_n'(\sqrt{\varepsilon} \kappa a)}{\Psi_n(\sqrt{\varepsilon} \kappa a)} + \frac{n}{\sqrt{\varepsilon}} \right\} \Psi_n(\kappa a) - \Psi_{n-1}(\kappa a)}{\left\{ \frac{\sqrt{\varepsilon} \Psi_n'(\sqrt{\varepsilon} \kappa a)}{\Psi_n(\sqrt{\varepsilon} \kappa a)} + \frac{n}{\sqrt{\varepsilon}} \right\} \xi_n(\kappa a) - \xi_{n-1}(\kappa a)} \quad (5)$$

$$\Psi_n(x) = x j_n(x) \quad (6)$$

$$\xi_n(x) = x h_n(x) \quad (7)$$

$$\Psi_n'(x) = \Psi_{n-1}(x) - \frac{n}{x} \Psi_n(x) = x j_{n-1}(x) - n j_n(x) \quad (8)$$

$$\xi_n'(x) = \xi_{n-1}(x) - \frac{n}{x} \xi_n(x) = x h_{n-1}(x) - n h_n(x) \quad (9)$$

where ε is the complex dielectric constant.

Table 4. Parameter values relevant to dust count prediction.

| Parameter | Symbol | Unit | Value |
|----------------------------------|------------|----------------------|--------------------------|
| <u>Spacecraft</u> | | | |
| Distance | h | m | 30 - 2 x 10 ⁴ |
| <u>Laser transmitter</u> | | | |
| Peak power of laser transmission | P_0 | W | 1 x 10 ⁶ |
| Optical efficiency | T_T | | 0.894 |
| <u>Receiver for long range</u> | | | |
| Optical efficiency | T_R | | 0.678 |
| Effective radius of telescope | R_R | m | 0.11 |
| Return power | W | W | |
| Detector sensitivity | S_A | A W ⁻¹ | 0.36 |
| Total noise equivalent power | NEP_{PB} | W Hz ^{-1/2} | 1.2 x 10 ⁻¹³ |
| Band width | B | Hz | 1 x 10 ⁸ |

 Table 5. Assumed physical values of dust particle and 1999 JU₃.

| Physical character | Symbol | Unit | Value |
|--|------------|-----------------|------------------------------------|
| Number density | N | m ⁻³ | 10 ⁵ - 10 ¹¹ |
| Mie backscatter cross section | S_b | m ² | |
| Dust radius | a | μm | 5, 10, 20 |
| Complex dielectric constant [Michel <i>et al.</i> , 1996] | ϵ | | 2.40+2.38i |
| Charge of an electron | e | C | 1.6 x 10 ⁻¹⁹ |
| Background noise | P_B | W | 2.79 x 10 ⁻¹⁰ |

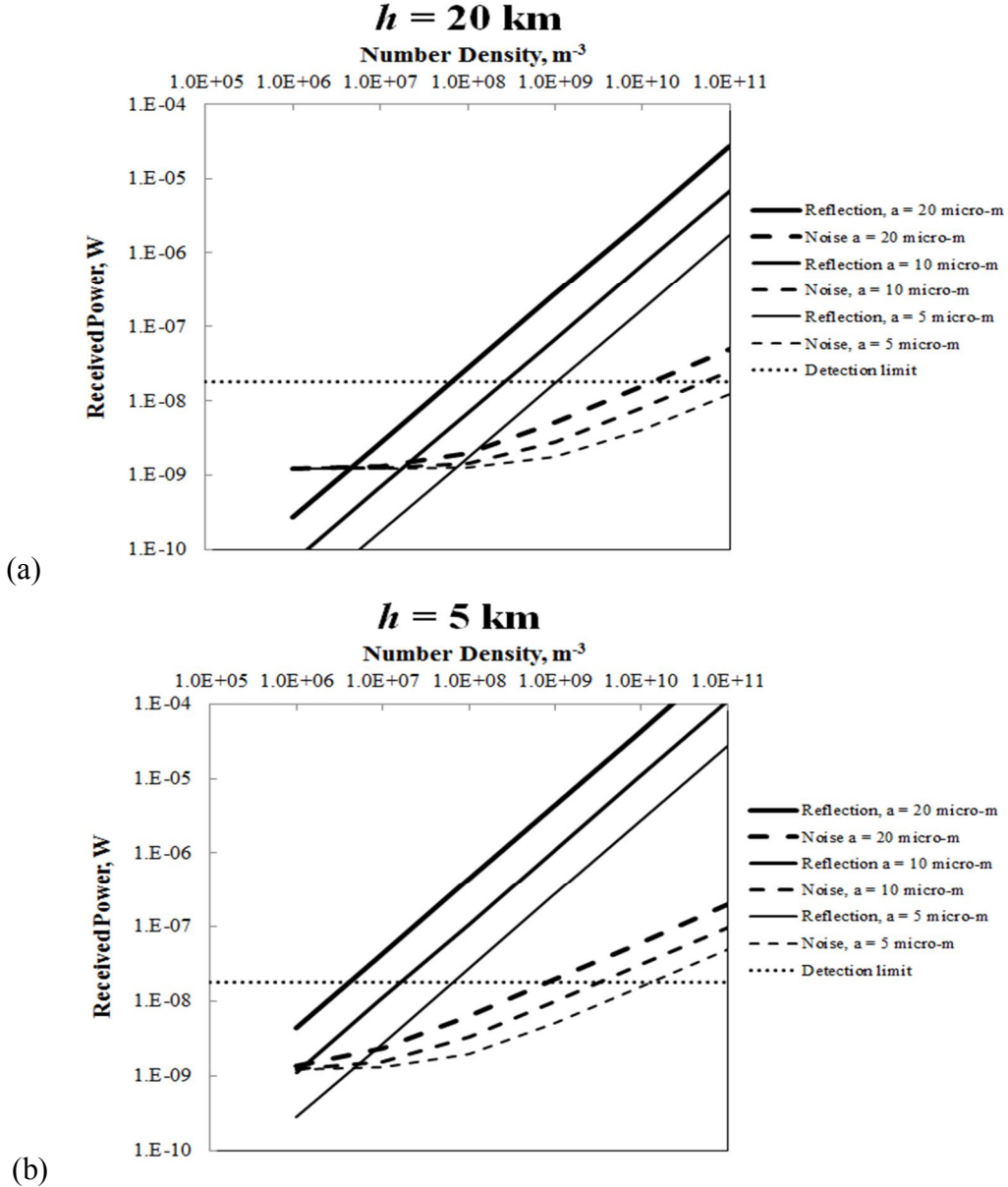
Using Equation (1), we calculate a peak power of backscattering light from a dust cloud for various sets of the distance, the number density, and the dust radius. In Figure 7a, $W(a)$ is shown for the dust radius of 5, 10, and 20 μm. The distance is assumed to be 20 km that is a nominal altitude of HP during rendezvous phase. An initial global mapping is planned at this altitude. The number density ranges from 1 x 10⁶ to 10¹¹. Also shown in Figure 7a is the detection limit of Si-APD (Table 3) and noise levels. The detection limit is 1.78 x 10⁻⁸ W. The noise level, P_N , is calculated from

$$P_N = \sqrt{2e \frac{W(a) + P_B}{S_A} B + NEP_{PB}^2 B} \quad (10)$$

where e is the charge of an electron, P_B is the power of the background, S_A is the sensitivity of detector, NEP_{PB} is the total noise equivalent power, and B is the band width of electric circuit attached to Si-APD (Table 4).

Also shown in Figures 7b and 7c are the peak powers calculated for h of 5 km and

1 km, respectively. In preparation for touchdown and sampling, the spacecraft stays at altitudes of 5 km and 1 km. At 5 km, the second global mapping is planned while only local mapping will be carried out at an altitude of 1 km. As shown in Figure 7, the peak power of reflection is generally stronger than noise level of the detector. However, the reflection from dust cloud is so weak that the targeted number density of 10^6 m^{-3} is hardly higher than the detection limit. Even at the lowest altitude (Figure 7c), the reflection from a dust cloud of 10- μm radius for 10^6-m^{-3} number density is equivalent to the detection limit. If a is 5 μm , N more than 10^7 m^{-3} is necessary to be detected. Therefore we plan to start the dust count operation from the HP and attempt to conduct as much operations as possible at low altitude.



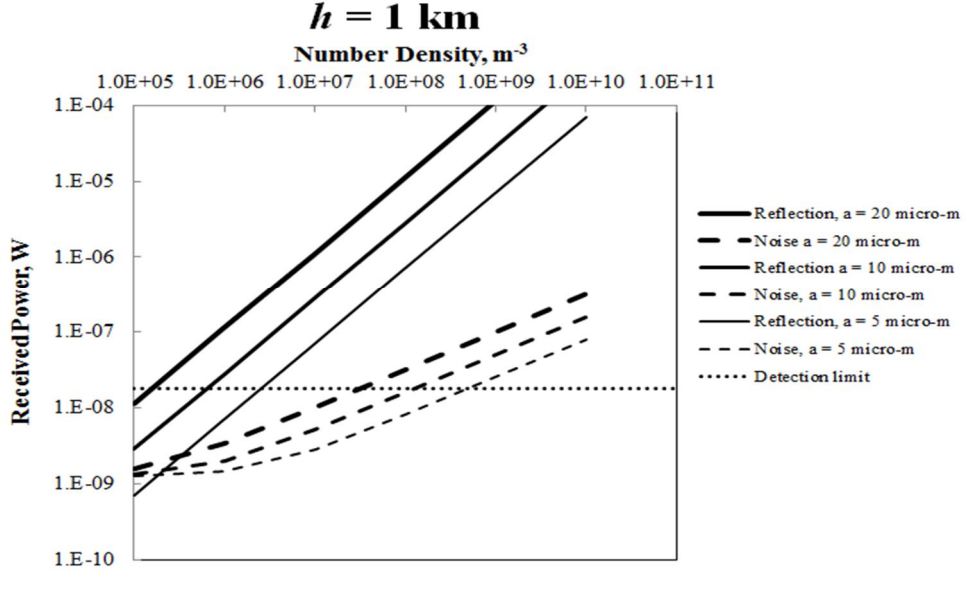


Figure 7. Expected peak power of reflection from dust cloud versus dust radius. The distance of (a) 20 km, (b) 5 km, and (c) 1 km is assumed. Calculated peak powers and noise levels are shown by solid and dashed lines, respectively. Thick, middle, and thin lines correspond to the particle radius of 20 μm , 10 μm , and 5 μm , respectively. Detection limit of the detector is also shown by dotted line.

7. Summary

Hayabusa-2 is the second asteroid mission of Japan, and is the first to return sample from C-type asteroid. Four remote-sensing instruments (ONC, TIR, NIRSS3 and LIDAR), one lander (MASCOT), three micro-rovers (MINERVA-II-1a, -1b and -2), and impactor and sampler (SCI and SMP) are being developed to be onboard Hayabusa-2 aiming to elucidate the missing link between early and present states of our solar system.

LIDAR is a part of bus subsystem, but its data will be used for studies of the asteroid, 1999 JU₃, as well. The ranging data are important for a measurement of the gravity that is crucial for subsequent touchdown and sampling operation. Also the ranging data are taken to construct the shape model of 1999 JU₃ with camera images. A new algorithm for 3-dimensional shape modeling is examined and is proved to be efficient and reliable. Roughness of the asteroid surface is not measured directly from the profile of returned pulse, but is calculated from a series of ranging data instead. The observation of albedo is planned, however, the observation error is too large to distinguish subtle variation on the surface of C-type asteroid. A new function for possible detection of asteroid dusts is implemented to Hayabusa-2 LIDAR. Because the reflection from dust cloud is weak, the dust-count experiments will be made mostly at an altitude lower than 1 km.

Contributions

This paper is based on mid-term report of Hayabusa-2 project. And all material comes from efforts of and a discussion within LIDAR Science Team. The gravity measurement is studied by Hitoshi Ikeda and Koji Matsumoto. The shape modeling is a joint work of ONC and LIDAR teams led by Naru Hirata. The observation of roughness and albedo is examined by Hirotomo Noda and Ryuhei Yamada helped by a discussion with Shinsuke Abe and Fumi Yoshida. The dust count is designed by

Hiroki Senshu and Shoko Oshigami. Hirotomo Noda and Makoto Shizugami take charge in preparation of quick look software.

Acknowledgements

We thank members of Hayabusa-2 mission. We are also grateful to NEC corporation who is manufacturing LIDAR instruments.

References

- Abe, S., T. Mukai, N. Hirata, O. S. Barnouin-Jha, A. F. Cheng, H. Demura, R. W. Gaskell, T. Hashimoto, K. Hiraoka, T. Honda, T. Kubota, M. Matsuoka, T. Mizuno, R. Nakamura, D. J. Scheeres, and M. Yoshikawa, Mass and local topography measurements of Itokawa by Hayabusa, *Science*, **312**, 1344-1347, 2006.
- Araki, H., S. Tazawa, H. Noda, Y. Ishihara, S. Goossens, S. Sasaki, N. Kawano, I. Kamiya, H. Otake, J. Oberst, and C. Shum, Lunar Global Shape and Polar Topography Derived from Kaguya-LALT Laser Altimetry, *Science*, **323**, 897-900, doi: 10.1126/science.1164146, 2009.
- Baer, J., Chesley, S. R., Matson, R. D., Astrometric masses of 26 asteroids and observations on asteroid porosity, *Astron. J.*, **141**, 143, 2011.
- Barnouin-Jha, O. S., A. F. Cheng, T. Mukai, S. Abe, N. Hirata, R. Nakamura, R. W. Gaskell, J. Saito, B. E. Clark, Small-scale topography of 25143 Itokawa from the Hayabusa laser altimeter, *Icarus*, **198**, 108–124, 2008.
- Barnouin, O., M. Daly, B. Bierhaus, C. Dickenson, D. Gaudreau, J. Tripp, M. Ilnicki, J. Garvin, J., and A. Hildebrand, The OSIRIS-REx laser altimeter, Asteroids, Comets, Meteors 2012, LPI Contribution No. 1667, id.6198, 2012.
- Bohren, C. F. and D. R. Huffman, Absorption and Scattering of Light by Small particles, A Wiley-Interscience Publication, pp. 530, 1983.
- Britt, D. T., D. Yeomans, K. Housen, and G. Consolmagno, Asteroid density, porosity, and structure. In *Asteroids III*, eds. W. F. Bottke Jr., A. Cellino, P. Paolicchi, and R. P. Binzel, pp. 485-500, 2002.
- Buczkowski, D. L., O. S. Barnouin-Jha, and L. M. Prockter, 433 Eros lineaments: Global mapping and analysis, *Icarus*, **193**, 39–52, 2008.
- Carr, M. H., R.L. Kirk, A. McEwen, J. Veverka, P. Thomas, J.W. Head, and S. Murchie, The geology of Gaspra, *Icarus*, **107**, 61-71, 1994.
- Chapman, C. R., Asteroid collisions, craters, regolith, and lifetimes, In *Asteroids*, eds D. Morrison and W. C. Wells, pp. 145–160, NASA Conf. Publ. 2053, 1978.
- Chapman, C. R., P. Paolicchi, V. Zappala, R. P. Binzel, and J. F. Bell, Asteroid families: Physical properties and evolution, In *Asteroids II*, eds. R. P. Binzel, T. Gehrels, and M. S. Matthews, pp. 386-415, 1989.
- Clark, B. E., J. Veverka,, P. Helfenstein,, P. C. Thomas,, J. F. Bell, A. Harch, M. S. Robinson, S. L. Murchie, L. A. McFadden, and C. R. Chapman, NEAR photometry of asteroid 253 Mathilde, *Icarus*, **140**, 53-65, 1999.
- Colwell, J. E., A. A. S. Gulbis, M. Horanyi, and S. Robertson, Dust transport in photoelectron layers and the formation of dust ponds on Eros, *Icarus*, **175**, 159-169, 2005.
- Criswell, D. R., Horizon-glow and motion of lunar dust, In *Photon and Particle Interactions With Surfaces in Space*, ed. R. J. L. Grard, Springer, New York, pp. 545-556, 1973.
- Demura, H., S. Kobayashi, E. Nemoto, N. Matsumoto, M. Furuya, A. Yukishita, N. Muranaka, H. Morita, K. Shirakawa, M. Maruya, H. Ohshima, M. Uo, T. Kubota, T. Hashimoto, J. Kawaguchi, A. Fujiwara, J. Saito, S. Sasaki, H. Miyamoto, and N.

- Hirata, Pole and global shape of 25143 Itokawa, *Science*, **312**, 1347-1349, 2006.
- Dickinson, C. S., M. Daly, O. Barnouin, B. Bierhaus, D. Gaudreau, J. Tripp, M. Ilnicki, and A. Hildebrand, An overview of the OSIRIS REx laser altimeter (OLA) (abstract), 43rd Lunar Planet. Sci. Conf., The Woodlands, Texas, LPI Contribution No. 1659, id.1447, 2012.
- Eugster, O., G. F. Herzog, K. Marti, and M. W. Caffee, Irradiation Records, Cosmic-Ray Exposure Ages, and Transfer Times of Meteorites, In *Meteorites and the Early Solar System II*, eds. D. S. Lauretta and H. Y. McSween, Jr., Univ. Arizona Press, Tucson, 943 pp., p. 829-851, 2006.
- Fernald, F. G., B. M. Herman, and J. A. Reagan, Determination of aerosol height distribution by Lidar, *J. Appl. Meteor.*, **11**, 482-489, 1972.
- Fiocco, G. and L. D. Smullin, Detection of scattering layers in the upper atmosphere (60–140 km) by optical radar, *Nature*, **199**, 1275 - 1276, 1963.
- Fujiwara, A., J. Kawaguchi, D. K. Yeomans, M. Abe, T. Mukai, T. Okada, J. Saito, H. Yano, M. Yoshikawa, D. J. Scheeres, O. Barnouin-Jha, A. F. Cheng, H. Demura, R. W. Gaskell, N. Hirata, H. Ikeda, T. Kominato, H. Miyamoto, A. M. Nakamura, R. Nakamura, S. Sasaki, and K. Uesugi, The rubble-pile asteroid Itokawa as observed by Hayabusa, *Science*, **312**, 1330-1334, 2006.
- Furukawa, Y. and J. Ponce, Accurate, dense, and robust multi-view stereopsis, *IEEE Trans. Pattern Analysis and Machine Intelligence*, **32**, 1362-1376, 2010.
- Gaskell, R. W. , O. S. Barnouin-Jha, D. J. Scheeres, A. S. Konopliv, T. Mukai, S. Abe, J. Saito, M. Ishiguro, T. Kubota, T. Hashimoto, J. Kawaguchi, M. Yoshikawa, K. Shirakawa, T. Kominato, N. Hirata, and H. Demura, Characterizing and navigating small bodies with imaging data, *Meteor. Planet. Sci.*, **43**, 1049-1062, 2008.
- Greenberg, R., W. F. Bottke, M. Nolan, P. E. Geissler, J-M. Petit, D. D. Durda, E. Asphaug, and J. Head, Collisional and Dynamical History of Ida, *Icarus*, **120**, 106–118, 1996.
- Hirata, N., and H. Miyamoto, Dust levitation as a major resurfacing process on the surface of a Saturnian icy satellite, *Atlas, Icarus* **220**, 106-113, 2012.
- Hirata, N., O. S. Barnouin-Jha, C. Honda, R. Nakamura, H. Miyamoto, S. Sasaki, H. Demura, A. M. Nakamura, T. Michikami, R. W. Gaskell, and J. Saito, A survey of possible impact structures on 25143 Itokawa, *Icarus*, **200**, 486–502, 2009.
- Ikeda, H., Y. Tsuda, Y. Mimasu, and M. Yoshikawa, A simulation study of gravity and ephemeris estimation of asteroid 1999 JU₃ using spacecraft radiometric tracking, optical, and altimeter measurements, *Adv. Astron. Sci.*, **148**, AAS 13-417, 23rd AAS/AIAA Space Flight Mechanics Meeting, 2013.
- Kawakami, K., M. Abe, S. Hasegawa, and T. Kasuga, Observation of asteroid (162173) 1999 JU₃ doe next asteroidal sample return mission (in Japanese), *Planetary People*, **19**, 4-11, 2010.
- Kimura, H. and I. Mann, The electric charging of interstellar dust in the solar system and consequences for its dynamics, *Astrophys. J.*, **499**, 454-462, 1998.
- Klett, J. D., Stable analytical inversion solution for processing lidar returns, *Appl. Opt.*, **20**, 211-220, 1981.
- Krivov, A.V., M. Sremčević, F. Spahn, V. V. Dikarev, and K. V. Kholshevnikov, Impact generated dust clouds around planetary satellites: Spherically-symmetric case, *Planet. Space Sci.*, **51**, 251–269, 2003.
- Lee, P., J. Veverka, P. C. Thomas, P. Helfenstein, M. J. S. Belton, C. R. Chapman, R. Greeley, R. T. Pappalardo, R. Sullivan, and J. W. Head, III, Ejecta Blocks on 243 Ida and on other asteroids, *Icarus*, **120**, 87–105, 1996.
- Liou, K. N., An introduction to atmospheric radiation, Academic Press, pp. 392, 2002.

- McCoy, J. E., and D. R. Criswell, Evidence for a high altitude distribution of lunar dust, *Proc. Lunar Sci. Conf.* 5th, 2991-3005, 1974.
- Michel, B., T. H. Henning, R. Stognienko, and F. Rouleau, Extinction properties of dust grains: A new computational technique, *Astrophys. J.*, **468**, 834-841, 1996.
- Michel, P., W. Benz, and D. C. Richardson, Disruption of fragmented parent bodies as the origin of asteroid families, *Nature*, **421**, 608-611, 2003.
- Michel, P., W. Benz, and D. C. Richardson, Catastrophic disruption of pre-shattered parent bodies, *Icarus*, **168**, 420-432, 2004.
- Miyamoto, H., H. Yano, D. J. Scheeres, S. Abe, O. Barnouin-Jha, A. F. Cheng, H. Demura, R. W. Gaskell, N. Hirata, M. Ishiguro, T. Michikami, A. M. Nakamura, R. Nakamura, J. Saito, and S. Sasaki, Regolith migration and sorting on asteroid Itokawa, *Science*, **316**, 1011-1014, 2007.
- Mizuno, T., K. Tsuno, E. Okumura, and M. Nakayama, Evaluation of LIDAR system in rendezvous touchdown sequence of Hayabusa mission., *Trans. Japan Soc. Aero. Space Sci.*, **179**, 47-53, 2010.
- Moskovitz, N. A., S. Abe, K.-S. Pan, D. J. Osip, D. Pefkou, M. D. Melita, M. Elias, K. Kitazato, S. J. Bus, F. E. DeMeo, R. P. Binzel, P. A. Abell, Rotational characterization of Hayabusa II target Asteroid (162173) 1999 JU₃, *Icarus*, **224**, 1, 24–31, 2013.
- Mukai, T., S. Abe, N. Hirata, R. Nakamura, O. S. Barnouin-Jha, A. F. Cheng, T. Mizuno, K. Hiraoka, T. Honda, H. Demura, R. W. Gaskell, T. Hashimoto, T. Kubota, M. Matsuoka, D. J. Scheeres, and M. Yoshikawa, An overview of the LIDAR observations of asteroid 25143 Itokawa, *Adv. Space Res.*, **40**, 187-192, 2007.
- Müller, T. G., J. Durech, S. Hasegawa, M. Abe, K. Kawakami, T. Kasuga, D. Kinoshita, D. Kuroda, S. Urakawa, S. Okumura, Y. Sarugaku, S. Miyasaka, Y. Takagi, P. R. Weissman, Y.-J. Choi, S. Larson, K. Yanagisawa, and S. Nagayama, Thermo-physical properties of 162173 (1999 JU3), a potential flyby and rendezvous target for interplanetary missions (Research Note), *Astron. Astrophys.*, **525**, A145, 2011.
- Nagao, K., R. Okazaki, T. Nakamura, Y. N. Miura, T. Osawa, K. Bajo, S. Matsuda, M. Ebihara, T. R. Ireland, F. Kitajima, H. Naraoka, T. Noguchi, A. Tsuchiyama, H. Yurimoto, M. E. Zolensky, M. Uesugi, K. Shirai, M. Abe, T. Yada, Y. Ishibashi, A. Fujimura, T. Mukai, M. Ueno, T. Okada, M. Yoshikawa, and J. Kawaguchi, Irradiation History of Itokawa Regolith Material Deduced from Noble Gases in the Hayabusa Samples, *Science*, **333**, 1128-1131, 2011.
- Nakamura, T., T. Noguchi, M. Tanaka, M. E. Zolensky, M. Kimura, A. Tsuchiyama, A. Nakato, T. Ogami, H. Ishida, M. Uesugi, T. Yada, K. Shirai, A. Fujimura, R. Okazaki, S. A. Sandford, Y. Ishibashi, M. Abe, T. Okada, M. Ueno, T. Mukai, M. Yoshikawa, and J. Kawaguchi, Itokawa dust particles: A direct link between S-type asteroids and ordinary chondrites, *Science*, **333**, 1113-1116, 2011.
- Poppe, A., and M. Horanyi, Simulations of the photoelectron sheath and dust levitation on the lunar surface, *J. Geophys. Res.*, **115**, 2010.
- Prockter, L., P. Thomas, M. Robinson, J. Joseph, A. Milne, B. Bussey, J. Veverka, and A. Cheng, Surface expressions of Structural Features on Eros, *Icarus*, **155**, 75-93, 2002.
- Rennilson J. J., and D. R. Criswell, Surveyor observations of lunar horizon glow, *Moon*, **10**, 121-142, 1974.
- Richardson, D. C., Z. M. Leinhardt, H. J. Melosh, and W. F. Jr. Bottke, Gravitational aggregates: Evidence and evolution, In *Asteroids III*, eds. W. F. Bottke Jr., A.

- Cellino, P. Paolicchi, and R. P. Binzel, pp. 501-515, 2002.
- Robinson, M. S., P. C. Thomas, J. Veverka, S. Murchie, and B. Carcich, The nature of ponded deposits on Eros, *Nature*, **413**, 396-400, 2001.
- Rowlands, D. D., D. E. Pavlis, F. G. Lemoine, G. A. Neumann, and S. B. Luthcke, The use of laser altimetry in the orbit and attitude determination of Mars Global Surveyor, *Geophys. Res. Lett.*, **26**, 1191-1194, 1999.
- Snavely, N., S. M. Seitz, and R. Szeliski, Photo tourism: Exploring image collections in 3D, *ACM Trans. Graphics*, 2006.
- Simonelli, D. P., M. Wisz, A. Switala, D. Adinolfi, J. Veverka, P. C. Thomas, and P. Helfenstein, Photometric properties of PHOBOS surface materials from Viking images, *Icarus*, **131**, 52-77, 1998.
- Sullivan, R., R. Greeley, R. Pappalardo, E. Asphaug, J. M. Moore, D. Morrison, M. J. S. Belton, M. Carr, C. R. Chapman, P. Geissler, R. Greenberg, J. Granahan, J. W. Head III, R. Kirk, A. McEwen, P. Lee, P. C. Thomas, and J. Veverka, Geology of 243 Ida, *Icarus*, **120**, 119-139, 1996.
- Thomas, P. C., M. J. S. Belton, B. Carcich, C. R. Charpman, M. E. Davies, R. Sullivan, and J. Veverka, The shape of Ida, *Icarus*, **120**, 20-32, 1996.
- Tsuchiyama, A., M. Uesugi, T. Matsushima, T. Michikami, T. Kadono, T. Nakamura, K. Uesugi, T. Nakano, S. A. Sandford, R. Noguchi, T. Matsumoto, J. Matsuno, T. Nagano, Y. Imai, A. Takeuchi, Y. Suzuki, T. Ogami, J. Katagiri, M. Ebihara, T. R. Ireland, F. Kitajima, K. Nagao, H. Naraoka, T. Noguchi, R. Okazaki, H. Yurimoto, M. E. Zolensky, T. Mukai, M. Abe, T. Yada, A. Fujimura, M. Yoshikawa, and J. Kawaguchi, Three-dimensional structure of Hayabusa samples: Origin and evolution of Itokawa regolith, *Science*, **353**, 1125-1128, 2011.
- Veverka, J., P. C. Thomas, M. Robinson, S. Murchie, C. Chapman, M. Bell, A. Harch, W. J. Merline, J. F. Bell III, B. Busey, B. Carcich, A. Cheng, B. Clark, D. Domingue, D. Dunham, R. Farquhar, M. H. Gaffey, E. Hawkins, N. Izenberg, J. Hoseph, R. Kirk, H. Li, P. Lucey, M. Malin, L. McFadden, J. K. Miller, W. M. Owen, Jr., C. Peterson, L. Prockter, J. Warren, D. Wellnitz, B. G. Williams, and D. K. Yeomans, Imaging of Small-Scale Features on 433 Eros from NEAE: Evidence for a Complex Regolith, *Science*, **292**, 484-488, 2001.
- Vilas, F., Spectral characteristics of Hayabusa 2 Near-Earth asteroid targets 162173 1999 JU₃ AND 2001 QC34, *Astron. J.*, **135**, 1101-1105, 2008.
- Yano, H., T. Kubota, H. Miyamoto, T. Okada, D. Scheeres, Y. Takagi, K. Yoshida, M. Abe, S. Abe, O. Barnouin-Jha, A. Fujiwara, S. Hasegawa, T. Hashimoto, M. Ishiguro, M. Kato, J. Kawaguchi, T. Mukai, J. Saito, S. Sasaki, and M. Yoshikawa, Touchdown of the Hayabusa spacecraft at the Muses sea on Itokawa, *Science*, **312**, 1350-1353, 2006.

Near Infrared Spectroscopy and Thermal Infrared Imagery on Hayabusa2: Hydrated and Physical State of C-Class Asteroid 1999JU3

Tatsuaki Okada and Takahiro Iwata

*Institute of Space and Astronautical Science, Japan Aerospace Exploration Agency
And JAXA Space Exploration Center
3-1-1 Yoshinodai, Chuo-Ku, Sagamihara, 252-5210, Japan
Okada.tatsuaki@jaxa.jp*

Abstract — Near infrared spectroscopy and thermal infrared imagery will be performed in Hayabusa2, the next Japanese near-Earth asteroid sample return mission, to map the surface hydrated minerals and physical state of C-class asteroid 1999JU3. NIRS3 is a point near-infrared spectrometer based on InAs linear array and observes reflectance spectrum from 1.9 to 3.2 μm , which covers 3 μm band indicating the amount and composition of hydrated minerals on the asteroid surface. TIR is a mid-infrared imager based on un-cooled micro-bolometer array and takes thermo-graphic images of the asteroid in 8 to 12 μm band, where thermo-physical properties of the asteroid surface are derived. Results from these instruments enable us to investigate the nature of asteroid 1999JU3 as well as its history of aqueous and thermal alteration. These results also help us to select the candidate sites for sample collection on asteroid. In addition, *in situ* experiments using surface robots will take place in Hayabusa2 for studying the asteroid science, obtaining geologic context for remote sensing or returned samples, and scouting for later landing site selection. MASCOT is a 10 kg class mobile surface element and has a six band thermo-pile based radiometer MARA and a near-infrared hyper-spectral microscope MicrOmega. They measure the asteroid by local and micro scale, contemporary to the global scale observations by TIR and NIRS3, and contribute to investigating the asteroid by multiple scales.

1. Introduction

Hayabusa2 is planned as the Japanese next near-Earth asteroid sample return mission. It is the immediate follow-on mission of Hayabusa, which successfully visited S-class asteroid 25143 Itokawa and recovered samples from there to Earth for the first time in history^{1,2)}. The mission and spacecraft of Hayabusa2 are based on the heritages of Hayabusa, which makes the short term development feasible. Hayabusa2 will be launched in 2014 by the H2-A launch vehicle with a backup in 2015, arrive 1999JU3 in 2018 to conduct asteroid observation and sample collection, and return the samples to Earth in 2020³⁾.

Science targets of Hayabusa2 are to understand the origin and evolution of solar system, our Earth, and life by investigating a volatile rich primitive small body which preserves ancient environments in materials. And the mission should explore a new frontier by visiting the body representative of outer solar system. C-class near-earth asteroid is considered as the best choice to be explored by Hayabusa2. The target asteroid is 1999JU3 which is the only C-class asteroid ever found for the Hayabusa class spacecraft to accomplish sample-return mission in the technical point of view. Taxonomy of the asteroid is most suited to a Cg class, the size is estimated 0.87 ± 0.03 km in diameter, its rotation period is 7.63 hours. Its solar distance is 0.9633 AU at perihelion and 1.4159 AU at aphelion, and the orbital period is 473.9 days. Details of 1999JU3 are shown in Table 1.

We know something about C (carbonaceous) chondrites by analysis of meteorites but little about C class asteroids although there were flybys of a C-class asteroid and some comets. As analogues of 1999JU3, we assume 253 Mathilde⁴⁾, the only imaged C-class asteroid, and 25143 Itokawa, the only explored small asteroid. Mathilde is a 50 km sized C-class asteroid, and its density is very low, 1300 ± 200 kg/m³. Several huge craters are found on the asteroid, where exposed interior looks homogeneous. The asteroid is considered as a primitive and very loosely packed rubble-pile body, formed primordially as a planetesimal in early solar nebula⁵⁾. Itokawa is a 535 x 294 x 209 m sized S-class asteroid¹⁾, its density is 1900 ± 130 kg/m³. No large craters are found but some huge boulders, a tenth size of the asteroid, exist on the asteroid. There are two kinds of geological units: rough areas covered with boulders and flat and smooth areas covered with a millimeter to centimeter sized pebbles. The latter is considered the sedimentation area of granular particles. Itokawa is like a rubble-pile body formed from an impact fragments from a larger parent asteroid. Images of Mathilde and Itokawa are shown in Fig.1, as well as the formation scenario of primordial and rubble-piled asteroids are shown in Fig.2.

In Hayabusa2, 1999JU3 will be investigated by remote sensing from spacecraft and surface measurements by surface robots, and by analyses of returned samples. Infrared observations are most essential to composition and thermo-physical properties of asteroid. Roles of infrared observations are described for asteroid science and sampling site selection in the next chapter, and infrared instruments are introduced in the following chapters.

Table 1. Compilation of 1999JU3 characteristics^{3),6),7)}

| | |
|-------------------------------|-------------------------|
| Taxonomic Type | Cg |
| Diameter (D_{eff}) | 0.87 ± 0.03 km |
| Axis ratio | 1.3 : 1.1 : 1.0 |
| Rotation period | 7.63 ± 0.01 Hr |
| Pole axis (°, °) | (73, -62), or (331, 20) |

| | |
|-------------------------------|---|
| Albedo (P_v) | 0.070 ± 0.006 |
| $H^6)$ | 18.82 ± 0.021 |
| $G^6)$ | -0.110 ± 0.007 |
| Thermal Inertia ⁷⁾ | $200 - 600 \text{ Jm}^{-2}\text{s}^{-0.5}\text{K}^{-1}$ |
| Orbit (solar distance) | $0.9633 - 1.4159 \text{ AU}$ |
| Semi-major axis | 1.1896 AU |
| Eccentricity | 0.1902 |
| Inclination | 5.8838° |
| Orbital Period | $473.9 \text{ days} = 1.30 \text{ years}$ |

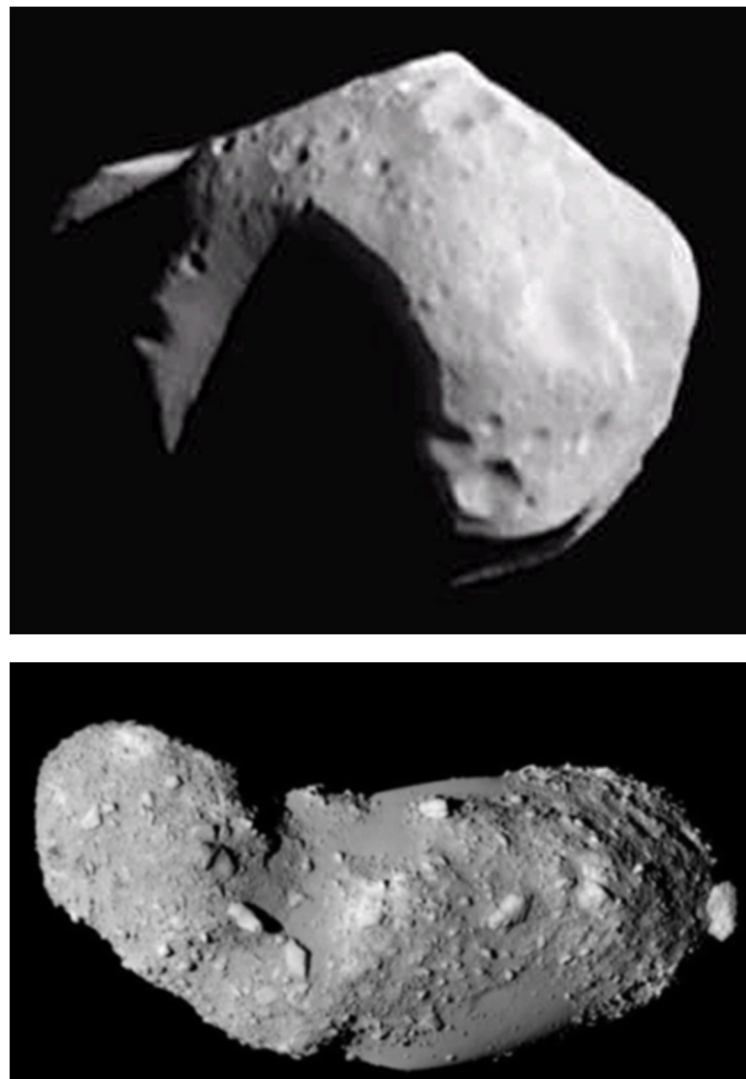


Figure 1. Images of C-class asteroid 253 Mathilde (top)⁴⁾ and S-class small asteroid 25143 Itokawa (bottom)⁸⁾ are shown as analogues of small C-class asteroid 1999JU3.

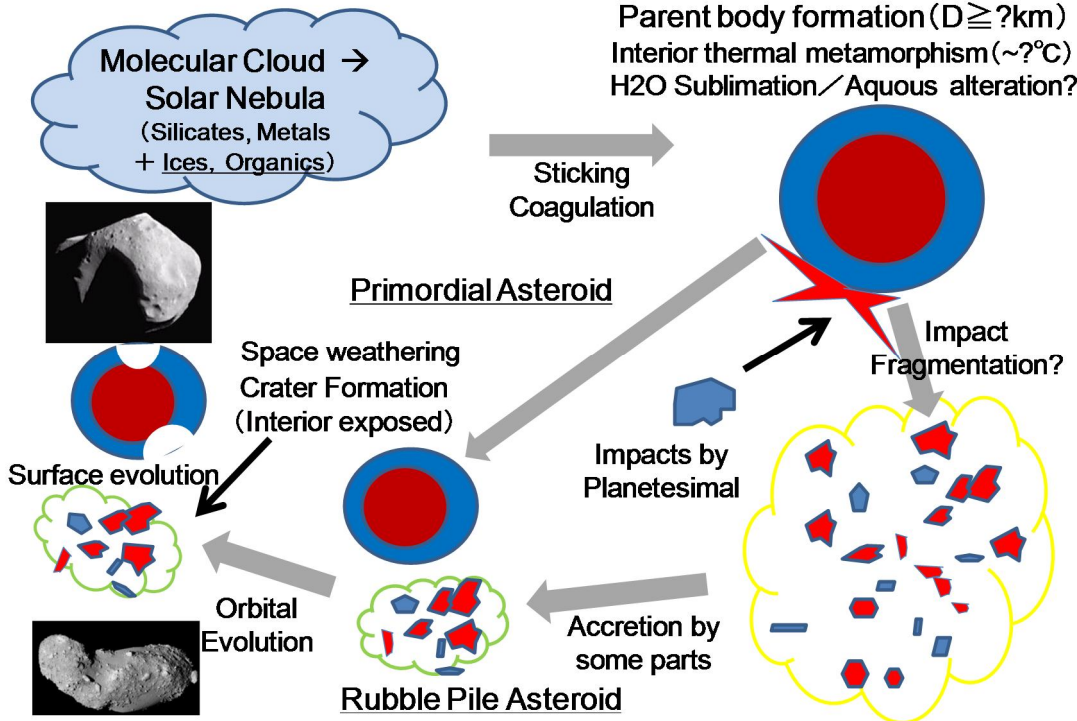


Figure 2. Possible formation scenarios of asteroid 1999JU3, a primordial and very loosely packed, or a re-accreted rubble-pile of impact fragments.

2. Infrared Observations in Hayabusa2

Infrared observations have been used in planetary missions for surface mineralogy and thermo-physical properties. Spectroscopy of near-infrared wavelength is often used to identify or distinguish each area in mineral composition by central wavelengths and depths of several absorption bands. C-class asteroid has a rather flat spectral profile in visible to near-infrared wavelength, but with remarkable absorption at about 3 μm . The shape and depth of the absorption band is most informative on the hydrated state or aqueous alteration of surface materials. Small and sharp absorption bands also exist at 1.4 and 1.9 μm indicating hydrated minerals. Since the C-class asteroid is associated with carbonaceous chondrite meteorites, the mineralogy and aqueous alterations inform the inter-connection between asteroids and those meteorites.

Physical properties of uppermost surface materials are most important to be investigated in asteroid material science, since some of inner materials must have been obtained as meteorites. Uppermost surface materials are considered as fragile due to its fluffy or highly porous structure and cannot survive during terrestrial atmospheric entry. Such fragile and porous materials might be well distinguishable by thermo-physical property, although it is also dependent on the particle size in case of regolith surface. The asteroid surface temperature varies 250 to 400 K at the sub-solar point depending on the distance from the sun and the thermal inertia of the material. Thermal infrared measurement at 10 μm wavelength is sufficiently sensitive to determine the thermo-physical properties of surface materials.

In Hayabusa2, a near-infrared point spectrometer NIR3 is developed to identify the surface hydrated materials for the spatial resolution of several tens of meters. It is used to understand the aqueous alteration and its regional distribution as well as to

provide information on sampling site selection. Figure 3 shows the near-infrared map of Itokawa in 0.9 to 2.1 μm wavelength⁹⁾.

A thermal-infrared imager TIR is mounted to take images of thermal radiation off the surface of asteroid, in order to investigate thermo-physical properties of asteroid as well as to provide information on the sanding site selection and the safe assessment of touchdown operation. Figure 4 shows a calculated temperature map of Itokawa assuming the thermal inertia of $135 \text{ Jm}^{-2}\text{s}^{-0.5}\text{K}^{-1}$ (regolith surface case) and the solar distance is 1.0 AU (under the same condition as the touchdown to Itokawa).

A small lander MASCOT is developed by German Aerospace Center (DLR) in cooperation with French Space Agency (CNES) and Japan Aerospace Exploration Agency (JAXA) for conducting in situ scientific observation of asteroid surface, obtaining the geologic context for remote sensing, and scouting the later landing sites for sampling¹⁰⁾. The 10 kg class lander carries an infrared hyper-spectral microscope MicrOmega and a multi-band thermal radiometer MARA. MicrOmega will observe the surface mineralogy and textures for each particle, especially for hydrated and organic materials. MARA will determine the thermal inertia of surface precisely by continuous measurement from day to night.

In Hayabusa2, infrared observations strongly contribute to understanding the nature of the asteroid, providing the information on landing site selection, as well as assessing the safe operation of spacecraft. Infrared measurements will be done both from remote sensing and by surface measurements. Characteristics of those instruments are summarized in Table 2. Details of each instrument are described in the following chapters.

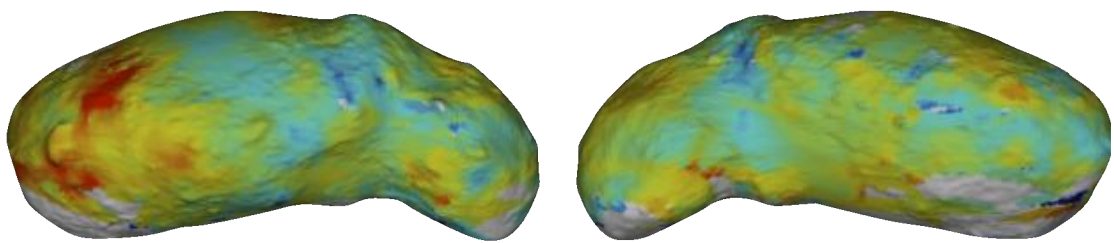


Figure 3. A near-infrared map of asteroid 25143 Itokawa observed by NIRS on Hayabusa⁹⁾. Its regional variation is not by mineral composition but by difference of surface freshness or space-weathering.

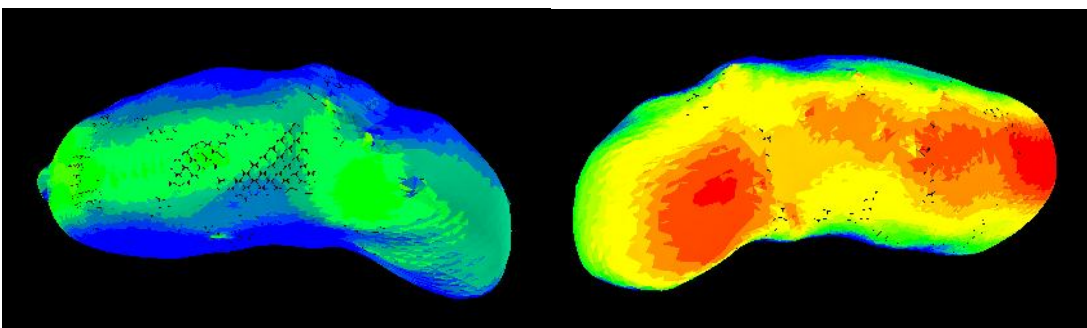


Figure 4. A calculated temperature map of asteroid 25143 Itokawa are shown, assuming that the surface thermal inertia is $135 \text{ Jm}^{-2}\text{s}^{-0.5}\text{K}^{-1}$ on the shape model of Itokawa. Its regional variation is due to the local time and the solar angle at each site.

Table 2. Summary of Specifications of Payload Instruments

| Payloads | Specifications |
|------------------------------|---|
| Near IR Spectrometer (NIRS3) | Wavelength: 1.9 – 3.2 μm , FOV: 0.1°x 0.1° (70m @HP, 2-3m@H=1km) Detector: 128 pix, (Hamamatsu, InAs linear array) Spectral Sampling: 30nm SNR: >50 Radiometric calibration: >90% |
| Thermal IR Imager | Wavelength: 8 -12 μm (1band) FOV: 12°x 16° (4km x 5km@HP, 200m x 280m @H=1km) Detector: 320 x 240 pix (NEC 320 un-cooled bolometer) IFOV: 0.877mrad (17.6m@HP, 0.88m@H=1km) NETD: <0.3K, Absolute Temperature: <3K, for 250-400K |
| Small Lander (MASCOT) | MicrOmega(IR spectro-microscope using AOTF) Wavelength: 0.9 – 3.5 μm , 10nm resolution Spatial Resolution: 128x128 pixels for 2.5mm (20 μm) Detector: HCT with Stirring Cooler, 128 x 128 pixels. MARA (thermal emission with 6 band filters) Wavelength: 6-band channels in 8-12 μm , 5-20 μm Detector: 6 thermopiles |

3. NIRS3

3.1 Science targets of NIRS3

NIRS3 is a near-infrared point spectrometer to characterize 3 μm band of reflectance spectra off the asteroid surface. Purposes of NIRS3 are for sampling site selection and for science of asteroid.

- 1) For sampling site selection:
 - NIRS3 is to assess surface mineralogy and the abundance of water/ice or hydrated features at 50 m spatial resolution.
- 2) For science:
 - NIRS3 is to identify the surface materials (meteoritic type) and to search for water-ice or hydrated materials and investigate aqueous alteration undergone in the parent body.
 - NIRS3 is to investigate the surface metamorphic processes by the spectral shape (dehydration by heating)
 - NIRS3 is to find underground volatile existence and activity by observing the SCI excavated ejecta.

Ground based near-infrared spectroscopy of C-class asteroids has proven to often bear 3 μm absorption band and there are some types of band shape such as round, checkmark, and weak features (see Fig.5). Similar features are observed for

meteorites in the laboratory. CI chondrites have 2.7 μm sharp band and 2.9 to 3.1 μm round band. CM chondrites have the main 2.8 μm and a weaker 3.0 μm double bands. CR chondrites have similar to CM but a single band. CV chondrites have only a weak or no band. The 3 μm band features of some silicates, carbonates, sulfates, hydroxides, and oxides are also shown in Fig.6, where the wavelength range covered by NIRS3 is shadowed in grey.

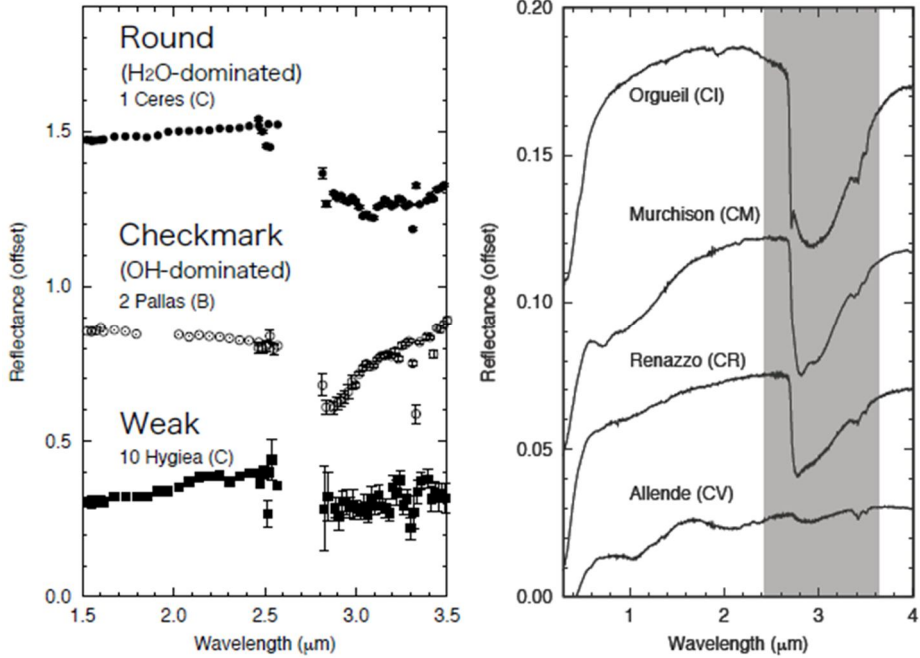


Figure 5. The 3 m band features of asteroids 1 Ceres, 2 Pallas, and 10 Hygrea by ground based observations are shown as well as those features of meteorites in laboratory such as Orgueil (CI), Murchison (CM), Renazzo (CR), and Allende (CV) (left: after Rivkin et al., 2002¹¹⁾, right: Hiroi et al., 1996¹²⁾).

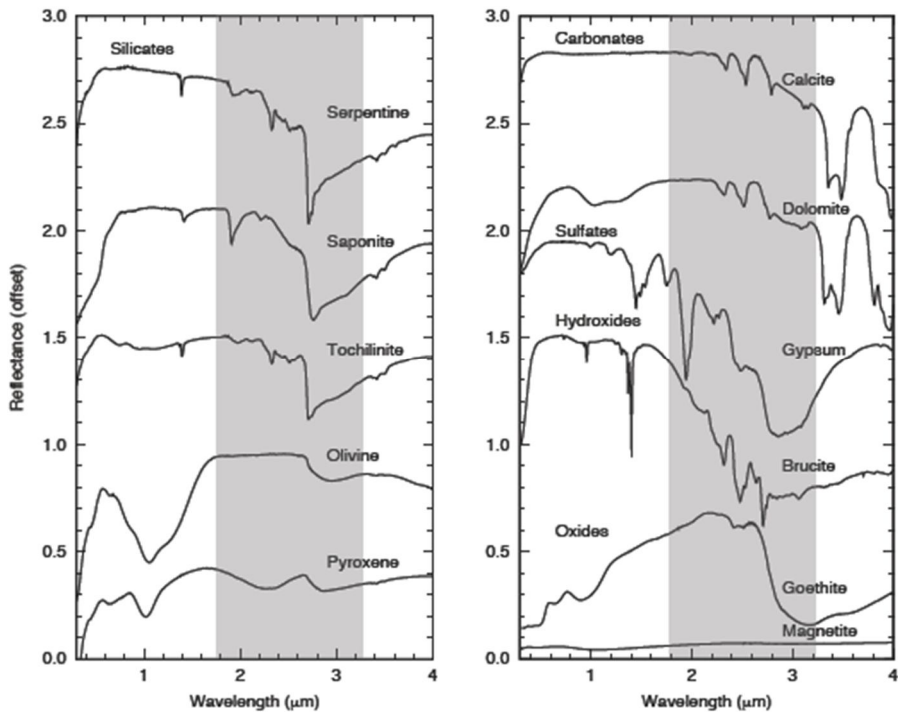


Figure 6. 3 m band features of minerals in laboratory such as silicates, carbonates, sulfates, hydroxides, and oxides. The wavelength in grey is covered by NIRS3 (data from RELAB, <http://www.planetary.brown.edu/relab/>).

3.2 Scientific Objectives of NIR3

Scientific objectives of NIR3 are 1) acquiring spatially resolved NIR reflectance spectra, relative to disc-integrated spectrum obtained by ground based spectroscopy, and 2) revealing surface characteristics of C-class asteroid.

1) Acquiring spatially resolved NIR reflectance spectra:

- NIR3 is to observe the surface near-infrared spectrum at medium spatial resolution (< 50 m) for global coverage.
- NIR3 is to observe the surface near-infrared spectrum at high spatial resolution (< 5 m) for selected areas such as sampling sites and impact experiment crater.

2) Revealing surface characteristics of C type asteroid:

- NIR3 is to determine mineral composition, and its similarity to meteoritic types such as CI, CM, CV, CO, CR.
- NIR3 is to search for traces of aqueous and/or thermal alteration by detailed spectroscopy of 3 m band feature.
- NIR3 is to find a link with meteorites by the similarity of 3 μm band feature.
- NIR3 is to investigate regolith properties, by measuring phase angle dependency of spectral feature.
- NIR3 is to determine space weathering process on 1999JU3, which is yet to be studied for C-class asteroid.
- NIR3 is to find water/hydroxyl formation by solar wind on the surface of 1999JU3, which is also found on the Moon.

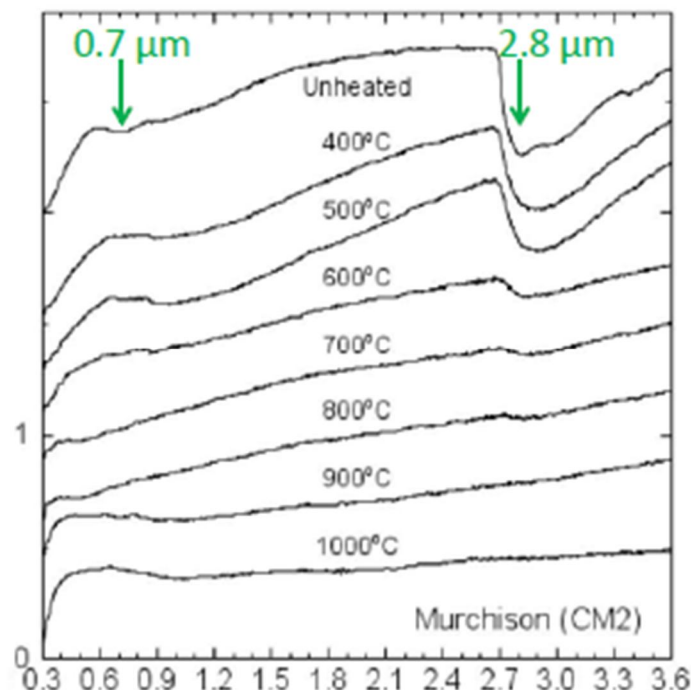


Figure 7. Change of 3 μm band feature by heating or dehydration (modified from Hiroi et al., 1996^[12]).

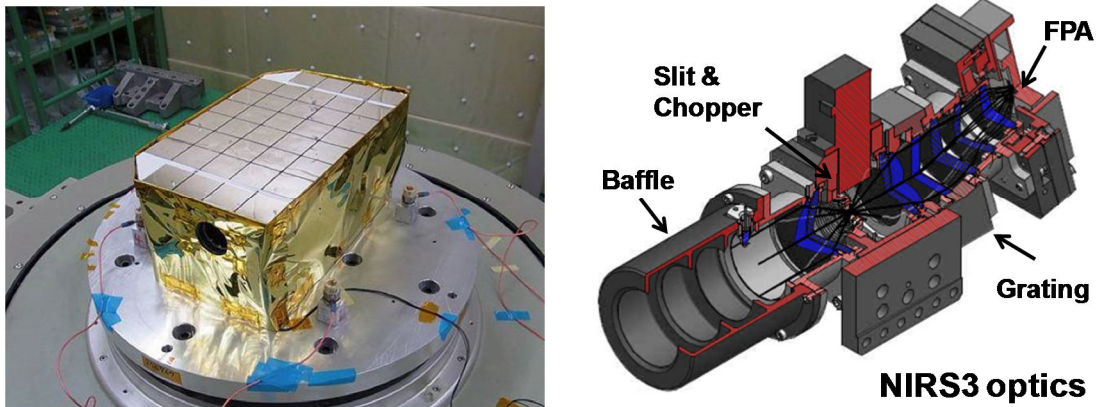


Figure 8. NIRS3-S proto-model and the schematics of NIRS3 optics

3.3 Optical Configuration of NIRS3

The concept of NIRS3 optical configuration is shown as follows. NIRS3 optics include an objective, collimator and imaging of Si-Ge lens, slit and flat transmission grating. The optical unit is passively cooled with radiator to a low temperature enough to reduce the background radiation emitted from the optics. An optical chopper is placed in front of the entrance slit to obtain a dark reference. The characteristics of NIRS3 optics are shown in Table 3, and the schematics of the NIRS3 optical configuration is shown in Figure 8.

Table 3. Specifications of NIRS3 optics

| Parameters | Value |
|---------------------------|--|
| Optical design | Entire transmission optics, Si-Ge lens system, grating spectrometer |
| Entrance pupil diameter | 30 mm |
| F number | 1 |
| Grating groove density | 100 gr/mm |
| Grating blazed wavelength | 2500 nm |
| Optical transmission | 0.6–0.9 |
| Slit size | 45 μm x 45 μm |
| Optics temperature | 193 to 183 K |

3.4 FPA (focal plane assembly) and Electronics

As the focal plane assembly, InAs photodiode linear array has been selected for acquiring spectral range of 1900 to 3200 nm at the temperature achievable by passive cooling. The FPA with electronic preamplifier and thermistor is manufactured by Hamamatsu Photonics K.K. FPA. The chopper serves to modulate the detected radiation, allowing the dark current level of the detector to be subtracted on a pixel-by-pixel basis. The dark current level subtraction and stacking of the subtracted radiation output are conducted on the FPGA.

The InAs photodiode package is shown in Fig.9, and the characteristics of FPA and electronics are shown in Table 4.

Table 4. Specifications of NIRS FPA

| Parameters | Value |
|----------------------|---|
| Detector type | InAs linear array, Hamamatsu Photonics. |
| Format | 1 x 128 pixels |
| Pixel size | 50 μm x 100 μm |
| Dark current | 1.3 x 10^{10} e/s |
| Quantum efficiency | 40% |
| Readout noise | 3000 e rms |
| Wavelength cut-off | 3200 nm |
| Detector temperature | 193 to 183 K (- 80 to -90 °C) |

**Figure 9.** Photograph of InAs linear array sensor

4. TIR

4.1 Outlines of TIR

TIR is a thermal infrared imager to take images of thermal emission off the surface of asteroid, or for “thermography” of near-earth object. TIR is being developed using the heritage of Long-wave Infrared camera (LIR)¹³⁾ onboard Akatsuki, a Japanese Venus climate orbiter, and successfully imaged the atmospheric clouds of the Earth and Venus.

Purposes of TIR are for operational use and for scientific use.

- 1) For sampling site selection and operation for touchdown:
 - Surface physical conditions (sand, pebbles, or rocks) at each geologic unit are derived from thermo-physical properties by TIR observations even if conducted from Home Position, and they are used for sampling site selection. About 1 mm size is most favorable for sampling.
 - Surface temperature measured and predicted by TIR observations are used for assessment of touchdown operation.
- 2) For *in situ* science:
 - TIR is to understand the surface physical properties of “C-class” asteroid: porosity, density, geologic features to investigate thermal evolution, heating or sedimentation processes
 - TIR is to know the surface condition to interpret NIR spectroscopy
 - TIR is to obtain the direct information on YORP/Yarkovsky

4.2 Concept of TIR

TIR is the very first experiment of thermal infrared imaging of NEA to determine thermo-physical properties of asteroid. TIR uses an un-cooled bolometer array and consequently it becomes a relatively small and light weighted instrument. TIR is developed using the heritage from LIR¹³⁾ on Akatsuki Venus climate orbiter, so that a short-term development is highly feasibility (off-the-shelf).

There is a well known relation of thermal inertia with asteroid size by ground based observations¹⁴⁾ (see Fig.10). Thermal inertia of 1999JU3 is estimated 200 to 600 $\text{J m}^{-2}\text{s}^{-0.5}\text{K}^{-1}$, with most suited value from 200 to 300 $\text{J m}^{-2}\text{s}^{-0.5}\text{K}^{-1}$ ⁷⁾. But this is a disc-integrated averaged value, so TIR will map the surface thermal inertia to construct a thermal model of 1999JU3 with 20 m spatial resolution. Verification of the relationship is an important problem to be solved by TIR observation.

TIR will also inform on the surface conditions, since there is an empirical relation between thermal inertia and surface conditions as summarized in Table 5. It is not only for scientific study to understand the nature of asteroid, but the surface condition, materials, and boulder existense information on favorable or hazardous place as a landing site.

Surface temperature varies in its maximum and minimum temperature as well as the time delay for max temperature. Such temperature profiles could allow us to estimate the thermal inertia. Temperature profiles of asteroid surface at sub-solar site at 1 AU from the Sun are calculated for thermal inertia ranging from 10 to 2000 $\text{J m}^{-2}\text{s}^{-0.5}\text{K}^{-1}$ (see Fig.11).

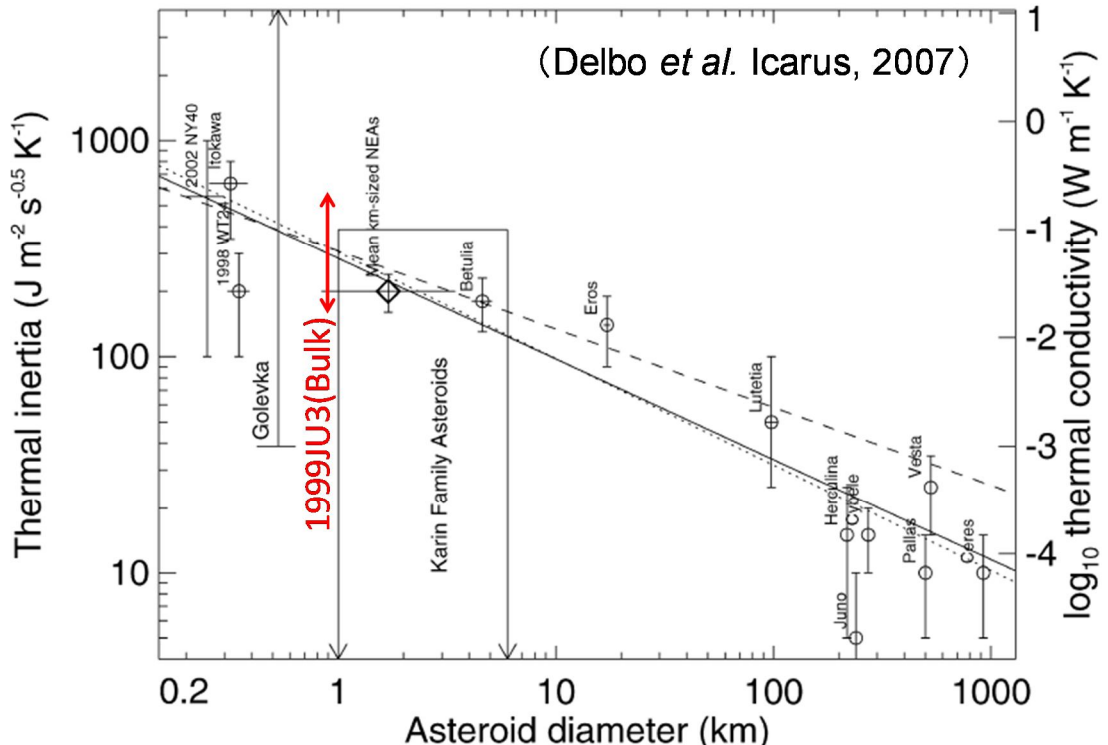


Figure 10. Relation of asteroid size to thermal inertia and thermal conductivity (modified from Delbo et al., 2007¹⁴⁾).

Table 5. Relation between thermal inertia and surface conditions.

| Thermal Inertia [J m ⁻² s ^{-0.5} K ⁻¹] | Surface Condition |
|---|---|
| about 10 | Very fluffy, high porosity (~80%), Ceres, Martian soils |
| about 50 | Fine sand : Lunar regolith ($d \sim 100$ mm or less) |
| 100 ~ 200 | Sandy regolith ($d \sim \text{mm}$): Eros soil |
| 200 ~ 400 | Pebbles ($d \sim \text{cm}$): Itokawa's Muses-Sea Regio |
| 400 ~ 1000 | Boulders, Rock fragments ($d < 1\text{m}$): Itokawa's rough terrain |
| 1000 ~ 2000 | Rocks with high porosity |
| 2000 ~ | Monolithic rocks |

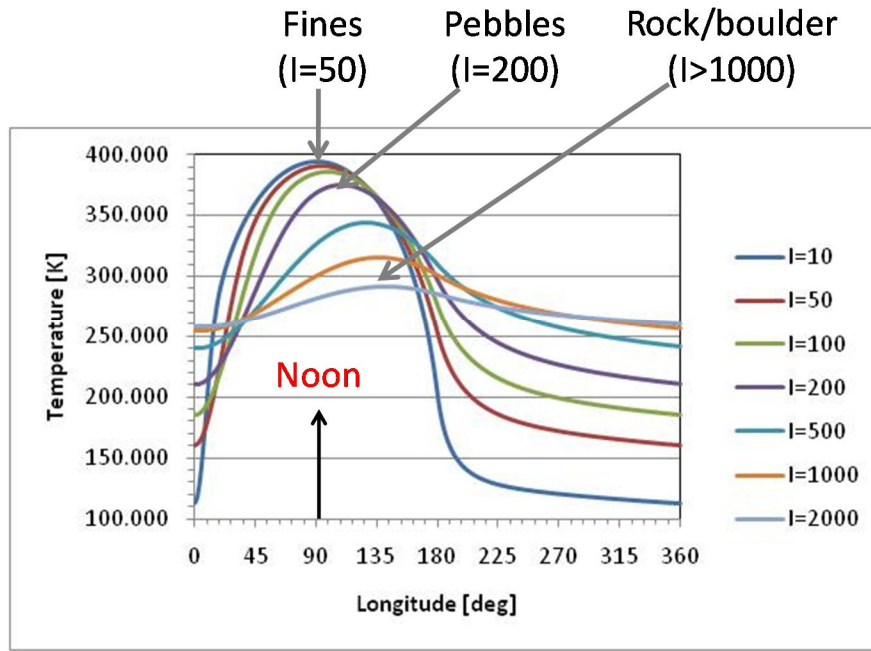


Figure 11. Temperature profile for various thermal inertia, assuming the solar distance is 1AU and the site is on the sub-solar point of asteroid whose polar axis perpendicular to the Sun.

4.3 Objectives of TIR

Details of the TIR observations are summarized in asteroid science and contribution to sample-return.

(1) Asteroid Science by in-situ Observations:

This is to understand the nature of asteroid 1999JU3 and C-class NEA in general. Thermal properties of rocks/boulders shows thermal processes indicators originated from various depth of parent body. Thermo-physical properties of inner wall of huge craters inform on the formation processes of asteroid. It suggests whether the asteroid is primordial since its formation or reconstructed as rubble-pile body. It also indicates whether the body is homogenous or heterogeneous from surface to interior. Thermo-physical properties of smooth plain, which is considered as the sedimentation under micro-gravity, will provide a new insight to understand sedimentation, granular flow, or accretion processes of asteroid. Comparison with ground observation will verify the asteroid thermal model, and much improvement in modeling the thermo-physical properties is expected in its dependency on particle size, surface roughness, and observation geometry.

(2) Contribution to Sample-Return

Thermal inertia map will be used for sampling site selection. Organic matters are

thermally altered at 370K or 420K depending on the species but the maximum temperature ever experienced during the asteroid history can be calculated if the past trajectory is traced by numerical simulation¹⁵⁾. Surface condition also constrains the landing sites. The favorable particle size is 1 mm which includes most of textures for petrologic study. Ultra-fine sand like lunar regolith is too small for petrology and 1 cm sized pebbles are too large for the sampling device. Rock distribution hazardous to touchdown operation of spacecraft is also indicated by thermal inertia.

Geologic context for sampling site is important to interpret the analyses of samples, especially for the thermo-physical properties, surface conditions, and rock distribution of the uppermost surface area. Such data will be mainly obtained by TIR observations at low altitude.

Thermal model of asteroid is constructed not only for science but also for safety descent operation for touchdown, and for lander deployment. The temperature, and thermal emission off the surface can be calculated when the spacecraft is planned to descend to the surface. Actually the worst case study shows that the touchdown is able to carry on only during the solar distance is 1.25AU or further away. But if the thermal model is updated using the TIR observations, more opportunity could be available for shorter distance from the Sun.

(3) Synergy of lander measurements and returned sample analysis is another important point to be conducted in Hayabusa2. Thermo-physical properties of returned sample could be related with TIR data, especially for the particle size and composition of materials. Mutual calibration of temperature, infrared flux between TIR and surface robot experiments is most required to interpret the data.

4.4 TIR Instrument

TIR is a thermal infrared imager based on un-cooled micro-bolometer array. Its characteristics are shown in Table 6. TIR consists of TIR-S and TIR-AE. TIR-S includes the optics, sensor, shutter, temperature controller, and electronics. A pair of images with the shutter closed and open must be taken and subtracted to construct a meaningful image. Onboard image summation improves the signal-to-noise ratio. Expected noise equivalent temperature difference (NETD) or relative accuracy of temperature is about 0.3K, and absolute accuracy of temperature is about 3K. It is sufficient to determine the thermal inertia of each geologic site by 20% uncertainty.

Optics is made of three pieces of germanium lens and germanium band pass filter to limit the wavelength from 8 to 12 μm . This is the typical wavelength for thermo-graph. The field of view is a wide angle of 16° by 12°, and has advantage in observation of larger area and surrounding environments such as dust clouds and satellites.

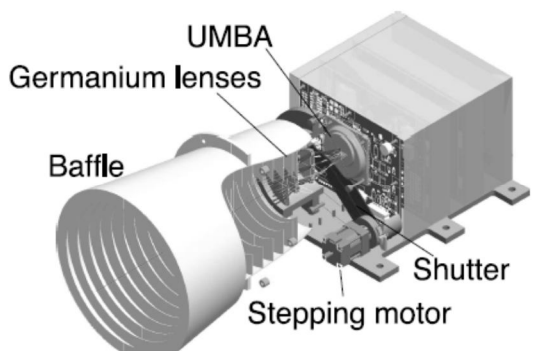
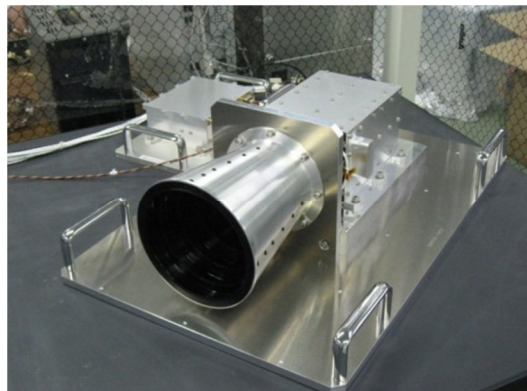


Figure 12. The photograph of TIR (LIR PM) and the schematic diagram of TIR¹³⁾.

Table 6. Performances of TIR

| Parameters | Values |
|--------------------|---------------------------|
| Wavelength | 8-12 μ m |
| FOV | 16°x12° |
| IFOV | 0.05° |
| Detection range | 250-400K |
| Pixel numbers | 344×260 (320 x 240) |
| Temp. resolution | 0.3K (@350K target) |
| Abs. temp accuracy | 3K |
| Ge Lens F-value | 1.4 |
| Total Mass | 3.3 kg |
| Total Power | 22 (in nominal operation) |

5. MASCOT: in situ characterization of asteroid

MASCOT is a small science lander with mobility, which will be deployed from Hayabusa2 spacecraft¹⁰. It is a 10 kg class lander with four scientific instruments. MARA and MicrOmega as well as an image(CAM) and a magnetometer (MAG) will be mounted on MASCOT. The configuration of MASCOT is shown in Fig.13.

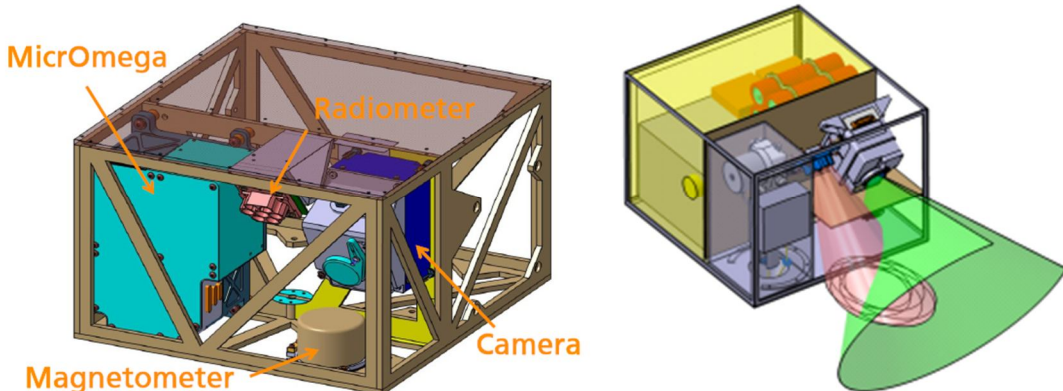


Figure 13. The outline of MASCOT is shown (left), and the schematic view shows the footprint of MARA is imaged by CAM (right).

MARA (a radiometer) is the instruments that has six thermopile sensors with different bandpath wavelength. Before deployment, MARA will calibrate by observing the temperature controled target plate mounted on the separation mechanism. Its science goals are for the derivation of surface thermal inertia, radiometric determination of surface temperature, determination of surface emissivity in selected wavelength regions, and constraints on mineralogy. MARA has two wide bands for temperature measurement to cover 2 to 50 μ m and 5 to 100 μ m, so that MARA measures almost full coverage of thermal emission. MARA also has four bands for obtaining mineral information to cover 5.5 to 7 μ m, 8 to 9.5 μ m, 9.5 to 11.5 μ m, and 14 to 16 μ m, respectively. More laboratory experiments are needed to identify mineralogy of carbonaceous materials with these four bands.

MicrOmega (NIR Hyper-spectral Microscope) is based on scanning 384 wavelength light source with acousto-optical tunable filter (AOTF) and HgCdTe pixel array sensor of 128 by 128 pixels¹⁶. The detector needs active cooling by a stirring cooler. Its science goals are to perform the first *in situ* microscopic characterization of C-asteroid, especially for hydrated minerals, oxidation state, organic matters, and

particle size distribution. It covers 0.9 to 3.5 μm wavelength which includes 1.4 and 1.9 μm bands for hydrated minerals, 2.7 μm and 2.8-3.1 μm bands for hydroxide and hydrated minerals, and 3.4 μm band for organics matters. MicrOmega will perform microscopic probing of 1999JU3, contrary to global scale of remote sensing and micro- to nano-scale of returned sample analyses.

MASCOT works continuously for 16 hours (two asteroid days), powered by Li primary batteries. It has mobility to relocate from site to site. Three or four sites will be observed, where the data for ground-truth could be obtained. Those data is important for understanding the nature of asteroid, obtaining the surface geologic context, and scouting the later landing operations.

6. Concluding Remarks

Near-infrared spectroscopy by NIRS3 and thermal infrared imaging by TIR around asteroid is important in the science of Hayabusa2. They are to investigate the nature of asteroid in mineralogy, state of aqueous or thermal alteration, thermo-physical properties, and physical conditions of asteroid surface. They are to inform for sampling site selection, and geologic context of returned samples. They are also to perform safe descent operation for sampling (SMP), and deployment of landers (MASCOT, MINERVA2) and impactor (SCI).

Remote and surface infrared measurements will be in good collaboration in Hayabusa2. Direct NIR spectral microscopy and multi-band thermal radiometry at local sites will be done by MASCOT, which will be good “ground truths” and contemporary to global remote sensing by NIR spectroscopy (NIRS3) and thermal imagery (TIR).

Acknowledgments

The authors appreciate all the members of Hayabusa2 project to propose, design and develop the spacecraft and the onboard science instruments. The authors would like to thank all the science members of Hayabusa2 and the Joint Science Team, especially of NIRS3, TIR, and MASCOT teams, to have many discussions and improve the science scenario and observation plans. The authors would give special thanks to local organizing committee members to hold the meeting in Macau.

References

- 1) Fujiwara, A. et al. (2006), The rubble-pile asteroid Itokawa as observed by Hayabusa, *Science* 312, 1330-1334.
- 2) Fujimura, A. et al. (2011), Processes to open the container and the sample catcher of the Hayabusa returned capsule in the Planetary material Sample Curation Facility of JAXA, 42th Lunar Planet. Sci. Conf., Houston, TX, #1829.
- 3) Yoshikawa, M. et al. (2012), Hayabusa2 – New challenge of next asteroid sample return mission, *Asteroids, Comets, Meteors* 2012, Niigata, #6188.
- 4) Veverka, J. et al. (1997), NEAR’s flyby of 253 Mathilde: Images of a C asteroid, *Science* 278, 2109-2114.
- 5) Yeomans D., et al. (1997), Estimating the mass of asteroid 253 Mathilde from tracking data during the NEAR flyby, *Science* 278, 2106-09.
- 6) Abe, M. et al. (2008), Ground-based observational campaign for asteroid 162173 1999JU3, COSPAR Scientific Assembly, B04-0061-08.
- 7) Mueller, T.G. et al. (2011), Thermo-physical properties of 162173 (1999JU3), a potential flyby and rendezvous target for interplanetary missions, *A&A*, 525,

- A145 (pp.6). There are other estimates such as Campins, H. et al. A&A 503, L17-L20 (2009), Spitzer observations of spacecraft target 162173 (1999 JU3), which indicates $>150 \text{ Jm}^{-2}\text{s}^{-0.5}\text{K}^{-1}$ for equatorial retrograde geometry, and $700\pm200 \text{ Jm}^{-2}\text{s}^{-0.5}\text{K}^{-1}$ if rotation axis by Abe et al.(2008) is adopted.
- 8) Saito, J. et al., (2006), Detailed images of asteroid 25143 Itokawa from Hayabusa, Science 312, 1341-1344.
 - 9) Kitazato, K. et al., (2008), Near-infrared spectro-photometry of asteroid 25143 Itokawa from NIRS on the Hayabusa spacecraft, Icarus 194, 137-145.
 - 10) Ho, T.M., et al., (2012), A mobile surface science package – MASCOT – for in situ characterization of asteroids, Asteroids, Comets, Meteors 2012, #6138.
 - 11) Rivkin, A.S. et al, (2002), Hydrated minerals on asteroids: the astronomical record, in Asteroid III, Bottke, W.F. et al. (Eds.), Univ. Arizona Press, Tucson, AZ, 235-253.
 - 12) Hiroi, T., et al. (1996), Thermal metamorphism of the C, G, B, and F asteroids seen from the 0.7 μm , 3 μm and UV absorption strengths in comparison with carbonaceous chondrites. Meteoritics Planet. Sci., 31, 321–327.
 - 13) Fukuhara, T. et al., (2011), LIR: Longwave infrared camera onboard the Venus orbiter Akatsuki, Earth Planets Space, 63, 1009–1018.
 - 14) Delbo, M., et al. (2007), Thermal inertia of near-Earth asteroids and implications for the magnitude of the Yarkovsky effects, Icarus 190, 236-249.
 - 15) Michel, P. and Delbo, M., (2010), Orbital and thermal evolutions of four potential targets for a sample return space mission to a primitive near-Earth asteroid, Icarus 209, 520-534.
 - 16) Bibring, J.-P., et al, (2012), MicrOmega: an hyper-spectral NIR microscope on board Hayabusa2, Asteroids, Comets, Meteors 2012, #6399.